Università degli Studi di Padova
Dipartimento di Ingegneria Industriale
Tesi di Laurea Magistrale in Ingegneria Elettrica

A MODEL FOR THE PERFORMANCE ANALYSIS OF A VANADIUM REDOX FLOW BATTERY STORAGE SYSTEM

Laureando:
Matteo Fiorindo
Matricola 1063584

Relatori:
Prof. Massimo Guarnieri
Dr. Federico Moro

Anno accademico 2014/2015

To all the people that helped me,
along my way.

Abstract

The Vanadium Redox Flow Battery Systems are a promising technology for large stationary storage. Their main advantages are a competitive cost and simplicity.

A key technology for the electrolyte feeding systems is based on interdigitated channels but most of the multiphysics models found in literature are based on simple flow fields. Therefore the aim of this work is to develop a multiphysics model to simulate a VRFB with interdigitated channels by the means of the finite element method. The model is based on the electrochemistry of VRFB and on the equations governing the fluid flow field for free and porous media.

It is therefore possible to analyze the distribution of the electrolyte into the cell, highlighting the areas with low intake of electrolyte, that are completely neglected in most of the models.

This model is also suited to determine the behavior of a VRFB under different operating conditions. It is possible to evaluate the equilibrium voltage, the overpotentials, the dissociation rate of the sulphuric acid species and the concentrations of the different vanadium species into the cell from a set of initial conditions.

Contents

Chapter 1

Introduction

1.1 Need for energy storage

The electricity industry is facing an increase of the production of energy from renewable sources due to their environmentally-friendly nature.

These sources are usually discontinuous, because the generated power depends on the weather. The sun can be overshadowed by the clouds and the wind can vary its direction and intensity very quickly. Hence the power variability can range from the hourly time-scale for photovoltaic systems to the seconds or minutes time-scale for wind generators.

The fluctuating production of these sources is therefore a big issue. Usually, the base-load power, i.e. the amount of power demanded in every moment of the day, is produced by coal and nuclear power plant while the power at peak time is produced by plants that can be easily powered up.

Due to an European legal requirement to encourage renewable sources,they have grid priority, meaning that the grid must take their electricity first. Wind and photovoltaic sources would have however grid priority because their marginal cost is zero.

Moreover their variation has a timescale faster than all the other plants and when the power varies too much, it may not be enough to lower the output of gas generators. Some plants may have to be switched off altogether and some coal-fired ones turned down.

In this scenario, the base-load power plants cannot be switched down, so the companies were having to pay the managers of the grid to take their electricity, transforming completely the established business model for utilities. Furthermore existing grids are not designed for distributed sources so they can become unstable if power from these sources exceed 20% of the total amount of generated power without solutions to compensate it. Distributed generation means small sized electric generation units at residential, commercial and industrial sites, e.g. small photovoltaic cells, wind turbines or small gas turbine [1]. Therefore, with an increase of grid connected renewable and distributed power plants with the simultaneous presence of large power plants, there is the need to design, control and manage the grid more accurately.

The most effective solution to these problems are Electrical Storage Systems

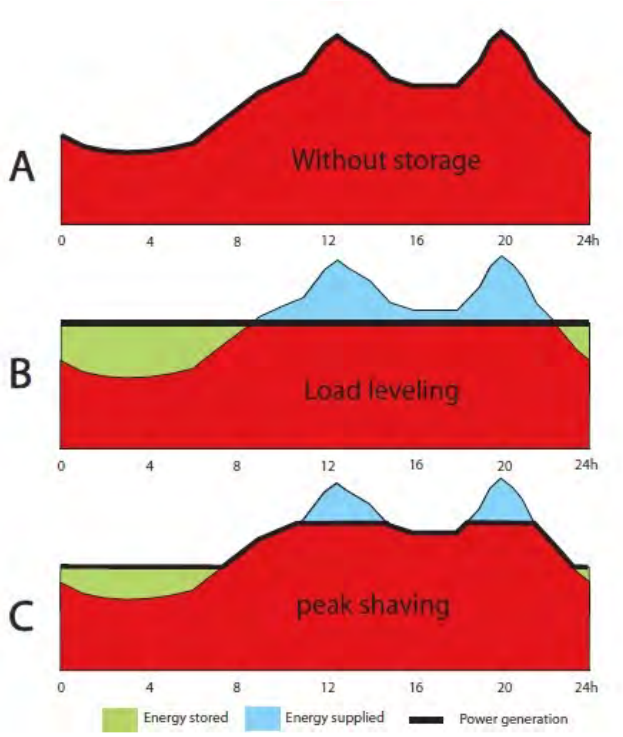

Figure 1.1: Allocation of different energy storage requirements in the power—discharge duration diagram (source: Electricity Storage Association [2])

ESS. In this way the exceeding energy generated by renewable sources can be stored until the demand of power overtake the capability of the generation units.

Another use of the energy storage is to reduce electricity costs when electric companies apply hourly pricing policies.

There are two main categories of energy servicies provided by ESS 1.1:

- Power Quality, that refers to a timescale quite short, in the range of minute/second.
- Energy Management, that concerns load leveling, power balancing and peak shaving

For both the categories the advantage in the use of Electrical Energy Storage Systems is the possibility to delay the use of the generated electricity. The choice of the ESS technology for each category of service is done according to the the operating time and the available power. The time ranges from the fraction of a second to several hours, with response time of millisecond for the fastest ESS while available power ranges from few kilowatt to gigawatt.

1.2 Energy Storage Systems

The ESS are categorized by storage capacity, power, lifetime (i.e. the ability to resist to many charge/discharge cycles), cost and response time.

Present days offer a wide range of technologies with different ranges of storable energy and different localization needs, e.g.

- *PHES*, Pumped Hydro Energy Storage, store the energy in the form of potential energy by pumping water at a certain height. It is the most exploited at present and can exceed $50MWh$ and $3GW$ but can be sited only in mountain regions. It also has high response time, so it is suitable for high-power long-time services.

Other technologies are:

- *CAES*, Compressed Air Energy Storage, store the energy by compressing air. The compression of air creates heat that can be stored and used during expansion. There is the need of large scale underground caves. Has the same rated power of *PHES*. The current R&D activity is developing adiabatic-operating systems to overcome present limitations.

- *FES*, Flywheel Energy Storage, store angular kinetic energy, with a flywheel that rotate at high velocity. It has very fast response but a fast auto-discharge due to friction, also with electromagnetic bearings. They are best suited for purposes such as frequency regulation. They are affected by containment problems and gyroscopic effects from the Earth's rotation due to the high rotational speed.

- *SMES*, Superconducting Magnetic Energy Storage, is made by superconducting coils that store magnetic energy. The superconductors need a huge amount of energy to be kept at very low temperatures, since superconductivity at high temperature is still under research. Due to the fast response, SMESs is suitable for power quality services.

- *ELDC*, Electric Double Layer Capacitor, store electrical energy by the means of the electric double layer effect. It is known also as *super-capacitor*, has a long life cycle but can store energy only for short time due to auto-discharge. It is used mainly to assist other power supplies for surge power requirements, such as during the acceleration of Electric/Hybrid Vehicles.

- *ECES*, Electro Chemical Energy Storage, store chemical energy into an electrolyte. It seems to be the only suitable solution to compensate the intermittency or variability of renewable energy generators. Due to the versatility and modularity that allows wide scalability, the time scale energy storage of this systems, can vary from short to long. It has a different location in the power/duration diagram from the other storage technologies (Fig. 1.2).

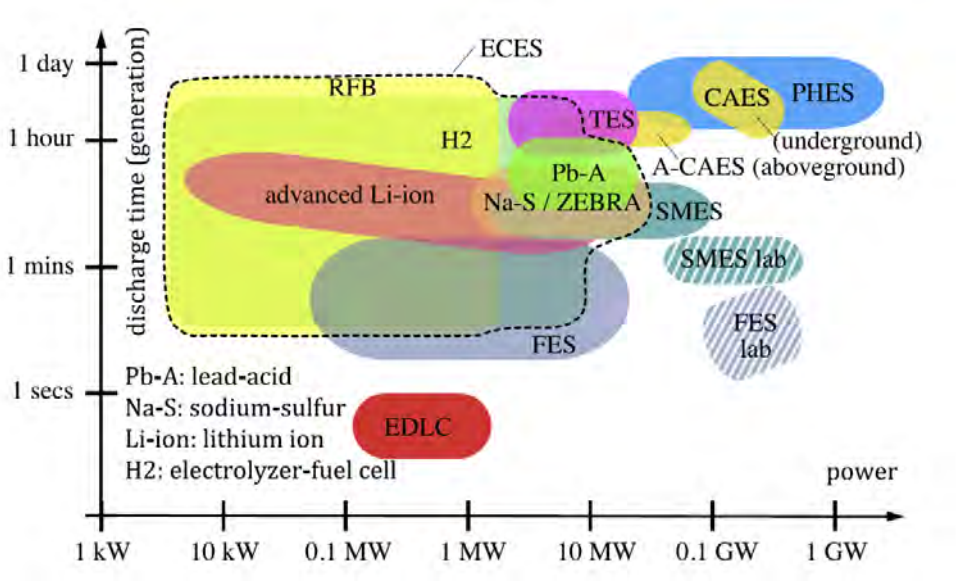

Figure 1.2: power duration diagram of energy storage systems [3]

1.3 Electro Chemical Energy Storage

Since Alessandro Volta's first voltaic pile in 1800, batteries have evolved from non-rechargeable primary cells to rechargeable secondary cells, and electrochemistry is commonly used to store electricity in consumer electronics.
Batteries consist of two types of electrochemical devices:

- Primary batteries, irreversibly transform chemical energy to electrical energy
- Secondary batteries, can be recharged

Batteries and Advanced Batteries can respond to changes in power demand within microseconds, have low standby losses and can have high energy efficiency, depending on the application and the details of the operation. Since in the majority of batteries toxic materials are used, their disposal must be always be considered.

Lead-Acid Batteries

Lead-acid is one of the oldest battery technology and the first that can be recharged. It was invented by Gaston Plantè in 1859 and consist of an alternated series of lead metal electrodes and lead oxide electrodes placed in a sulphuric acid electrolyte. This is one of the cheapest solutions for power quality and UPS but, due to the short cycle life and the inability to withstand deep discharges, has limited application for energy management.

Sodium Sulphur Batteries

Sodium sulphur batteries (NaS) were initially developed in 70*s* and the research on them is still underway.

These batteries are based on liquid sodium in the negative electrode and liquid sulphur at the positive electrode. The electrolytes at room temperature do not work and require to be heated up. The main problem is therefore the high operating temperature, that is about $300° \ C$.

Lithium-Ions batteries

One of the most diffused type of battery is the lithium-ions battery, that combine the lightness of the lithium (the lightest metal) with a high electrochemical potential. This makes the Li-ion battery as the battery with the highest electrical density, with a specific energy ranging between $100 Wh/kg$ and $150 Wh/kg$ [4]. The main limitation is the high cost per kWh.

Redox Flow Batteries

This kind of batteries (RFBs) is one of the most recent and promising technology for the stationary energy storage. The electrochemical conversion of the energy is exploited through redox processes of fluid electrolytes, which are stored in external tanks.
This technology is presented in the following section.

1.4 Redox Flow Battery: Introduction

Redox Flow Batteries are a promising technology [3] that in the recent years has increasingly studied. These batteries operate with redox reactions of two electrolyte solutions through a polymer ion-exchange membrane that only allows for transport of protons between two cell sectors. The concentration of metal ions into the electrolytes depends strongly on the chemistry used, and it ranges from 0.1 to $9M$ [5]. The liquids are stored into two separate tanks and are introduced into the RFB when needed.

The advantages of this technology are:

- flexibility and scalability, because of the independent sizing of power and energy, the capacity can be increased simply by expanding the capacity of the tanks
- high round trip efficiency,
- high DOD, depth of discharge
- long durability, since RFBs operate by changing the valence of the metal ion, the components of the electrolyte solution are not consumed
- fast responsiveness (small electrical time constant $\sim [ms]$)
- reduced environmental impact
- long stand-by periods on full discharge without ill effects

- rapid refueling by solution exchange, in case of need
- low maintenance

The disadvantages of RFBs are:

- low power and energy density ($10 - 50 Wh/kg$), compared to other technologies. This makes them unsuitable for mobile applications
- the operating temperature is limited to a small range $[15 \div 35°C]$ to avoid solution precipitation
- shunt currents, due to the conductivity of the electrolyte solution, that cause additional losses and reduce the efficiency

1.4.1 Vanadium Redox Flow Battery

Among the Redox Flow Batteries, the technology with the best chance to be widely adopted is the *Vanadium Redox Flow Battery*.

The main advantage is the ability of vanadium to exist in four oxidation states, making possible a battery with only one electroactive element instead of two. In this way are used vanadium redox couples in both half-cells and the problem of cross contamination by diffusion of ions across the membrane is therefore avoided.

Differently from other RFBs, this technology is cheaper ($3.7 \div 4.5 €/L$ for the electrolyte) and an higher simplicity, avoids the use of highly toxic materials and does not require recirculating external devices to keep the electrolyte homogeneous because vanadium starts to precipitate only if the temperature overcomes a limit temperature.

The first patent of the VRFB has been deposited by Maria Skyllas-Kazacos and co-workers in 1986, while their first papers are from 1985 [6, 7]. Their work has been developed at the University of New South Wales in Australia.

A VRFB is made by many power cells, connected in series and/or in parallel. Each cell contains two half cells divided by an ion-permeable membrane, that theoretically allows only the diffusion of protons as can be seen in Fig. 1.3. The half-cells electrochemical reactions take place into porous electrodes, which are made by carbon felt and are connected to graphite current collectors. The stack of cells is connected to the tank by pipes and the electrolytes flow thanks to pumps. To make an electrolyte with vanadium, there is the need to dissolve it. This is done by the means of a dilute sulphuric acid solution. The two electrolyte solution, due to the different oxidation states of the vanadium are different. The negative half-cell electrolyte contains only V^{2+} and V^{3+} ions and the positive half-cell electrolyte contains only $VO^{2+}(V^{4+})$ and $VO_2^+(V^{5+})$ ions.

1.5 Large-scale storage with VRFBs

One of the first papers that showed the possible use of VRFBs for the energy storage is from the 2004, where L. Joerissen et al. [9] studied a possible use of the

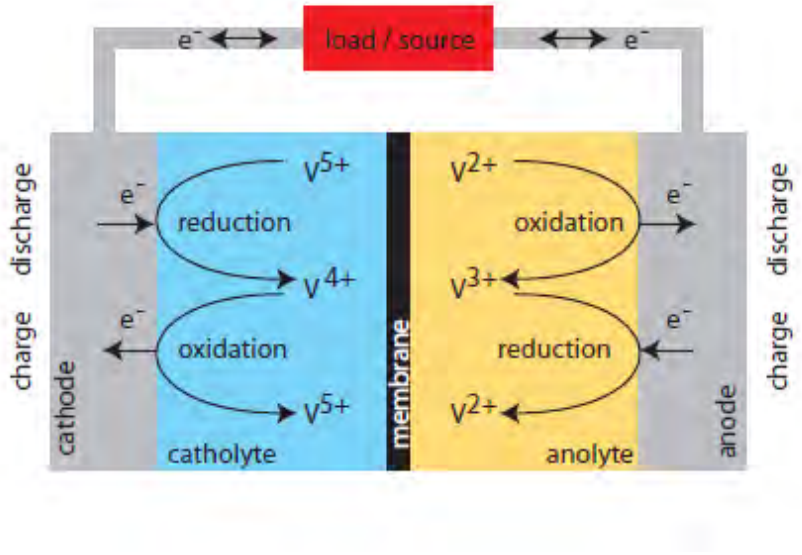

Figure 1.3: Basic scheme of a VRFB [8]

VRFB in small grids and stand-alone photovoltaic systems. They stated that this technology allows the use of inexpensive components, and made a cost analysis. The result of the cost estimation is 30000 € for a $2[kW]$ and $30[kWh]$ system.

In 2011 Shigematsu [10] published a paper that reviewed the technical development of the redox flow battery (RFB). The RFBs are compared with other storage technologies in the first part, then it describes the characteristics of the RF batteries then explains the history of the development of this batteries. In particular explains that after the patent of M. Skillas-Kazacos in 1986 [11], in Japan the development of VRFB started after a new technology of recovering vanadium included in petroleum and heavy fuels from the soot of the fuels burned at thermal power plants. Therefore the development in Japan started in 1989 and the first trial VRFB system were manufactured by Kashima Kita in 1997, a $200[kW]$ and $800[kWh]$ system. After this system the development of various systems continued and in 2001 Sumitomo Electric started to sell practical products for load leveling, instantaneous voltage sag compensation and emergency power supply.

In another 2011 review, A. Weber et al. [12] examined some of the more common RFBs, their individual components and underlying governing physical phenomena. They state also that any RFB chemistry has a particularly advantageous solution with respect to the other chemistry, making fundamental industrial and academic research.

During the discharge the electrolyte solutions flow through the carbon felt of the electrodes and the V^{2+} oxidizes in the anolyte, releasing electrons which are collected by the graphite current collector and flow trough an external load, and subsequently they are transferred to the cathode. Finally, the V^{5+} ions of the catholyte are reduced by these electrons.

During the charge an external source reverses the flow of electrons. This reverses the reactions in both the half-cells.

1.5.1 Electrochemistry

VRFB is based on redox reactions involving four oxidation states of the vanadium:

$$V^{2+} \rightleftarrows V^{3+} + e^- \tag{1.1}$$

$$V^{5+} + e^- \rightleftarrows V^{4+} \tag{1.2}$$

where $\rightarrow$ represents the discharge and $\leftarrow$ represents the charge of the battery. In a redox reaction the species that loses electrons is said to be *oxidized* while the species that gains electrons is *reduced*. It is possible to write therefore the following equations to explain:

$$reductant \quad \rightarrow \quad product + e^- \tag{1.3}$$

$$oxidant + e^- \quad \rightarrow \quad product \tag{1.4}$$

Since a battery is a device that convert stored chemical energy in electrical energy by a redox reaction, it is possible to write the reactions that occurs during the charge and the discharge of the VRFB.

During the discharge the electrons move from the anolyte to the catholyte, by flowing through the external load:

$$\begin{array}{lccccccc} oxidation & & & V^{2+} & \rightarrow & V^{3+} & + & e^- \\ reduction & V^{5+} & + & e^- & \rightarrow & V^{4+} & & \\ \hline & V^{2+} & + & V^{5+} & \rightarrow & V^{3+} & + & V^{4+} \end{array} \tag{1.5}$$

During the discharge V^{5+} takes an electron from V^{2+} while during the charge the reversed flow of electrons gives the following redox reaction:

$$\begin{array}{lccccccc} reduction & V^{3+} & + & e^- & \rightarrow & V^{2+} & & \\ oxidation & & & V^{4+} & \rightarrow & V^{5+} & + & e^- \\ \hline & V^{3+} & + & V^{4+} & \rightarrow & V^{2+} & + & V^{5+} \end{array} \tag{1.6}$$

Previous equations are a simple form of the reactions that actually occur into the VRFB. The V^{4+} and V^{5+} exist as oxides, respectively VO^{2+} and VO_2^+. The redox equation therefore must be modified to guarantee the balance of charges and the stoichiometry, by considering also the dissociation of H_2O. The equation 1.2 becomes:

$$VO_2^+ + 2H^+ + e^- \quad \rightleftarrows \quad VO^{2+} + H_2O \tag{1.7}$$

while the equation 1.1 remains the same.
The equation 1.6 can be therefore modified in:

$$V^{2+} + VO_2^+ + 2H^+ \quad \rightleftarrows \quad VO^{2+} + V^{3+} + H_2O \tag{1.8}$$

Nernst Equation

The individual potential of any electrode with respect to the standard hydrogen electrode measured at standard conditions, i.e. $25°C$, $100kPa$ and a concentration of $1M$ is called standard electrode potential $E^{\ominus}$. When the operating conditions are different from the standard conditions the relation between the electrode potential E and the operating conditions is given by the Nernst equation.

This equation can be obtained by thermodynamics considerations: By starting from the Gibbs free energy, which represents the maximum amount of extractable energy from a chemical reaction, it is possible to write it as:

$$\Delta G = \Delta H - T\Delta S \quad [J/mol] \tag{1.9}$$

where ΔH indicates the variation of enthalpy and ΔS is the variation of entropy. The free energy can also be expressed as the sum of a constant term, the free change of energy with activity of each product and reactant equal to one $\Delta G^{\ominus}$ and a variable term, function of the temperature and the equilibrium constant K:

$$\Delta G = \Delta G^{\ominus} + RTlnK \quad [J/mol] \tag{1.10}$$

Since the equilibrium constant K can be expressed, for a generic reaction

$$aA + bB \rightleftarrows cC + dD \tag{1.11}$$

as

$$K = \frac{a_C^c a_D^d}{a_A^a a_B^b} \tag{1.12}$$

where $c^{\ominus}$ is the standard molarity, c_i is a concentration, $a_i = \gamma_i^c \frac{c_i}{c^{\ominus}}$ is the activity and γ_i is the activity coefficient. The equilibrium constant K can also be represented as:

$$K = \frac{(\gamma_C^c)^c(\gamma_D^c)^d}{(\gamma_A^c)^a(\gamma_B^c)^b} \cdot \frac{c_C^c c_D^d}{c_A^a c_B^b} \tag{1.13}$$

therefore the Gibbs free energy can be expressed as

$$\Delta G = \Delta G^{\ominus} + RTln\left[\frac{c_C^c c_D^d}{c_A^a c_B^b} \cdot \frac{\gamma_C^c \gamma_D^d}{\gamma_A^a \gamma_B^b}\right] [J/mol] \tag{1.14}$$

The last step is obtained from the conservation of energy, that states the variation of energy is equal to the transfer of n moles of electrons to the difference of potential E, with F the Faraday constant

$$\Delta G = -nFE \quad [J/mol] \tag{1.15}$$

so

$$E = E^{\ominus} - \frac{RT}{nF} ln\left[\frac{c_C^c c_D^d}{c_A^a c_B^b} \cdot \frac{\gamma_C^c \gamma_D^d}{\gamma_A^a \gamma_B^b}\right] \quad [V] \tag{1.16}$$

that is equal to

$$E = E^{\ominus'} - RTln\left[\frac{c_C^c c_D^d}{c_A^a c_B^b}\right] \quad [V] \tag{1.17}$$

$E^{\ominus\prime}$ is a formal redox potential that is introduced because it is directly measurable. Since it is defined as

$$E^{\ominus\prime} = E^{\ominus} + \frac{RT}{nF} ln \left[\frac{\gamma_C^c \gamma_D^d}{\gamma_A^a \gamma_B^b} \right] \quad [V] \tag{1.18}$$

it allows to write eq. 1.17, that does not take into account the activities and the activity coefficients which are not directly measurable.

For dilute solutions activity coefficients tend to the unity so activities can be replaced by the concentrations, giving the standard electrode potential but for VRFB this is not valid because the electrolytes are concentrated, not diluted, solutions.

By starting from the equation 1.8 instead of 1.6 it is possible to get a Nernst equation that can be expressed as:

$$E = E^{\ominus} + \frac{RT}{F} ln \left\{ \left(\frac{c_{VO_2^+} \cdot c_{H^+}^2}{c_{VO^{2+}}} \right)_c \left(\frac{c_{V^{2+}}}{c_{V^{3+}}} \right)_a \right\} \quad [V] \tag{1.19}$$

This equation gives a good approximation of the potential of the cell until the concentration of one of the species of vanadium becomes very high with respect to the other. Normally the operating range of a battery does not exceed high state of charges, so the approximation is acceptable.

The Nernst equation is therefore a useful relation between the standard potential and the deviation from the standard conditions, allowing to determine the equilibrium voltage for any condition.

The standard cell potential is $E^{\ominus} = 1.255V$ and it is obtained by summing the standard reduction potentials of the half-cell reactions [8], i.e. for the anode

$$E_{anode}^{\ominus} = -0.255V, \quad V^{3+} + e^- \rightleftarrows V^{2+} \tag{1.20}$$

and for the cathode

$$E_{cathode}^{\ominus} = 1.000[V], \quad VO_2^+ + 2H^+ + e^- \rightleftarrows VO^{2+} + H_2O \tag{1.21}$$

To account also for the temperature dependence it is possible to modify eq. 1.19 as

$$E = E^{\ominus} \left(1 + \frac{\partial E^{\ominus}}{\partial T} \Delta T \right) \quad [V] \tag{1.22}$$

where

$$\frac{\partial E^{\ominus}}{\partial T} = -\frac{1}{nF} \left(\frac{\partial \Delta G^{\ominus}}{\partial T} \right) \simeq -1.26[mV/K] \tag{1.23}$$

State of Charge

To evaluate the available energy with respect to the maximum stored energy it is possible to use the State of Charge, usually written as SoC.It is expressed as a ratio between the different vanadium species:

$$SoC = \frac{c_{V^{2+}}}{c_{V^{2+}} + c_{V^{3+}}} = \frac{c_{VO_2^+}}{c_{VO^{2+}} + c_{VO_2^+}} \tag{1.24}$$

This parameter is equal to 0 when the battery is completely discharged and it is equal to 1 when the battery is completely charged.

Since the total concentration of vanadium $c_{V_{tot}}$ is equal to the sum of the concentrations of the vanadium species of each electrolyte

$$c_{V_{tot}} = c_{V^{2+}} + c_{V^{3+}}, \quad c_{V_{tot}} = c_{VO^{2+}} + c_{VO_2^+} \quad [mol/L] \tag{1.25}$$

the SoC can be written also as:

$$SoC = \frac{c_{V^{2+}}}{c_{V_{tot}}} = \frac{c_{VO_2^+}}{c_{V_{tot}}} \tag{1.26}$$

The SoC can be expressed as a function of the concentrations because, with the concentration $c_i = \frac{M_i}{Vol}[mol/L]$, the total amount of electroactive species is

$$M_{tot} = M_{V^{2+}} + M_{V^{3+}} = C_{V^{2+}}Vol + C_{V^{3+}}Vol = (C_{V^{2+}} + C_{V^{3+}})Vol \quad [mol] \tag{1.27}$$

so

$$C_{V_{tot}} = \frac{M_{tot}}{Vol} = C_{V^{2+}} + C_{V^{3+}}[mol/L] \tag{1.28}$$

and the same for $C_{V^{4+}}$ and $C_{V^{5+}}$.

Overpotentials

The potential difference between the equilibrium potential, evaluated with the Nernst equation, and the potential at which the redox reaction is experimentally observed is called *overpotential* and occurs when a current flows into the electrode. In this case there is the need to force the redox reaction to proceed and this energy is given by this overpotential. Since there are diffenent types of overpotentials and they are electrode phenomena, i.e. they are phenomena related only to the electrodes, they may affect either or both the electrodes.

- **Activation overpotential, $\eta_{\mathbf{act}}$**

  One of them is the activation overpotential, that represents the energy needed to start a charge transfer. Therefore when an overpotential is applied the equilibrium conditions are modified and a current starts flowing. The magnitude of the current is limited by the mass transfer of the reactants or by the rate of electron transfer between the electrodes and the reactant. Furthermore the magnitude of the overpotential depends on the rate of the reaction that is taking place, i.e. a fast reaction requires a lower overpotential than a slow reaction. This overpotential can be seen as the energy required to overcome the activation barrier of a redox reaction. If the concentration of reduced and oxidized species are equal, the activation barrier is symmetrical, while if they are not equal, this barrier is not symmetrical. In this last case, the activation energy required for the cathode and the anode reaction are not equal.

- **Concentration overpotential, $\eta_{\mathbf{conc}}$**

  Another overpotential, called concentration overpotential is related to the difference in concentration between the bulk solution and the solution near the surface of the electrode. The electroactive species have different concentration between the bulk solution and the surface of the electrodes. This causes a concentration overpotential, η_{conc}. If the rate of the reaction is high, the reactant species do not came in contact with the surface of the electrode fast enough. But to mantain a steady current the surface of the electrode must came in contact with new electrolyte reactant from the bulk of the solution, since the reaction occurs only in a thin layer next to the electrode, otherwise a concentration overpotential occurs. The movement of species into the electrolyte can be operated by convection, migration or diffusion; each one has different characteristics and velocities. Diffusion is regulated by the Fick's first law:

  $$J_{diff,i} = -D_i \left(\frac{\partial c_i}{\partial x} \right) \quad [mol/m^2 s] \tag{1.29}$$

  that can be written, for two or more dimensions as:

  $$J_{diff,i} = -D_i \nabla c_i \quad [mol/m^2 s] \tag{1.30}$$

  where D_i is the diffusion coefficient of the species i and is function of the electrochemical mobility, the viscosity and the radius of the particle.
  The migration term refers to the movement of the ions through a solution, that is an electric current. Their movement is caused by an electric field: the rate of the migration depends on the intensity of the field i.e. as the electrode potential increases. The equation of the drift velocity reached for a charged particle is given by:

  $$V_d = uE \quad [m/s] \tag{1.31}$$

  where $u[m^2/Vs]$ is the electric mobility and $E[V/m]$ is the electric field.

  The third term is the convective term, that refers to other ways to generate motion into the solution, e.g. density differences, temperature gradients or mechanical stirring. In this way it is also possible to decrease the contribute of the concentration overpotential.

  The expressions of the concentration potential are mainly relations with empirical parameters.

- **Ohmic and Ionic overpotentials, $\eta_{\mathbf{ohm}}$ and $\eta_{\mathbf{ion}}$**

  Other overpotentials, which are analytically determinable, are the Ohmic and the Ionic overpotentials, that are another way to consider the losses caused by the electrical resistance of the carbon felt electrodes, the bipolar

plates and the carbon collector plates. Therefore the ohmic overpotential η_{ohm} can be seen as:

$$\eta_{ohm} = R_{ohm} I \quad [V] \tag{1.32}$$

where R_{ohm} is the sum of the resistances previously described.

Furthermore the current flow is hindered by the resistance of the electrolyte itself and by the resistance of the membrane. To consider this effect, analogously to the ohmic overpotential, is possible to refer to a ionic overpotential η_{ion}. The conductivity of the electrolyte is a function of the number, the charge and the mobility of the ions dissolved in it. This parameter can be written therefore as:

$$\sigma_e = F \sum |z_i| c_i u_i \quad [S/m] \tag{1.33}$$

where z_i is the charge of the ion i and u_i is the mobility and depends on the size of the ion and its interactions with the other components of the electrolyte. In this way it is possible to write the ionic overpotential as:

$$\eta_{ionic} = R_{ionic} I = \left(\frac{1}{\sigma_e} \frac{L}{S} + R_m \right) I \quad [V] \tag{1.34}$$

where $L[m]$ is the length and $A[m^2]$ is the cross section. $R_m[Ohm]$ is the resistance of the membrane.

Given the operating conditions of the cell or the stack, it is possible to determine the operating voltage of the stack as:

$$U_{tot} = N(E - \sum \eta_i) \quad [V] \tag{1.35}$$

where N is the number of cells that compose the stack and η_i are the various overpotentials mentioned above.

An useful table, found in [1] allows to see the variables dependency on the operating conditions. • means direct dependency, ∘ denotes indirect dependency and \ means no dependency.

Variable	I	$C_{V^{2+}}$	$C_{V^{3+}}$	$C_{V^{4+}}$	$C_{V^{5+}}$	C_{H^+}	T	Q
SoC	\	•	•	•	•	\	\	\
E	\	•	•	•	•	•	•	∘
η_{act}	•	•	•	•	•	\	•	∘
η_{conc}	∘	•	•	•	•	\	•	∘
η_{ohm}	•	\	\	\	\	\	∘	\
η_{ionic}	•	∘	∘	∘	∘	∘	∘	\
U_{tot}	∘	∘	∘	∘	∘	∘	∘	∘

Table 1.1: Variables dependency on the operating conditions [1]

Current: the Butler-Volmer Equation

From thermodynamic considerations and by taking into account the activation overpotential η_{act} it is possible to write the *Butler-Volmer* equation, that make possible an evaluation of the current into the cell (a detailed explanation can be found in [1]):

$$I = I_0 \left[e^{\alpha n F \eta_{act}/RT} - e^{-(1-\alpha) n F \eta_{act}/RT} \right] \quad [A] \tag{1.36}$$

where $I_0[A]$ is the exchange current, i.e the value of the anodic current or the cathodic current, in absolute value and α is the charge transfer coefficient i.e. the fraction of the interfacial potential at an electrode-electrolyte interface that helps in lowering the free energy barrier for the electrochemical reaction. It is possible to refer this coefficient for each side of the battery, by considering the following relation, where a and c refers to anode and cathode respectively [13]:

$$\alpha_{pos} = 1 - \alpha_{neg} \tag{1.37}$$

By doing this, the Butler-Volmer equation can be written as:

$$I = I_0 \left[e^{\alpha_{pos} n F \eta_{act}/RT} - e^{-(\alpha_{neg}) n F \eta_{act}/RT} \right] \quad [A] \tag{1.38}$$

1.6 Multiphysics models

In 2008 were published the first multiphysics models. One by Blanc and Rufer [8] and combined an electrochemical model with a mechanical model that describes the hydraulic circuit of the electrolyte. The second model, the hydraulic one, determines the power required to the pump. The last part shows a way to increase the efficiency of the stack by the mean of a variable flow rate.

A 2D model has been published by Shah et al. [14] makes possible to analyze the overpotentials and the current densities of a VRFB cell. This is done with a $2D$ model, solved with COMSOL® but it consider a fluid flow only in the y direction, with the fluid entering directly into the porous electrode.

Another model of the beginning of 2009 has been performed by D. You et al. [15]. They developed a two-dimensional stationary model based on the approach of Shah [14]. They showed that the overpotential rises sharply when the battery is charged near $100\% SoC$. Therefore a VRFB battery usually operates with a maximum SoC of 95%. This model neglects completely electroneutrality and ionic migration but it is good to compare the effect of different parameters with the same conditions.

A different approach has been shown by Vynnyky [16] with a more detailed model. He states that with a plug-flow type velocity profile the model, using an appropriate coordinate transformation, the equations of the model are mathematically equivalent to one-dimensional diffusion equation. The obtained model is therefore an *asymptotically* reduced model, that led to lower computational time preserving geometrical resolution. It shows inconsistencies with the model of Shah et al. [14] due to the computation of the water profile in the carbon felt, that Vynnyky states as not necessary.

An enhancement to all the VRFB models has been performed by Knehr and Kumbur [17]. They proposed a more complete description of the Nernst equation. By incorporating the proton concentration at the positive electrode and adding the Donnan potential the accuracy of the equation has been improved. When compared with experimental data, the complete form of the Nernst equation showed a much better agreement.

A more complete and detailed model has been proposed by Knehr et al. in 2012 [18]. They presented a $2D$ transient, isothermal model that can predict species crossover and related capacity loss during operation. The model incorporates the species transport across the membrane due convection, diffusion and migration and also accounts for the transfer of water between half-cells to evaluate the variation of the volume of the electrolyte fluid. This model evaluates also the species concentrations at the membrane/electrolyte interfaces and the effects of side reactions due to vanadium crossover, as a capacity loss and efficiency and power output losses.

In 2014 Chen et al. [19] proposed an enhancement to the model of Vynnyky [16] by including the Donnan potential and the complete Nernst equation [17]. In this model they used the same assumption and simplification of the starting model, i.e. they suppose also a plug-flow type velocity profile. The enhancement operated gives an increase of the accuracy with a negligible increase of the computational cost.

1.7 3D models

All the previous models are based on simple fluid flow fields. The work of Xu et al. [20] is based on the investigation of the flow field design to minimize the mass transport polarization at a minimum pressure drop. For this reason they analyzed the performance of a VRFB with three different flow fields:

- one with no flow field
- one with a serpentine channel
- one with parallel flow fields

They state that the serpentine flow field appears to be the most suitable because it can improve the uniformity of the electrolytes through the electrode, it reduces the overpotential due to a more even electrolyte distribution over the electrode surface and enhances convective mass transport towards the membrane and furthermore the serpentine has the highest efficiency at the optimal flow rate i.e. the flow rate that gives the maximum power-based efficiency 1.4.

A $3D$ model that gives a rigorous explanation of pore-level transport resistance and pumping power, with the analysis of time constants of heat and mass transfer has been proposed by Yun and Sung [21]. Their dynamic model is solved by the finite volume method and shows the distribution of the temperature into the electrode and the time required to the temperature to stabilize.

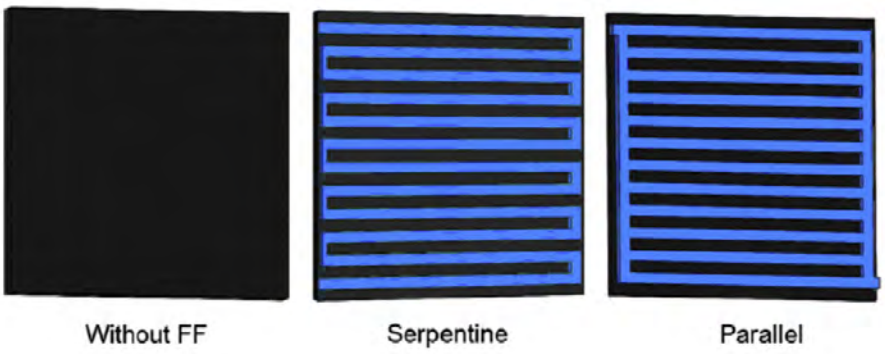

Figure 1.4: Different flow fields [20]

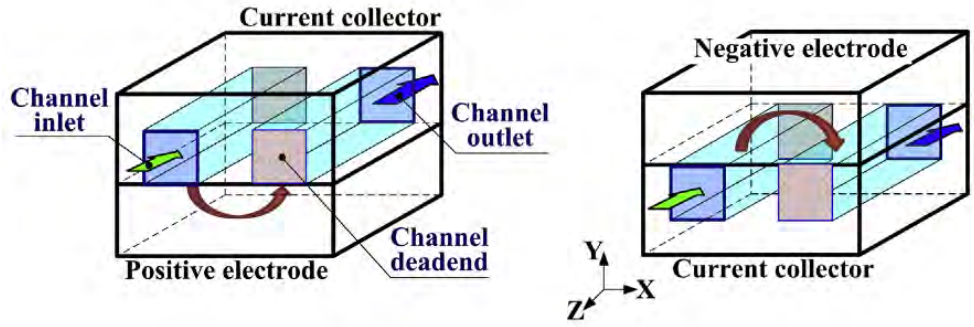

Figure 1.5: Example of interdigitated channels [22]

One of the most recent models, published during the development of this thesis, is that one presented by Cong et al. [22]. They proposed a $3D$ model with interdigitated flow channel design e.g. Fig. 1.5. The choice of an interdigitated flow channels is due to a lower pressure drop than the serpentine design and due to a more efficient mass transfer than the parallel design (the flow field designs presented by Xu, [20]). In their work, they analyzed a small cell of $10 \times 7mm^2$ with single inlet and two other multi-inlet cells of $10 \times 35mm^2$ and $10 \times 70mm^2$. They showed that the the pressure of electrolyte drops significantly in the side inlet of porous electrode at *low flow rates*, resulting in uneven distribution of electrolyte flow field and cell potential, while at higher electrolyte flow rates the potential distribution becomes uniform.

1.8 Thermal and large scale models

In 2012 Tang et al. published a couple of works on the thermal modeling of the VRFB [23, 24]. The first model [23] is used to predict the battery temperature as a function of time under different operating conditions and structure designs. The results that they have obtained have shown that the electrolyte temperature in both the tanks and the stack is influenced by multiple effects of flow rate,

surrounding temperature and heat generated by cell resistance losses. In the second model [24] the effect of the self-discharge reactions was incorporated into the thermal model previously analyzed. The model is therefore suited to investigate the thermal effect of the self-discharge reactions on both continuous charge and discharge cycling and during standby periods. They showed also that the stack resistance has a dominant impact on total heat generation and the electrolyte flow also plays an important role in heat transfer and dissipation.

Furthermore, a model for large scale applications of VRFB systems has been proposed by Turker et al. [25] in 2013. They developed a simulation model based on measurements with a kW-scale real life VRFB unit and obtained values for the round-trip efficiencies in good agreement with values reported in literature. They also state that pumping losses are crucial at very low power levels.

Another investigation has been performed by Bromberger et al. [26] in 2014. They introduced in a $2D$ model of a VRFB the effects of electrode compression on voltage losses and hydraulics. As a results of the parametric studies they state that the compression of the electrode lowers the area specific resistance (ASR), the porosity and the hydraulic permeability, increasing therefore the pressure drop. They state also that the ASR is highly sensitive to changes in the specific surface area $a \quad m^2/m^3$ and in the reaction constant k.

In the same year Tang et al. [27] operated a study on the optimization of the flow rate of VRFB. By modeling the concentration overpotential and analyzing the pressure losses in all the components they found a value for the flow factor of 7.5 for their VRFB system as an optimal choice, since it maximizes the efficiency. The flow factor is the ratio between the actual flow rate and the stoichiometric flow rate, which is evaluated from the Faraday's law. With this model it is possible to find a trade-off between concentration overpotential and pump losses, which are both closely related to the flow rate.

Chapter 2

COMSOL Multiphysics® Model

In order to analyze how a vanadium redox flow battery works it is useful to develop a model to be solved with a finite element multiphysics software.

Therefore the first part of the work is the analysis of an already developed model, found in the COMSOL® model library [28]. In this way it is possible to describe a system by a set of variables and a set of equations that establish relationships between the different variables [29]. These equations represent the key characteristics or behaviors of the selected system.

A computer simulation is an attempt to model a real or hypothetical situation on a computer so it can be studied to see how the system works. By changing variables in the simulation, predictions may be made about the behavior of the system. Computer simulation has become a useful part in engineering to gain an insight into the operation of a process or a system.

Traditionally, the formal modeling of a system has been via a mathematical model, which attempts to find analytical solutions enabling the prediction of the behavior of a system from a set of parameters and initial conditions. Computer simulation is often used for modeling systems for which simple closed form analytic solutions are not possible. [30]

2.1 Finite Element Method

The finite element method (FEM) is a numerical technique used for finding approximate solutions to the boundary value problems for partial differential equations (i.e. a differential equations together with a set of additional restraints, called the boundary conditions). FEM encompasses all the methods for connecting many simple element equations over many subdomains, named finite elements, to approximate a more complex equation over a larger domain.[31]

For elliptic partial differential equations, frequently no classical solution exists, and often there is the need to work with a so-called weak solution. This has consequences for both the theory and the numerical treatment. While it is true that classical solutions do exist under appropriate regularity hypotheses, for numerical calculations the analysis cannot be set up in a framework in which the existence of classical solution is guaranteed. One way to get a suitable framework for solving

elliptic boundary-value problems using finite elements is to pose them as variational problems: variational methods are used to minimize an error function and produce a stable solution (i.e. minimizing or maximizing functionals)[32].

In the case of ordinary differential equations initial or boundary conditions can be specified, while in the case of partial differential equations of the second order, the type of equation determines whether initial, boundary or initial-boundary conditions should be imposed.

The main feature of the FEM is the discretization of the domain through the creation of a grid (mesh), composed by small and simple elements, the so-called *finite elements*. Elements in $1D$ are segments, in $2D$ can be triangles or quadrilaterals and in $3D$ can be hexahedra, tetrahedra, square based pyramids and prisms. There is freedom in the choice of the elements so it is quite easy to fill with good approximation domains of any shape.

In classical FEM formulation the mesh must be conform to interfaces, that means that no element can fill portions of different regions with different material parameters. The domain must be completely covered and there cannot be intersections between elements. Two elements can have in common: nothing, a node, an entire edge ($2D$ and $3D$) or an entire face ($3D$). If the domain is not completely covered, the mesh is a non-conform mesh and the problem can be solved only with special methods.

The elements are connected by points called nodes (which are the vertices of the elements or internal points). Each node i has an interpolating function $N_i(x)$, that usually is a piecewise polynomial function, always continuous in the domain Ω. On each element the solution of the problem is expressed as the linear combination of *shape functions*. The coefficients of the shape functions (degrees of freedom) are the unknowns of the algebraic problem. Shape functions usually are linear functions, but they can also be of the second degree or more. For each element there are as many interpolants as the number of the vertexes of the element if the interpolants are of the first degree, while in general is equal to the number of nodes on the element.

There are two main approaches to solve a FEM problem, one is called *variational* and the other is called *weighted residual*. In the first case there is the need of a *functional* to be minimized, while it is not needed with the second approach, since there is the need of only the differential equation that describes the problem. Usually it is hard to write the functional to be minimized, but it is easier to solve.

The evaluated function minimizes the error on the whole solution. One of the advantages of the FEM is that the interpolation is included in the method itself and it is not done arbitrarily *a posteriori*.

The mesh usually can be made by the use of two techniques, *Advancing Front* and Delaunay triangulation. The first technique starts from the boundary and, by knowing the spacing function, finds next points. For each iteration a new front is created and must be avoided any overlapping of triangles. The advantage is that gives a good accuracy on the boundary, but has the disadvantage of being slow. Instead Delaunay triangulation is used to maximize the minimum angle of every triangle, avoiding sharp triangles.

Since the number of the test functions is equal to the number of the shape function

coefficients, the number of the constraint is equal to the number of the unknowns and the process gives a linear system of equations that has an unique solution if the boundary conditions are well-defined and well-posed.

These kind of problems can be expressed as a matrices problem $Ax = I$ where A is the matrix of the parameters and I is the vector of the known terms. Matrices and vectors of the matrices problem are obtained by assembling the contribution of each finite element: the goal is to determine the matrix relative to the global coordinate system, the stiffness matrix.

The solution of the matrices problem is obtained by iterative techniques such as *Gauss-Siedel method* or by direct solver as *Cholesky decomposition*.

The boundary conditions define the interfaces between the subdomains of the model. Together with initial conditions, boundary conditions are required to correctly define and solve the model. They are usually divided in three groups: Dirichlet condition, that sets the value of a function on the boundary; Neumann condition, that sets the derivative of a function and Robin condition, that imposes a combination of the value of a function and its derivative (mixed condition).

2.2 Finite element analysis software

The computational complexity to perform a simulation with FEM requires the use of a computer with appropriate software to solve systems of partial differential equations. Examples of software are ANSYS®, COMSOL® and SIMULIA®.

The complexity of some processes required to develop specialized software, that makes easier the implementation of some models, by *ad hoc* implementation, compilation and graphical interfaces.

The main component of the software is the solver, that uses a predefined formulation and integration method. The solver can compile an input file in the format required by the software. Together to the solver, there are also components of the software that facilitate the user in building the input file without the need of a text editor, called *pre-processor*. The components that allow the visualization and the organization of the output, to make it easily understandable whether the result is acceptable or not, are called *post-processor*.

2.2.1 COMSOL Multiphysics®

Comsol Multiphysics® is a powerful interactive environment for modeling and solving coupled problems based on FEM. The software provides a powerful integrated desktop environment with a *Model Builder*, where it is possible to get full overview of the model and access to all functionality [33].

Modules

In the present work are used the Fluid Flow branch and the Electrochemistry branch of the *Batteries and Fuel Cells Module*, in particular:

- the *Free and Porous Media Flow* interface

- the *Tertiary Current Distribution, Nernst-Plank* Interface
- the *Secondary Current Distribution* Interface

Geometry

The software has an internal CAD graphic interface, to create 1D, 2D or 3D geometries with Boolean operators, extrusions and rotations.
It can also import geometries created with external software like *AutoCAD®* or *CATIA®*.

Parameters and Equations

The software has a tool to specify or modify parameters and properties of materials with constant values, interpolating or analytic functions and much more. The values can be applied to the whole domain, to subdomains, surfaces, edges, points or contours of the geometry.

Boundary Conditions

Comsol allows both Neumann and Dirichlet conditions on internal or external contours. It is possible to define also other boundary conditions. All the conditions can be set by constant values or functions.

Mesh

The software can create free meshes that can be used in any geometry. These meshes do not have any restrictions on the distribution of the elements. It is also possible to create mapped mesh with fixed sizes and distributions. The boundaries of the domain and the subdomains are also faces or edges of the elements of the mesh.

Solver

COMSOL Multiphysics® includes different linear solvers, e.g. GMRES, PARDISO and Conjugate gradient. Iterative solver are not always converging. To improve convergence, it is possible to set preconditioning and other parameters, to obtain an optimal solver for the model.

Convergence

The convergence of the approximated solution with the exact solution depends on various parameters. If the model is well defined, the approximated solution is very near to the exact solution.

The precision of the results depends on the grade of the polynomial function and on the shape and the size of the finite elements. With the same polynomial function, the error decreases by reducing the size of the elements.

The main causes of errors are:

- errors in the code
- pre-processing or post-processing errors
- numerical approximations
- errors in the physical model
- use of elements not suitable with the real problem

Due to this errors the result must be verified e.g. with the entity of the values or with known solutions. Another check is to use a finer mesh and then make a comparison between the two results.

Validation

To be sure that the model is suited to the prediction of data, it must be validated, by comparing the results of the model with experimental results.

For every kind of model, the difference from the result of the model and the experimental result is acceptable when the deviation is compatible with both the characteristics of the input data and the variations of the phenomenon.

If the deviation is high, there must be done a check of all the input data and the parameters. When the difference is small enough, the model can be used as a reliable forecasting tool.

2.3 Starting point: COMSOL® VRFB model

The starting point of the present work is a simplified version of the model proposed by Knehr and Agar [18]. By neglecting the dependency of the model on the third spatial dimension, it is possible to develop a $2D$ model, that is easier to compute than a 3D model.

In this work the complete development of a new model has been avoided since a simple and useful model is found on the model library of COMSOL® [28].

The first thing that can be noted in this model is that the electrode is fed from the bottom with the electrolyte containing a solution of sulfuric acid and a vanadium redox couple. This fluid is supposed to enter in the electrode with constant velocity, along the *y axis*. The negative electrode, on the left, is grounded and the current leaves the cell from the side on the right with a fixed current density. The spatial regions used are three, made by rectangles of the same height but with different thickness. The external regions are the electrodes, while the central region is the membrane (as can be seen in fig. 2.1). For each rectangle must be set:

- a model of its behavior, with constitutive relations
- interface conditions
- boundary conditions

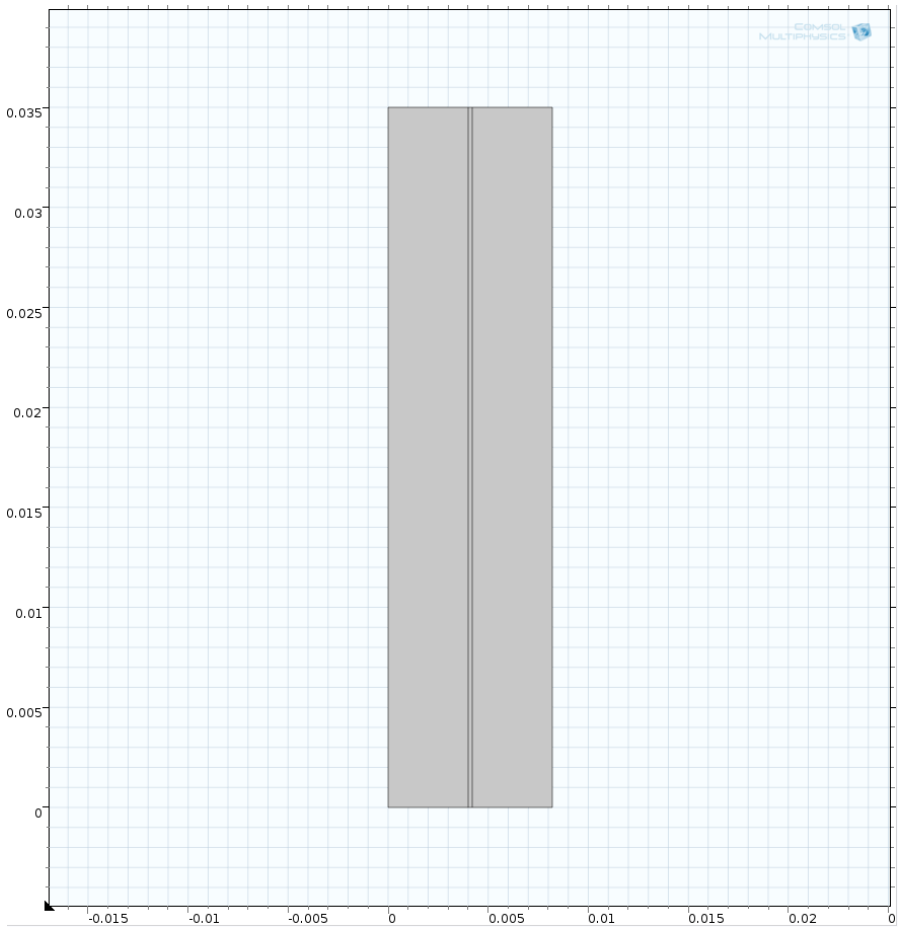

Figure 2.1: Geometry of the VRFB COMSOL model

In this case the model is solved for a stationary case, with a given set of inlet conditions, as the concentration of the species entering the cell and the velocity of the flow.

This is possible because the time required to measure a significant variation of the concentration of the species into the electrolyte is higher than the electrical and chemical time constants. Therefore the system can be studied as a sequency of stationary systems.

2.3.1 Positive and negative electrolyte solutions

Negative Electrolyte

The species contained in the negative electrolyte are:

- H^+
- HSO_4^-
- SO_4^{2-}
- V^{3+}

- V^{2+}

The equation used to calculate the equilibrium potential is the Nernst equation (eq. 1.16)

$$E_{eq,neg} = E_{0,neg} + \frac{RT}{F} ln\left(\frac{a_{V^{3+}}}{a_{V^{2+}}}\right) \quad [V] \tag{2.1}$$

where $E_{0,neg}[V]$ is the reference potential for the anode reaction and a_i is the chemical activity of the species i.

The current follows a Butler-Volmer equation 1.38

$$I = Ai_{0,neg}\left[e^{(1-\alpha_{neg}nF\eta_{act}/RT} - e^{-\alpha_{neg}nF\eta_{act}/RT}\right] \quad [A/m^3] \tag{2.2}$$

where $A[m^2/m^3]$ is the specific surface area of the porous electrode and α_{neg} is the transfer coefficient.

The reference current density is given by the following relation:

$$i_{0,neg} = Fk_{neg}(a_{V^{2+}})^{1-\alpha_{neg}}(a_{V^{3+}})^{\alpha_{neg}} \quad [A/m^2] \tag{2.3}$$

where k_{neg} is the rate constant.

The overpotential of the negative electrode is defined as:

$$\eta_{neg} = \phi_s - \phi_l - E_{eq,neg} \quad [V] \tag{2.4}$$

where $\phi_s[V]$ is the electric potential of the solid phase and $\phi_l[V]$ is the electrolyte potential. For this model it takes into account only the ohmic and the ion overpotentials.

Positive Electrolyte

The species contained in the positive electrolyte are:

- H^+
- HSO_4^-
- SO_4^{2-}
- VO^{2+}
- VO_2^+

In this case the Nernst equation, according to 1.8 becomes:

$$E_{eq,pos} = E_{0,pos} + \frac{RT}{F} ln\left(\frac{a_{VO_2^+}\left(a_{H^+}\right)^2}{a_{VO^{2+}}}\right) \quad [V] \tag{2.5}$$

The Butler-Volmer equation are modified as follows:

$$I = Ai_{0,pos}\left[e^{(1-\alpha_{pos}nF\eta_{act}/RT} - e^{-\alpha_{pos}nF\eta_{act}/RT}\right] \quad [A] \tag{2.6}$$

where the reference current density is:

$$i_{0,pos} = Fk_{pos}(a_{VO^{2+}})^{1-\alpha_{pos}}(a_{VO_2^+})^{\alpha_{pos}} \quad [A/m^2] \tag{2.7}$$

2.3.2 Sulphuric acid

As reported in the previously cited [18], the first dissociation of the sulphuric acid is assumed to be complete:

$$H_2SO_4 \rightarrow H^+ + HSO_4^- \tag{2.8}$$

while the second step

$$HSO_4^- \rightarrow H^+ + SO_4^{2-} \tag{2.9}$$

is considered incomplete and its state of dissociation is described by:

$$r_d = k_d \left(\frac{a_{H^+} - a_{HSO_4^-}}{a_{H^+} + a_{HSO_4^-}} - \beta \right) \tag{2.10}$$

where r_d is a rate parameter, k_d is a dissociation constant and β is the level of dissociation. This is an important parameter since the dissociation of the sulphuric acid varies the concentration of the available H^+.

2.3.3 Current distribution

The molar flux of species is described by means of the Nernst-Planck equation, that takes into account diffusion, migration and convection:

$$\mathbf{N}_i = -D_i \nabla c_i - z_i u_{mob,i} F c_i \nabla \phi_l + c_i \mathbf{n} \quad [mol/m^3 s] \tag{2.11}$$

The first term $-D_i \nabla c_i$ is the diffusion flux, the second, $-z_i u_{mob,i} F c_i \nabla \phi_l$, is the migration term, where $u_{mob,i}$ is the mobility of the species i, and the third term, $c_i \mathbf{n}$ is the convection term, where $\mathbf{n} \quad m/s$ is the fluid velocity vector.

The convective term summed up for all the species gives a null contribution due to the electroneutrality. For this reason the electrolyte current density, evaluated by means of the Faraday's law, sums up the contributions of all the diffusion and migration terms. Each of these terms is multiplied by its charge and then multiplied by the Faraday's constant:

$$\mathbf{i}_l = F \sum_n z_i (-D_i \nabla c_i - z_i u_{mob,i} F c_i \nabla \phi_l) \quad [A/m^2] \tag{2.12}$$

2.3.4 Interface conditions

To match field problems in subdomains, there is the need to set up the interface conditions between the membrane and the free electrolytes.

The first condition is the equality of the current density across the membrane:

$$\mathbf{n} \cdot \mathbf{i}_{l,e} = \mathbf{n} \cdot \mathbf{i}_{l,m} \tag{2.13}$$

where $i_{l,e}[A/m^2]$ is the current density in the electrolyte and $i_{l,m}[A/m^2]$ is the current density in the membrane.

Since the only species crossing the membrane are protons H^+ (neglecting the crossover of other species) the current in the membrane, according to the Faraday's law is proportional to the flux of H^+, while for the other species the contribute is zero:

$$\mathbf{n} \cdot \mathbf{N}_{H^+,e} = \mathbf{n} \cdot \frac{\mathbf{i}_{l,m}}{F} \quad [mol/m^2 s] \tag{2.14}$$

Usually, the Nernst equation is in the form adopted in the fuel cell literature. That is, for the positive electrode:

$$E_{pos} = E_{0,pos} + \frac{RT}{F} ln \left(\frac{c_{VO_2^+}}{c_{VO^{2+}}} \right) \quad [V] \tag{2.15}$$

For the VRFB this is an incomplete representation, because the potential across the membrane is not negligible, i.e. the activity of the hydrogen must be incorporated. This gives a more complete description of the equilibrium potential:

$$E_{pos} = E_{0,pos} + \frac{RT}{F} ln \left(\frac{c_{VO_2^+} c_{H^+}^2}{c_{VO^{2+}}} \right) \quad [V] \tag{2.16}$$

Another important factor, ignored in the standard form of the Nernst equation, is the Donnan potential, as reported in [17] that has the following form:

$$E_{m,\pm} = \frac{RT}{F} ln \left(\frac{c_{H^+,\pm}}{c_{h^+,m}} \right) \quad [V] \tag{2.17}$$

where $\pm$ is the positive or the negative electrolyte and m represents the membrane. By introducing it, the relation between the potentials and the concentration (or activity, supposed equivalent) becomes:

$$\phi_{l,m} = \phi_{l,e} + \frac{RT}{F} ln \left(\frac{a_{H^+,m}}{a_{H^+,e}} \right) \quad [V] \tag{2.18}$$

2.4 Analysis of the model in COMSOL®

The VRFB model implemented in the COMSOL® library relies on the following physics of the Batteries and Fuel Cells Module:

- Tertiary current distribution, Nernst-Planck
- Secondary current distribution

The first physics include reactions, mass and electric charge transport. It is related to the positive and negative electrodes because the concentrations in the porous electrode domains are of the same order of magnitude and the gradients of the concentrations are not negligible. For the second physics reactions do not occur inside the membrane is instead related to the membrane because the negative ions are fixed inside the polymer membrane so their concentration is constant.

Therefore, the general equations to be solved are respectively

$$\nabla \cdot \mathbf{i_l} = F \sum_n z_i R_i \quad [A/m^3] \tag{2.19}$$

and

$$\mathbf{i_l} = -u_{mob,+} F^2 c_+ \nabla \phi_l = -\sigma_l \nabla \phi_l \quad [A/m^2] \tag{2.20}$$

where the $R_i[mol/m^3 s]$ are the reaction sources due to the porous electrode reactions and σ_l is the electrolyte conductivity.

The Table 2.1 shows the parameters used for the model and where they can be found in the literature. In *Appendix A* can be found a detailed insight on the equations of the model.

2.4.1 Porous electrodes: Tertiary current distribution

The Tertiary current distribution physics is used to model the electrolyte into the porous electrodes. The relations found in the negative electrode Tertiary Current Distribution Physics are in Table 2.2 while the relations of the positive electrode physics are in Table 2.3. In both the tables $E_{eq,\pm} = Nernst(a, b, c)$ are the Nernst equations 2.1 and 2.5 where a, b, c are the input parameters.

The main nodes of this Tertiary current Distribution physics (i.e the interfaces of the software to set the parameters of each physics) are:

- electrolyte,
- insulation,
- no flux,
- initial values

To study VRFBs must be added to the physics other components (nodes), as:

- porous electrode,
- reactions,

  and nodes to set boundary and interface conditions as, for the negative electrode:

- electric ground,
- concentration,
- outflow, while for the second, the positive electrode, are:
- electrode current,
- concentration
- outflow

parameter	value	unity	definition	
H_{cell}	0.035	$[m]$	Cell height	[18]
W_{cell}	0.0285	$[m]$	Cell depth	[18]
L_e	0.004	$[m]$	Electrode thickness	[20]
L_m	203e-6	$[m^2/s]$	Membrane conductivity	[20]
D_{V_2}	2.4e-10	$[m^2/s]$	V^{2+} diffusion conductivity	[34]
D_{V_3}	2.4e-10	$[m^2/s]$	V^{3+} diffusion conductivity	[34]
D_{V_4}	3.9e-10	$[m^2/s]$	VO^{2+} diffusion conductivity	[34]
D_{V_5}	3.9e-10	$[m^2/s]$	VO_2^+ diffusion conductivity	[34]
D_H	9.312e-9	$[m^2/s]$	H^+ diffusion conductivity	[35]
D_{SO4}	1.065e-9	$[m^2/s]$	SO_4^{2-} diffusion coefficient	[18]
D_{HSO_4}	1.33e-9	$[m^2/s]$	HSO_4^- diffusion coefficient	[18]
v	300	$[ml/min/m^2]$	Inlet velocity	
T	293.15	$[K]$	Cell temperature	
σ_e	66.7	$[s/m]$	Electrode conductivity	[18],[36]
ε	0.93		Electrode porosity	[18],[36]
a	3.5e4	$[m^2/m^3]$	Electrode specific area	[18]
$E_{0,pos}$	1.004	$[V]$	Standard potential,positive	[37]
k_{pos}	2.5e-8	$[m/s]$	Rate constant,positive	[18]
α_p	0.55		Transfer coefficient,positive	[18]
$E_{0,neg}$	-0.255	$[V]$	Standard potential,negative	[37]
k_{neg}	7e-8	$[m/s]$	Rate constant, negative	[18]
α_n	0.45		Transfer coefficient, negative	[18]
β	0.25		Dissociation constant	[18]
kd	1e4	$[m^3s]$	HSO_4^- dissociation rate	[18]
$a_{H,m}$	1.99		Membrane proton activity	[18]
σ_m	10	$[s/m]$	Membrane conductivity	[18]
$c_{V_2,0}$	156	$[mol/m^3]$	V^{2+} initial concentration	[18]
$c_{V_3,0}$	884	$[mol/m^3]$	V^{3+} initial concentration	[18]
$c_{V_4,0}$	884	$[mol/m^3]$	VO^{2+} initial concentration	[18]
$c_{V_5,0}$	156	$[mol/m^3]$	VO_2^+ initial concentration	[18]
$c_{H,0,neg}$	4447.5	$[mol/m^3]$	H^+ initial concentration,ne	[18]
$c_{H,0,pos}$	5097.5	$[mol/m^3]$	H^+ initial concentration,pe	[18]
$c_{HSO_4,neg}$	2668.5	$[mol/m^3]$	HSO_4^- initial concentration,ne	[18]
$c_{HSO_4,pos}$	3058.5	$[mol/m^3]$	HSO_4^- initial concentration,pe	[18]
i_{avg}	-100	$[mA/cm^2]$	Average current conductivity	

Table 2.1: Table of the parameters and their references in the literature

equations of electrode, tertiary current distribution

After having set the nodes of the physics, must be analyzed the equations of each component to adjust it correctly.

- **Electrolyte**: For both cases the equations of the **electrolyte** are overwritten by the porous electrode equations, since there are no domains that contain only electrolyte and not the porous electrode.

	Negative Electrode	
a_{V^3}	$max(cV3, eps)$	V^{3+} activity
a_{V^2}	$max(cV2, eps)$	V^{2+} activity
a_H	$max(c_{H,neg}, eps)$	H^+ activity
a_{HSO_4}	$max(c_{HSO_4^-,neg}, eps)$	HSO_4^- activity
a_{SO_4}	$max(c_{SO_4,neg}, eps)$	SO_4^{2-} activity
$E_{eq,neg}$	$Nernst(E_{0,neg}, T, a_{V^{3+}}/a_{V^{2+}})$	Equilibrium potential
$i_{0,neg}$	$Fk_{neg}a_{V^{2+}}^{1-\alpha_{neg}}a_{V^{3+}}^{\alpha_{neg}}$	Exchange current density
rd	$kd\left(\frac{a_H - a_{HSO_4}}{a_H + a_{HSO_4}} - \beta\right)$	Dissociation rate
ϕ_l	$\phi_{l,neg}$	Electrolyte potential
ϕ_s	$\phi_{s,neg}$	Electrode potential

Table 2.2: Negative Electrode relations

	Positive Electrode	
a_{V^5}	$max(cV5, eps)$	VO_2^+ activity
a_{V^4}	$max(cV4, eps)$	VO^{2+} activity
a_H	$max(c_{H,pos}, eps)$	H^+ activity
a_{HSO_4}	$max(c_{HSO_4^-,pos}, eps)$	HSO_4^- activity
a_{SO_4}	$max(c_{SO_4,pos}, eps)$	SO_4^{2-} activity
$E_{eq,pos}$	$Nernst(E_{0,pos}, T, a_{V^{5+}}a_H^2/a_{V^{4+}})$	Equilibrium potential
$i_{0,pos}$	$Fk_{pos}a_{V^{4+}}^{1-\alpha_{pos}}a_{V^{5+}}^{\alpha_{pos}}$	Exchange current density
rd	$kd\left(\frac{a_H - a_{HSO_4}}{a_H + a_{HSO_4}} - \beta\right)$	Dissociation rate
ϕ_l	$\phi_{l,neg}$	Electrolyte potential
ϕ_s	$\phi_{s,neg}$	Electrode potential

Table 2.3: Positivee Electrode relations

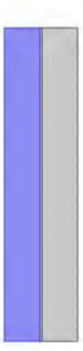

(a) *negative electrode electrolyte.*

(b) *positive electrode electrolyte.*

Figure 2.2: Negative and positive domains

- **Insulation**:
  For the electrical **insulation** the equations are $-\mathbf{n} \cdot i_e = 0$ and $\mathbf{n} \cdot i_s = 0$, and describe the wall or the boundary of a cell that is not in contact with

a conductor, therefore it is overwritten by **electric ground** and **electrode current**. The vector **n** represents the normal vector to the insulated surfaces, i_l represents the current into the electrolyte and i_s represents the current of the electrode. For this system it acts with the contribution of **no flux**, **concentration** and **outflow**.

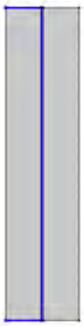

(a) *negative electrode insulation* .

(b) *positive electrode insulation.*

- **No flux**:
  it is a boundary condition that sets zero the flux of chemical species i in the direction orthogonal to the boundary: $-\mathbf{n} \cdot \mathbf{N_i} = 0$ where $\mathbf{N_i}$ is the flux of chemical species. It is applied only into the long sides where acts with **insulation** and **electric ground**, while for the short sides is overridden by **outflow** and **concentration**.

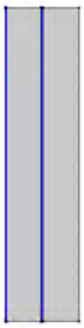

(a) *negative electrode no flux* .

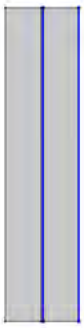

(b) *positive electrode no flux.*

- **Initial values**:
  initial values sets the initial values of the electric and electrolyte potentials and the initial values of the concentrations in the whole region (see fig 2.2). It is recommended to start from good initial values to ensure the convergence of the system, due to the exponential nature of some equation. The values to use are: $cHSO_{4,\pm,0}, cH_{\pm,0}, cV_{2,0}, cV_{3,0}$ and $-E_{0,\pm}$.

- **Porous electrode**:
  porous electrode imposes a balance of charges for the electrode and the

electrolyte in the pores. It imposes also a balance of mass for the species of the electrolyte. It works with the contribution of **initial values** and **reaction** (see fig. 2.2). The mass balance equation is:

$$\begin{cases} \nabla \cdot (-D_{i,eff}\nabla c_i - z_i U_{m,i,eff} F c_i \nabla \phi_l) + \mathbf{n} \cdot \nabla c_i = R_{i,tot} \\ R_{i,tot} = \sum_m R_{i,m} + \varepsilon_l R_{i,src} \end{cases} \tag{2.21}$$

Where $R_{i,tot}$ is the reaction source due to the porous electrode reactions, where the total reaction source is the sum of the contributes of the reaction sources.

The current in the electrolyte is

$$\nabla \cdot \mathbf{i_l} = \varepsilon_l F \sum_i z_i R_{i,src} + Q_l + i_{v,total} \tag{2.22}$$

where $i_{v,tot}$ is the current density of the Butler-Volmer equation 1.38 and Q_l is the electric charge stored in a infinitesimal volume. Due to the stationary model, $Q_l = 0$.
Due to the stationarity of the problem, $Q_l = 0$. From the Butler-Volmer equation Due to the electroneutrality, another equation is:

$$\sum_i z_i c_i = 0 \tag{2.23}$$

The Nernst-Planck equation can be written as in eq. 2.11.
The current can be evaluated from the Faraday's law, by considering the flux of the active species into the electrode:

$$\mathbf{i_l} = F \sum_i z_i (-D_{i,eff}\nabla c_i - z_i U_{m,i,eff} F c_i \nabla \phi_l) \tag{2.24}$$

The diffusion coefficient must be redefined by considering also the porosity of the porous electrode by the so-called Bruggemann correction where ε_l is the porosity of the electrode:

$$D_{i,eff} = \varepsilon_l^{1,5} D_i \tag{2.25}$$

The components of the current are evaluated as follow:

$$\nabla \cdot \mathbf{i_s} = Q_s - i_{v,total}, \quad \mathbf{i_s} = -\sigma_s \nabla \phi_s \tag{2.26}$$

where Q_s is a current source and it is equal to 0.
The conductivity σ_s must be computed by taking into account the Bruggeman correction:

$$\sigma_{s,eff} = \varepsilon^{1,5} \sigma_s \tag{2.27}$$

$$i_{v,total} = \sum_m i_{v,m} \tag{2.28}$$

The input of this component are the vector field **u**, the temperature T, the electrical conductivity of the electrode σ_s, the diffusion coefficients D_{SO_4}, D_{HSO_4},D_H, D_{V_2}, D_{V_3}, the migration in the electric field, with the Nernst-Einstein relation $U_{m,i,eff} = \frac{D_{i,eff}}{RT}$, the charge numbers if SO_4, HSO_4, H, V_2 and V_3, the electrolyte volume fraction (porosity) ε_l and the Bruggeman diffusion.

- **Porous electrode reaction**:
  By adding **porous electrode** it is added by default also the **porous electrode reaction** node that defines the electrode kinetics for the charge transfer reaction that occurs between the pore electrolyte and the electrode in the electrocatalyst sites in a porous electrode. The equation is (see eq. 2.4):

$$\eta = \phi_s - \phi_e - E_{eq} \tag{2.29}$$

  Where the potential can be corrected by considering the temperature, as in eq. 1.22:

$$E_{eq} = E_{eq,ref} + \frac{dE_{eq}}{dT}(T - T_{ref}) \tag{2.30}$$

  the equilibrium potential at reference temperature is set while its derivative, for this system is null. The kinetic expression of the electrode is of Butler-Volmer type, defining an equation such:

$$i_{loc} = i_0 \left(e^{\frac{\alpha_a F \eta}{RT}} - e^{\frac{-\alpha_c F \eta}{RT}} \right) \tag{2.31}$$

  where are set the exchange current density i_0, the anodic transfer coefficient α_a and the cathodic transfer coefficient α_c. Other parameters to set are the active specific surface area a_v, the number of participating electrons and the stoichiometric coefficients to evaluate $r_{i,m} = \frac{\nu_{i,m} i_v}{n_m F}$.

- **Reactions**:
  Must be added also the **reactions** node to add the reaction that are not electrochemical reactions, i.e. the reactions that do not gives a contribute to the Nernst equation. These equations are:

$$\nabla \cdot (-D_i \nabla c_i - z_i U_{m,i} F c_i \nabla \phi_l) + \mathbf{u} \cdot \nabla c_i = R_{i,src} \tag{2.32}$$

  and

$$\nabla \cdot \mathbf{i_l} = F \sum\nolimits_i z_i R_{i,src} + Q_l \tag{2.33}$$

  To consider a detailed model, must be added also the chemical reaction, i.e. the dissociation rate of the sulphuric acid, defined in eq. 2.10.

- **Electric ground**:
  for the negative electrode there is the **electric ground** node, to bound the electric potential to zero:

$$\phi_s = 0 \tag{2.34}$$

- **Electrode current**:
  for the positive electrode instead is set the **electrode current** $i_{s,average}$, that corresponds to the current of the collector, where

$$\int_{\partial\Omega} \mathbf{i_s} \cdot \mathbf{n} dl = i_{s,avg} \int_{\partial\Omega} dl \tag{2.35}$$

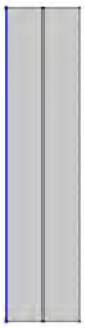

(a) *electric ground* .

(b) *electrode current* .

- **Concentration**:
  the node **concentration** gives the concentration field of the electrolyte on a boundary:

$$c_i = c_{0,i} \tag{2.36}$$

  and needs to set the concentrations $c_{0,HSO4_\pm}$, $c_{0,H_\pm}$, c_{0,V_2} and c_{0,V_3} for the negative electrode, while for the positive c_{0,V_2} and c_{0,V_3} are substituted with c_{0,V_4} and c_{0,V_5}.

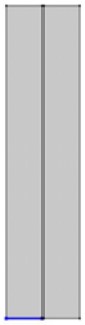

(a) *negative electrode concentration* .

(b) *positive electrode concentration.*

- **Outflow**:
  The **outflow** node sets on a boundary that the flux of chemical species through advection and migration is perpendicular to the selected boundary, with no contribution from diffusion to the flux over the selected boundary.

$$-\mathbf{n} \cdot D_i \nabla c_i = 0 \tag{2.37}$$

(a) *negative outflow.*

(b) *positive outflow.*

2.4.2 Membrane: Secondary current distribution

The secondary current distribution component corresponds to the membrane. It defines the transport of charged ions in an electrolyte uniform composition, using Ohm's Law and charge balance. It takes into account also for activation overpotentials, where the relation between charge transfer and overpotential can be described by Butler-Volmer equations.

electrode current, secondary current distribution

The equations of the model of the membrane and its interface conditions are described in the following part.

- **Electrolyte**:
  the node **electrolyte** defines the balance of charges into the electrolyte with:

$$\nabla \cdot \mathbf{i_l} = Q_l \tag{2.38}$$

  where

$$\mathbf{i_l} = -\sigma_l \nabla \phi_l \tag{2.39}$$

  with the electrolyte conductivity σ_m to be set.

- **Insulation**:
  the node **insulation**, as for the tertiary current distribution, gives

$$-\mathbf{n} \cdot \mathbf{i_l} = 0, -\mathbf{n} \cdot \mathbf{i_s} = 0 \tag{2.40}$$

  and it is valid on the boundary and not on the interface with the electrodes.

- **Initial values**:
  Into the node **initial values** are specified the values of the electrolyte potential ϕ_{l_m} and of the electric potential ϕ_s.

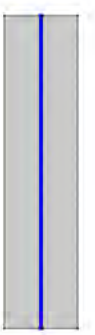

(a) *membrane insulation* .

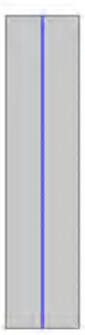

(b) *membrane initial values* .

- **Pointwise Constraint**:
  To add interface conditions are used two pointwise constraint, the first with expression that take into account the Donnan potential.

$$\phi_{l_{neg}} - \frac{RT}{F} ln(\frac{a_H}{a_{H_m}}) - \phi_{l_m} = 0 \tag{2.41}$$

  and constraint force expression, that should help in case the previous equation does not work, that has no physical meaning:

$$test\left(\phi_{l_{neg}} + \frac{c_{H_{neg}}}{F} - \phi_{l_m} = 0\right) \tag{2.42}$$

  and for the second expression

$$\phi_{l_{pos}} - \frac{RT}{F} ln(\frac{a_H}{a_{H_m}}) - \phi_{l_m} = 0 \tag{2.43}$$

  and constraint force expression

$$test\left(\phi_{l_{pos}} + \frac{c_{H_{pos}}}{F} - \phi_{l_m} = 0\right) \tag{2.44}$$

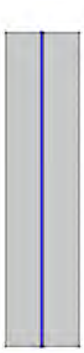

(a) *negative pointwise constraint.*

(b) *positive pointwise constraint.*

2.4.3 Mesh

For this model, the mesh required is quite simple, because of the geometry. The only issue to be treated with particular care is the mesh density, which has to be higher close to the membrane where reactions occurs (fig 2.3).

Figure 2.3: mesh of the simple model

2.4.4 Solution

The solution is found with a Newton-Raphson algorithm, where each step is solved with an iterative solver. In this case the solver is set with *GMRES* and fully coupled iterations, which means all the physics are computed together. The independent variables of the fully coupled system are:

- electric potential
- concentration c_H for the positive electrode
- concentration c_{HSO_4} for the positive electrode
- electrolyte potential $\phi_{l,m}$
- concentration c_{HSO_4} for the negative electrode

- electrolyte potential $\phi_{l,neg}$
- electric potential $\phi_{s,pos}$
- electrolyte potential $phi_{l,pos}$
- concentration cV^{5+}
- concentration cV^{4+}
- concentration cV^{3+}
- concentration cV^{2+}
- terminal voltage

Results

From this model it is possible to get many informations, such as the distribution of the concentration of the different species into the cell, like the vanadium ions in Fig 2.4, or the second dissociation of the sulphuric acid. It is possible also to

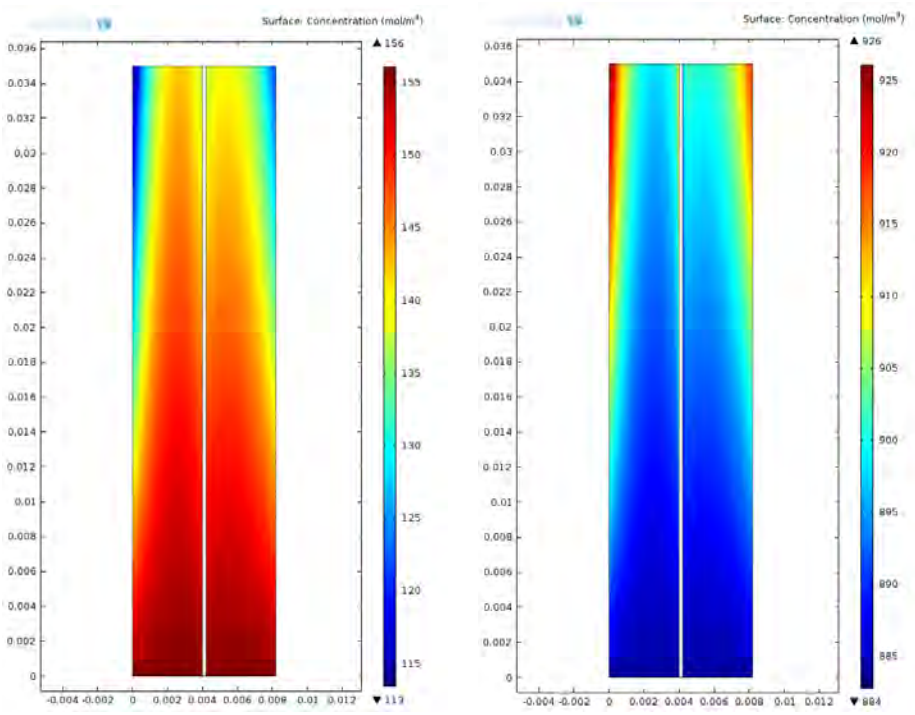

(a) *distribution of concentration of* V^{2+} *and* V^{5+} *species.*

(b) *distribution of concentration of* V^{3+} *and* V^{4+} *species.*

Figure 2.4: concentration of the vanadium species in the cell

get only part of the solution, defined on a subspace of the whole system, or values along a cut-line (Fig:2.5)

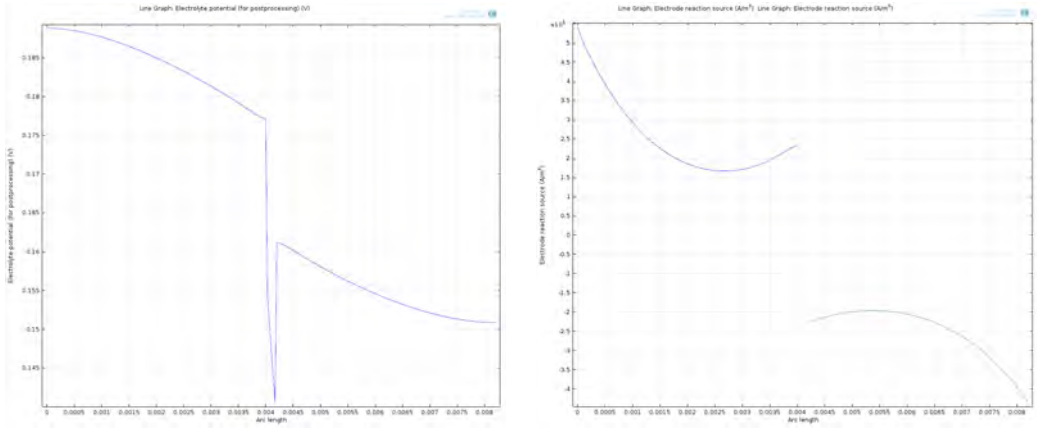

(a) *electrolyte potential.* (b) *Electrode current density.*

Figure 2.5: Behaviors of Electrolyte potential and Electrode current density along a line parallel to the $x - axis$, at half the height of the cell

Chapter 3

Multiphysics model with fluid flow field

The model previously analyzed neglects completely the flow field of the electrolyte solution by supposing that the flow is only along the $y - axis$, with a constant velocity in the whole section. This approximation is not well suited for the simulation of a practical cell. In a practical cell the electrolyte solution does not enter directly in the porous electrode but enters from one or more pipes, e.g. in Fig. 3.1. The same is for the outflow of the cell.

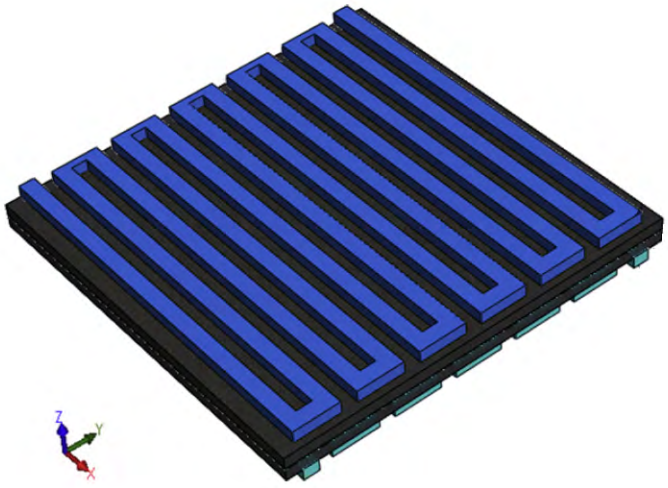

Figure 3.1: Example of serpentine flow field [20]

For these reasons an enhanced version of the model will consider the fluid flow of a practical cell.

3.1 Flow field model

The approximation of a simple flow field allows only the study of flow cells with simple geometries. To analyze the effect of different inlet geometries, the model

must take into account also the fluid flow field.

This work analyze and develop a model that combine the flow field analysis with the electrochemical analysis.

To develop the model are made some assumptions to describe the behavior of the electrolyte into the channels and into the porous electrode. The electrode is composed by a graphite porous matrix, so the general equation that describes the fluid flow in it is the Darcy's law

$$q = \frac{-\kappa}{\mu}\nabla p \quad [m/s] \tag{3.1}$$

where q is the Darcy flux i.e. discharge per unit area, which is related to the average velocity by the porosity

$$v = \frac{q}{\varepsilon_p} \quad [m/s] \tag{3.2}$$

The flow field in a porous media can be described also by the Brinkman equation

$$\begin{aligned}\frac{\rho}{\varepsilon_p}\left(\frac{\partial \mathbf{u}}{\partial t} + (\mathbf{u}\cdot\nabla)\frac{\mathbf{u}}{\varepsilon_p}\right) = &-\nabla p + \nabla\cdot\left[\frac{1}{\varepsilon_p}\left\{\mu(\nabla\mathbf{u} + (\nabla\mathbf{u})^T - \frac{2}{3}\mu(\nabla\cdot\mathbf{u})\mathbf{I}\right\}\right] + \\ &-\left(\kappa^{-1}\mu + \frac{Q_{br}}{\varepsilon_p^2}\right)\mathbf{u} + \mathbf{F} \quad [N/m^3]\end{aligned} \tag{3.3}$$

where $\mathbf{I}$ is the identity matrix, $\mu[Pas]$ is the dynamic viscosity, ε_p is the porosity, $\kappa[m^2]$ is the permeability tensor of the porous medium, $\beta_f[kg/m^4]$ is the Forchheimer drag that adds a viscous force proportional to the square of the fluid velocity and $Q_{br}[kg/m^3 s]$ is a mass source.
Usually the Darcy's law 3.4 is a good approximation.

$$\langle \mathbf{v} \rangle = \frac{-k}{\varepsilon_p \mu}\nabla p \quad [m/s] \tag{3.4}$$

but the previous considerations suggest the use of the Brinkman form of the Darcy's law, due to the presence of the Brinkman term, which is used to account for transitional flow between boundaries. The previous equation is therefore well suited to describe the fluid flow into the electrode, but the empty pipes cannot be represented in the same way.

This problem requires a model which can analyze the fluid flow in two adjacent regions, one with a free flow and one with a porous flow. The flow in the open regions, i.e. where free flow occurs, can be described by the Navier-Stokes equation,

$$\rho\left(\frac{\partial \mathbf{u}}{\partial t} + \mathbf{u}\cdot\nabla\mathbf{u}\right) = -\nabla p + \nabla\cdot T + F \quad [N/m^3] \tag{3.5}$$

where $\rho[kg/m^3]$ is the density of the fluid, $\mathbf{u}[m/s]$ is the velocity field, $p[Pa]$ is the pressure, $T[N/m^2]$ is the total stress and $F[N/m^3]$ is the volume force.
Since the fluid flow is defined in two different regions, must be defined interfacial

conditions to take into account the transition from a domain to another. There are various possibilities to describe the interface boundary between the different domains. The interface conditions used in this model are one of the simplest possibilities. In particular are imposed the continuity of the pressure and of the velocity on the interface.

A detailed analysis of the possible interface conditions is done in [38], where the best approximation is obtained by defining a viscous transition zone, as a subdomain of the porous region. This space is supposed to have a behaviour still represented by the Navier-Stokes equation. Therefore the continuity of velocity and pressure is imposed across it.

The following part therefore describes the physics of Comsol that allows this calculation, i.e. the Free and Porous Flow physics.

3.1.1 Equation of the Free and porous flow physics

The present model is developed to give the solution of a stationary problem. For this reason the Navier-Stokes and the Brinkman equation are modified, neglecting the time-varying terms.

Equations of the Free Flow

The equation in free flow is the Navier-Stokes equation without time derivatives

$$\rho(\mathbf{u}\cdot\nabla)\mathbf{u} = \nabla\left[-p\mathbf{I} + \mu(\nabla\mathbf{U} + (\nabla\mathbf{u})^T)\right] + \mathbf{F} \quad [N/m^3] \tag{3.6}$$

and steady-state continuity equation,

$$\rho\nabla\cdot\mathbf{u} = 0 \quad [kg/m^3 s] \tag{3.7}$$

Equations of the Porous Flow

The flow in the porous domain is described by Brinkman equation, without time derivatives

$$\begin{aligned} 0 = \nabla\cdot\left[-p\mathbf{I} + \frac{\mu}{\varepsilon_p}\left(\nabla\mathbf{U} + (\nabla\mathbf{U})^T\right) - \frac{2\mu}{3\varepsilon_p}(\nabla\cdot\mathbf{u})\mathbf{I}\right] + \\ - \left(\mu\kappa^{-1} + \beta_f|\mathbf{u}| + \frac{Q_{br}}{\varepsilon_p^2}\right)\mathbf{u} + \mathbf{F} \quad [N/m^3] \end{aligned} \tag{3.8}$$

and the continuity equation, that contains also a source term

$$\rho\nabla\cdot\mathbf{u} = Q_{br} \quad [kg/m^3 s] \tag{3.9}$$

Boundary conditions

The other components of this physic are mentioned in this part.

- **Inlet**
  The **inlet** has a simple equation, that sets the initial velocity.

$$\mathbf{u} = \mathbf{u_0} \quad [m/s] \tag{3.10}$$

- **Outflow**
  The **outflow** node allow the exit pressure of the flow field to be set by:

$$\left[-p\mathbf{I} + \mu\left(\nabla\mathbf{u} + (\nabla\mathbf{u})^T\right)\right]\mathbf{n} = -\hat{p_0}\mathbf{n} \quad [Pa] \tag{3.11}$$

  and the pressure on the boundary $\hat{p_0}$ has to be

$$-\hat{p_0} \leq p_0 \quad [Pa] \tag{3.12}$$

  where the p_0 pressure for this model is set to zero

$$p_0 = 0 \quad [Pa] \tag{3.13}$$

- **Fluid Properties**
  The **fluid properties** are explained by the Navier-Stokes equation 3.6 and the continuity equation 3.7

- **Porous Matrix Properties**
  The **porous matrix properties** are described by the Brinkman equation 3.8

3.1.2 Variables of the new model

The advanced model requires to define new variables such as the inlet velocity, the velocity field into the whole domain, the porosity and the outlet pressure.

The inlet velocity is chosen by taking into account that there are losses in the mass transport and the current flowing through the electrodes depends also on the concentration of V^{2+} and V^{5+} in the negative and positive electrodes.

A useful way to optimize the efficiency is to vary the flow rate. In order to do that, has been proposed the use of a flow factor, that multiplies the value of flow rate calculated on the basis of Faraday law for electrolysis 3.14. From literature can be found that the optimal results are obtained considering a flow factor α with $1 \leq \alpha \leq 8$ [23, 27]. Hence

$$Q_{electrode} = \frac{I}{Fc_V SoC} \quad [kg/m^3 s] \tag{3.14}$$

becomes

$$Q_\alpha = \alpha\frac{I}{Fc_V SoC} \quad [kg/m^3 s] \tag{3.15}$$

where $I[A]$ is the electric current, $c_V \quad [mol/m^3]$ is the concentration of the decreasing vanadium species and SoC is the state of charge.
Usually the SoC ranges from the 10% to the 90%, but it is also possible to set $SoC_{min} = 20 \div 25\%$.

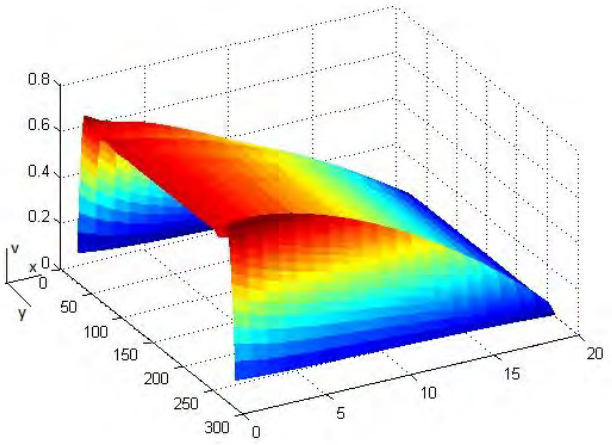

Figure 3.2: MATLAB® processing of the y component of the velocity field

3.2 Coupling between 2D analysis and 3D flow field model

In this work the first investigation about the implementation of a realistic flow field to a VRFB is done by adding a flow field calculated with a separated model, composed only by a free and porous flow physics and then scaled and introduced in the electrochemical model. The Cartesian components of the velocity computed on a rectangular grid by 3D flow field model were exported as matrices. These tables then have been imported in the 2D VRFB model as functions (see fig 3.2), then used as input functions to describe the velocity of the electrolyte into the electrode.

In this way has been investigated the feasibility of the combination of the flow field physics with the electrochemistry physics.

In the second step the free and porous flow field physics have been added to the VRFB model, to be solved in the same simulation, with a segregated solver.

3.3 Interdigitated flow field

The laboratory of Computational Electrical Engineering of the University of Padua is currently studying a VRFB system prototype. In this system, whose layout can be seen in Fig. 3.3, the electrolyte fluid enters through the porous electrode via interdigitated channels (see Fig 3.5).

The VRFB cell under study in the laboratory has interdigitated serpentine channels, that make all the electrolyte pass through the porous electrode (Fig. 3.4). Performing a $3D$ multiphysics simulation of the whole cell will require a tremendous computational cost. Therefore an equivalent $2D$ model would reduce drastically the time required for the computation.

The following part of the work is done to find a model which can perform a simulation of a cell of this system.

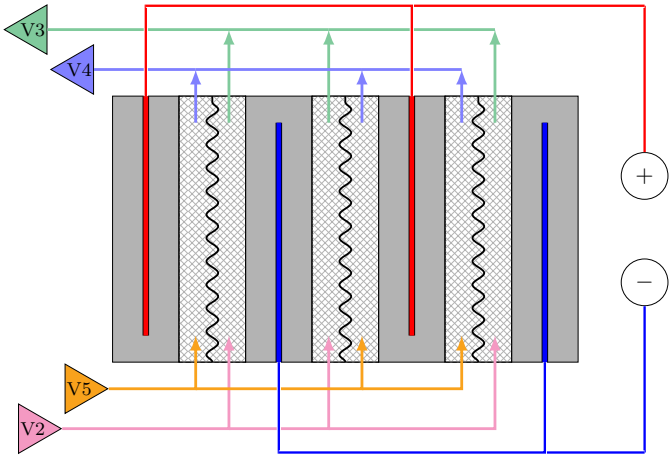

Figure 3.3: Layout of the monopolar cell

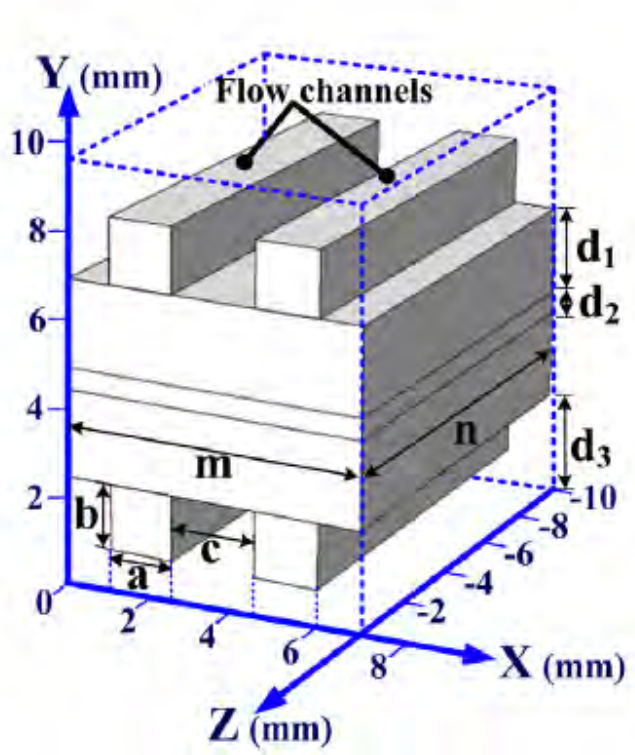

Figure 3.4: Simplified 3D model of interdigitated flow channels, You et al. [22]

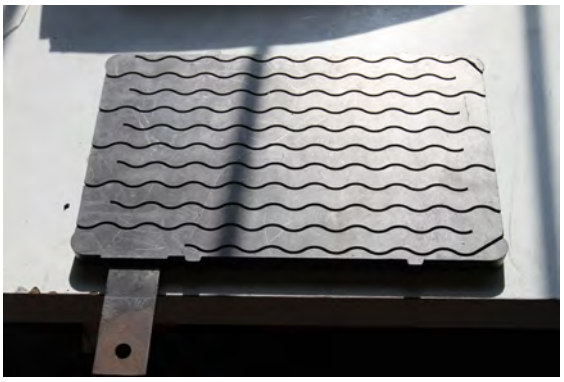

Figure 3.5: Monopolar plate with interdigitated channels

The single cell has a height $h_{cell} = 260mm$ and a width $w_{cell} = 160mm$, that are the dimensions of the membrane. The current density is set to obtain a current density of $i = 2000A/m^2$, therefore the current is

$$I = i \times h_{cell} \times w_{cell} \simeq 83A \tag{3.16}$$

The total concentration of vanadium is set at

$$c_{V_{tot}} = 1600mol/m^3 \tag{3.17}$$

The feeding system is made by interdigitated serpentine, $5 \sim 6$ for the inflow and $4 \sim 5$ for the outflow (fig 3.5).

With this concentration of vanadium and a concentration of sulphuric acid $\sim 6M$ the two electrolytes have different characteristics.

For the negative electrolyte the main parameters are:

- **Density**
  The density of the negative electrolyte is $\rho_{neg} = 1300kg/m^3$
- **Viscosity** The viscosity of the negative solution is $\eta_{neg} = 0.0025Pa \cdot s$

while for the positive electrolyte the parameters are:

- **Density** The density of the positive solution is $\rho_{pos} = 1354kg/m^3$
- **Viscosity** The viscosity of the positive solution is $\eta_{pos} = 0.005Pa \cdot s$

Due to the difference of viscosity the behavior of the cell is not anymore symmetric as in the case of the previous simple model.

Another important parameter is the permeability. This value has a wide range in the literature since it is determined with the Kozeny-Carman equation,where the Kozeny-Carman constant is a fitting parameter, obtained by measuring the permeability, known the porosity and the diameter of the fibers or the diameter of the pores:

$$k = \frac{d_f^2 \varepsilon^3}{K_{CK}(1-\varepsilon)^2} \quad [m^2] \tag{3.18}$$

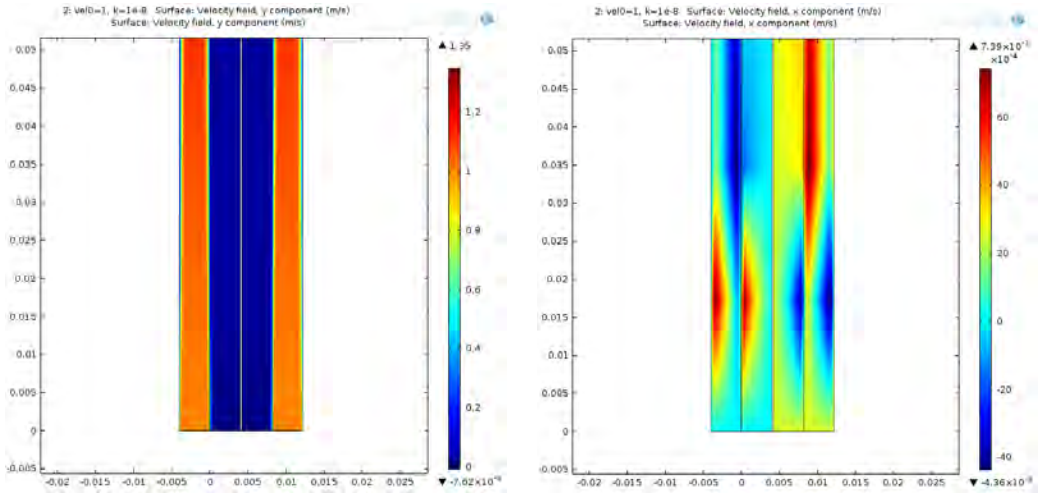

(a) *y component of the velocity field.* (b) *x component of the velocity field.*

Figure 3.6: Flow field into a vrfb with pipes in parallel to the electrodes

where $d_f[m]$ is the graphite fiber diameter, ε is the porosity and K_{CK} is the Kozeny-Carman constant, that characterize the shape and the orientation of the material [20].
Another expression of the Kozeny-Carman equation, used in VRFB modeling [18, 26] is

$$k = \frac{d_p^2 \varepsilon^3}{16 K_{CK}(1-\varepsilon)^2} \quad [m^2] \tag{3.19}$$

where $d_p[m]$ is the pore diameter, usually measured by mercury porosimeter.

For a more detailed analysis of the Kozeny-Carman equation, also by means of fractal geometry, there is a work of P. Xu and B. Yu [39].

In the literature, the Kozeny-Carman constant K_{CK} goes from a value of 4.28 in the work of D. You et al. [15] to a value of 180 and more [20]. The value of the permeability $k[m^2]$ therefore must be obtained experimentally.

This parameter, due to its proportionality with the pressure gradient (see Darcy's law 3.4), has a direct relation with the sizing of the pumps (in the Brinkman equation the permeability κ is still related to the pressure gradient).

In the present work some of the trial simulation were performed with a value of $k = 1 \times 10^{-9}[m^2]$, that is in good agreement with the values found in the literature.

The simple $2D$ model with the serpentine in parallel with the electrode, where the external rectangles are the pipes and the three internal rectangles are the electrodes and the membrane, was not feasible due to the small flow of electrolyte into the porous electrode (fig 3.6). This happened because of the high permeability $k[m^2]$ of the porous graphite electrode.

To avoid this problem the flow has to pass completely through the porous electrode.
In order to have an idea of how the fluid goes through the graphite electrode a $3D$ fluid flow model has been done. This model has only one inlet pipe and one outlet

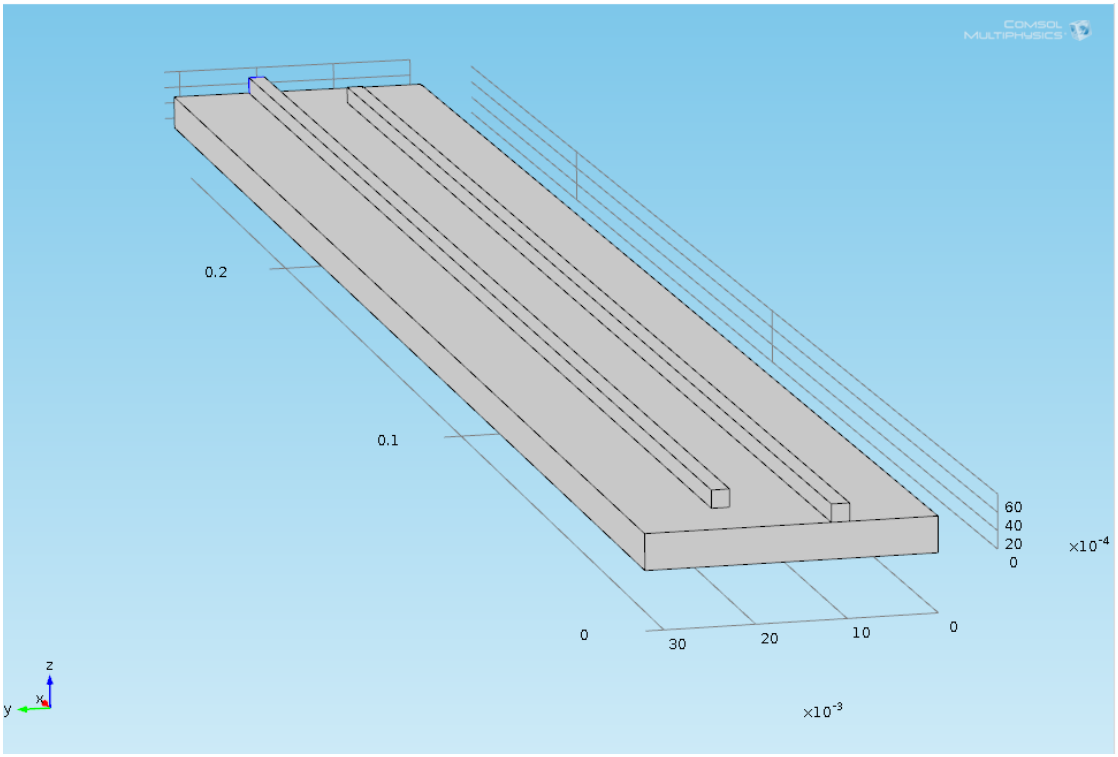

Figure 3.7: 3D flow field model with two pipes and a part of porous electrode

pipe (fig 3.7).

The mesh of this model was made thiner near the inlet and the outlet and coarser near the end of the pipes (fig 3.8). It is also as fine as possible to obtain a convergent solution. Every pipe is long $l_p = 250mm$.

The flow rate is calculated from the Faraday's law (3.15), with a current density of $i = 2000A/m^2$ and a state of charge $SoC_{min} = 0.25$, that is the condition that requires the highest flow rate.

As a result, it is possible to see how the fluid is distributed into the porous electrode, with the magnitude of the velocity field in fig. 3.9. A better understanding is given by the y and z component of the velocity field, respectively in fig. 3.10 and in fig. 3.11 As can be seen from fig. 3.10, fig. 3.11 and 3.12, with the parameters set above, the majority of the electrolyte passes through the porous electrode at the beginning and at the end of the cell, creating two zones with a good amount of fresh electrolyte solution, in the rest of the cell velocity of the flow is very low. This consideration neglects the fact that the real cell has serpentine channels, that should increase the passage area of the electrolyte solution through the porous electrode.
A solution to make a $2D$ model of an interdigitated channel cell is to simulate a slice of the cell along a $x - z$ plane (fig 3.13).

This can be done by supposing that the flow rate at the inlet (fig 3.14) passes through the electrode homogeneously distributed. By doing this, the equivalent flow rate can be calculated as the inlet flow rate multiplied by the area of the inlet

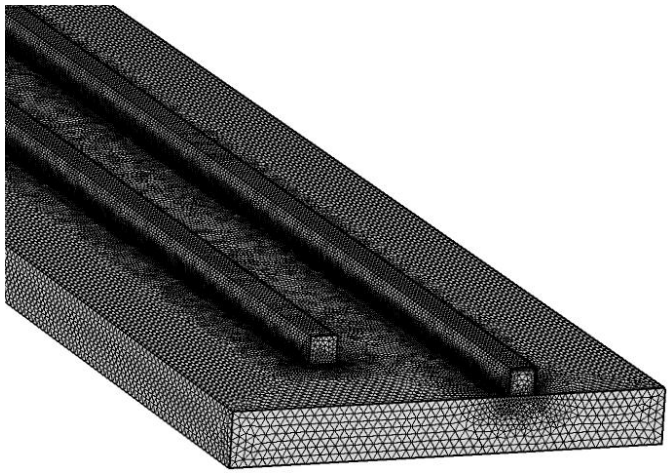

Figure 3.8: Partial view of the mesh of the 3D flow field model

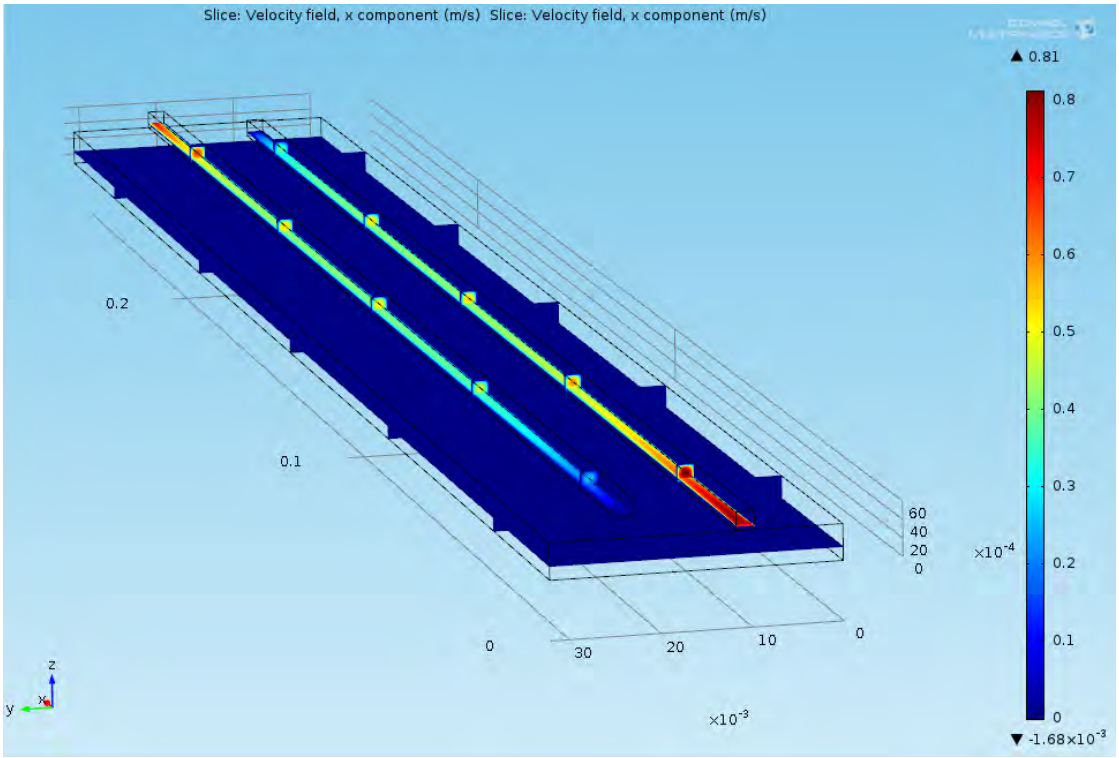

Figure 3.9: 3D velocity field magnitude

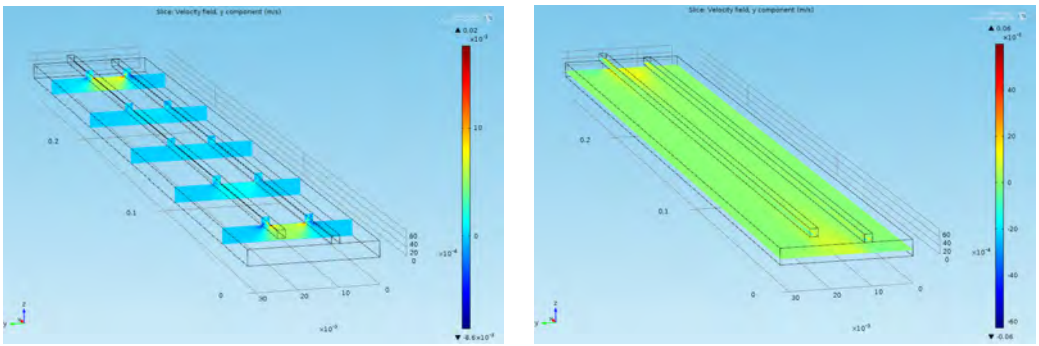

(a) *y component of the velocity field on a* $x - y$ *plane.*

(b) *y component of the velocity field on* $y-z$ *planes.*

Figure 3.10: y component of the velocity field

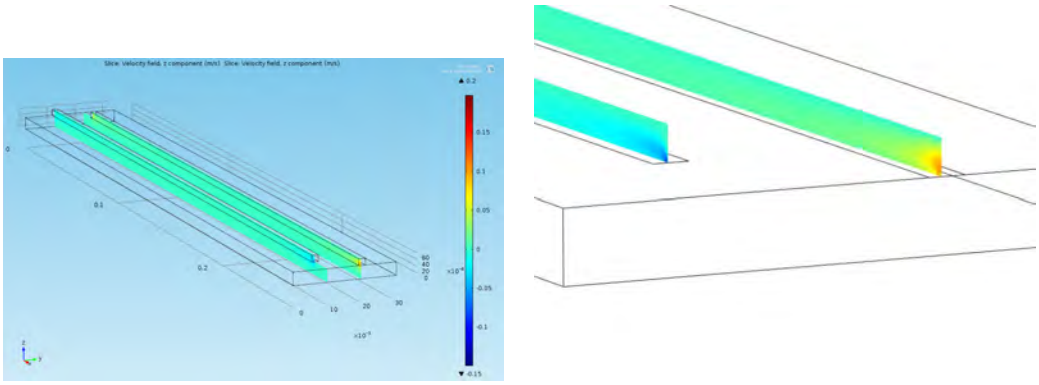

(a) *z component of the velocity field on* $x-z$ *planes.*

(b) *particular of the z component of the velocity field on* $x - z$ *planes.*

Figure 3.11: z component of the velocity field

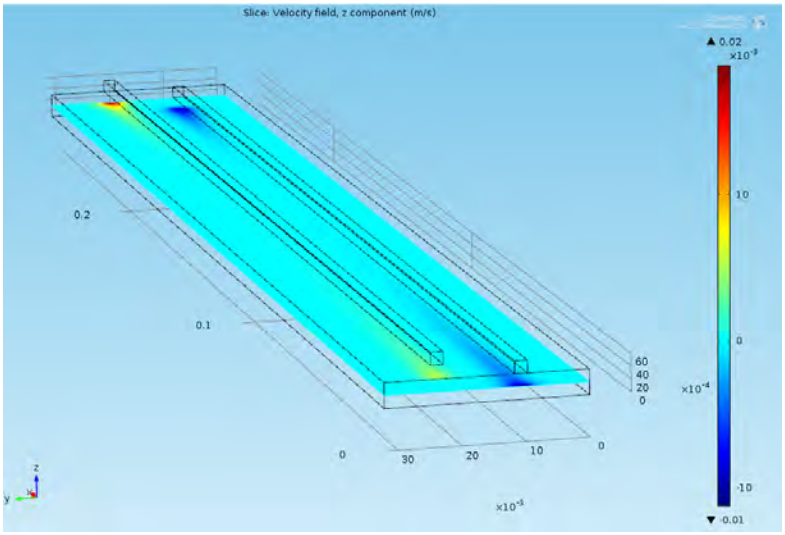

Figure 3.12: z component of the velocity field on a $x - y$ plane

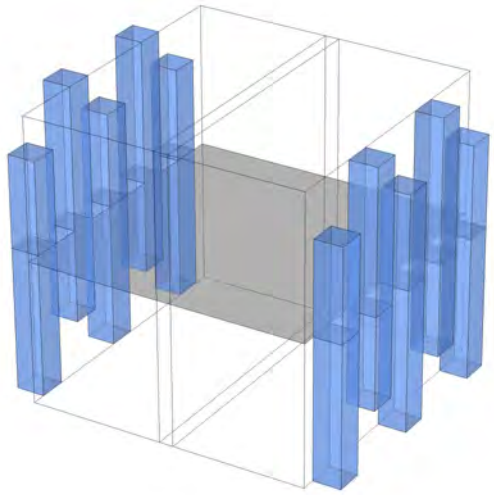

Figure 3.13: Example of cell with interdigitated channels, with a section on a xz plane

and divided by the area of the interface between the electrode and the pipe

$$Q_{eq} = Q_{inlet} \frac{A_{inlet}}{A_{interface}} \quad [m^3/s] \tag{3.20}$$

This assumption allows to perform a $2D$ simulation. As a result of the interdigitated channels flow field, the concentration of the electroactive species (Fig. 3.15) is homogeneous the whole cell except in the side areas.

3.3.1 Voltage driven analysis

With this model it is also possible to set the electric potential instead of the current density. This is done by adding a node **Electrode Potential** to the Tertiary Current Distribution of the positive electrode and by removing the **Electrode Current**. If this process is done to a model that has been already solved, it is necessary to create another solution. By doing this COMSOL makes a new system to be solved, with the electrode potential as a parameter and the electrode current as an unknown term.

3.3.2 Current driven analyis

One of the most important things to note is that it is possible to perform a parametric sweep, i.e. the solution of the same model with different sets of parameters e.g.: By defining the state of charge SoC and the total concentration of vanadium per each electrolyte solution cV_{tot} $[mol/m^3]$ the concentrations of vanadium species result

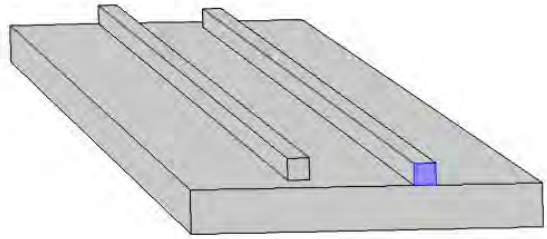

Figure 3.14: Inlet of the cell

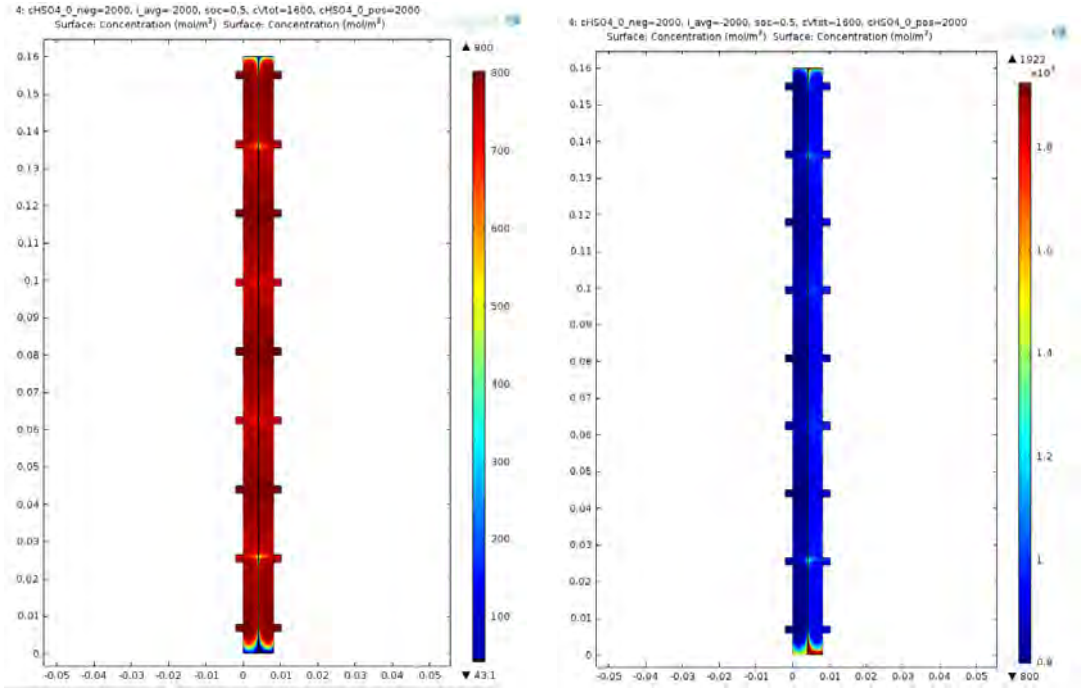

(a) V^{2+} *and* V^{5+} *concentrations.* (b) V^{3+} *and* V^{4+} *concentrations.*

Figure 3.15: Concentration of the vanadium species in a VRFB with interdigitate channels

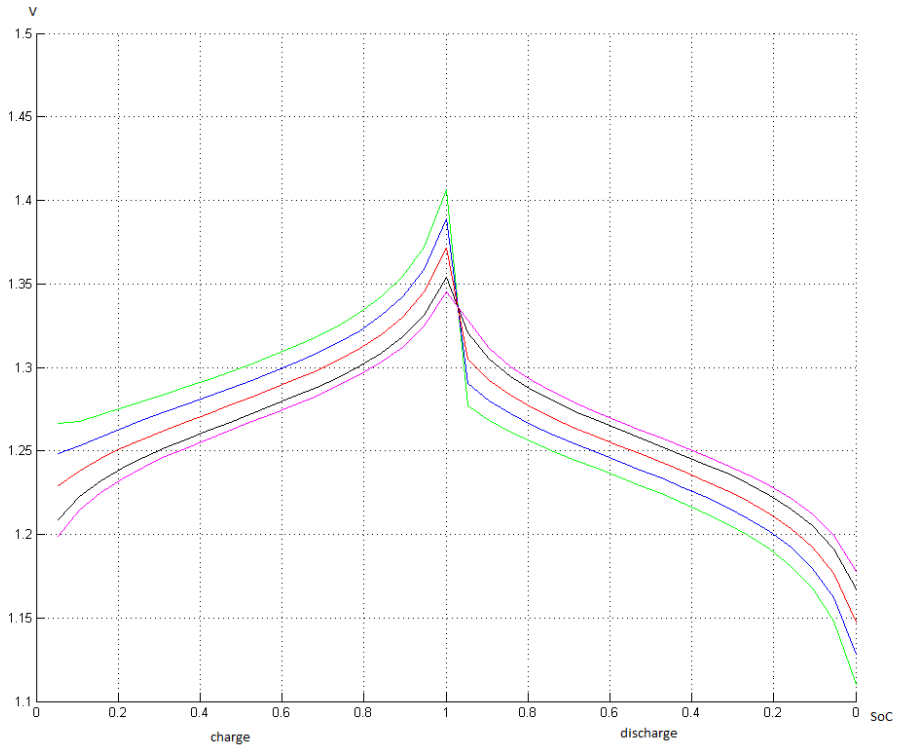

Figure 3.16: Curves of charge and discharge cycles with different current densities

- $cV_0^{2+} = cV_{tot} \times SoC \quad [mol/m^3]$
- $cV_0^{3+} = cV_{tot} \times (1 - SoC) \quad [mol/m^3]$
- $cV_0^{4+} = cV_{tot} \times (1 - SoC) \quad [mol/m^3]$
- $cV_0^{5+} = cV_{tot} \times SoC \quad [mol/m^3]$

Therefore by performing a parametric sweep of the SoC parameter, it is possible to see the behavior of the cell for each value of SoC.

By varying both the state of charge SoC and the electrode current density $i_{avg}[A/m^2]$ it is possible to get the curves of the electric potential during a cycle of charge and discharge (see Fig. 3.16 and Fig. 3.17). The postprocessing is done with MATLAB® (see Appendix 2). The values has been exported from COMSOL® in a *.cvs* file and then imported with a MATLAB script. The imported data were subsequently rearranged in order to create a figure with the curves of the electric potential, during both the charge, with a positive current density, and the discharge, with negative current density, but the same magnitude.

Another possibility is to analyze how the concentration of vanadium species changes into the cell, making possible to see if there are some "blind spots", where there is an higher discharge of the electrolyte due to a low flow (Fig. 3.18).

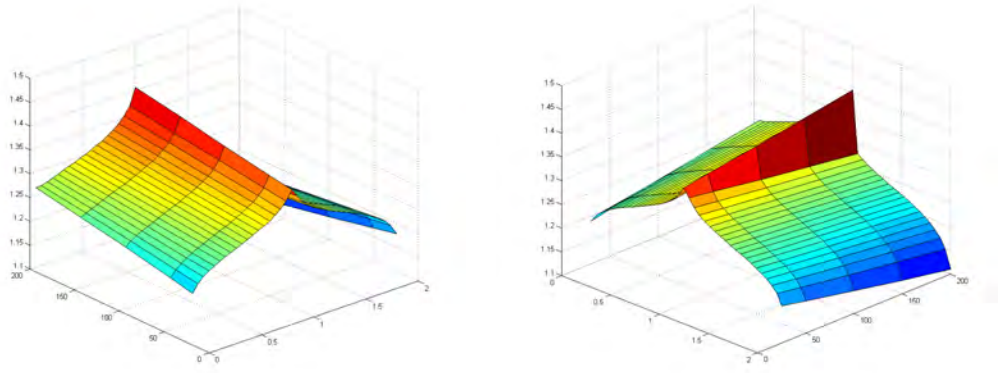

(a) *Electric potential with different SoC and current density,1.*

(b) *Electric potential with different SoC and current density,2.*

Figure 3.17: Curves that shows the behavior of the electric potential during charge and discharge with different values of current density

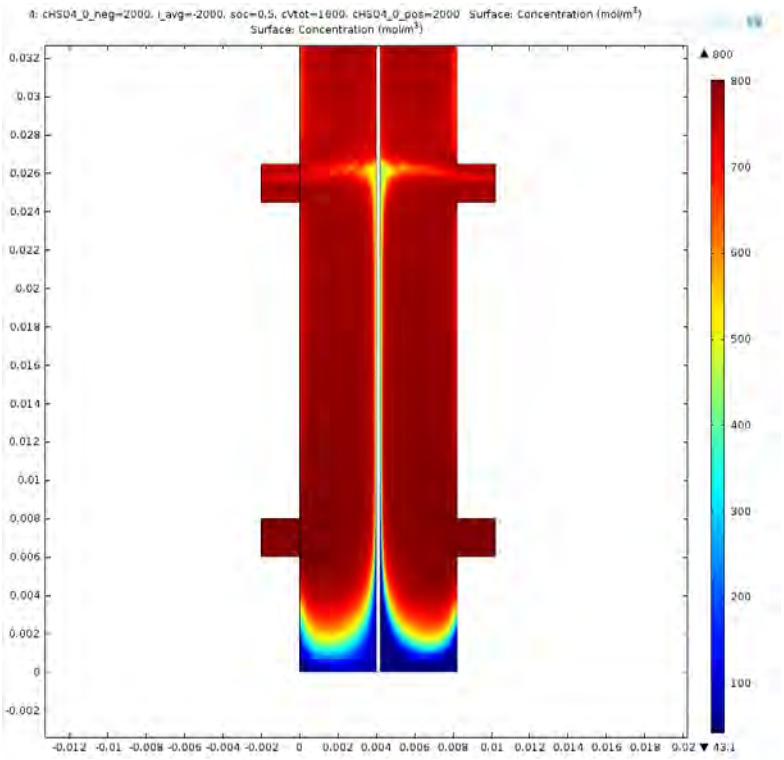

Figure 3.18: View of a portion of a VRFB with interdigitated channels, concentration of V^{2+} and V^{5+} species

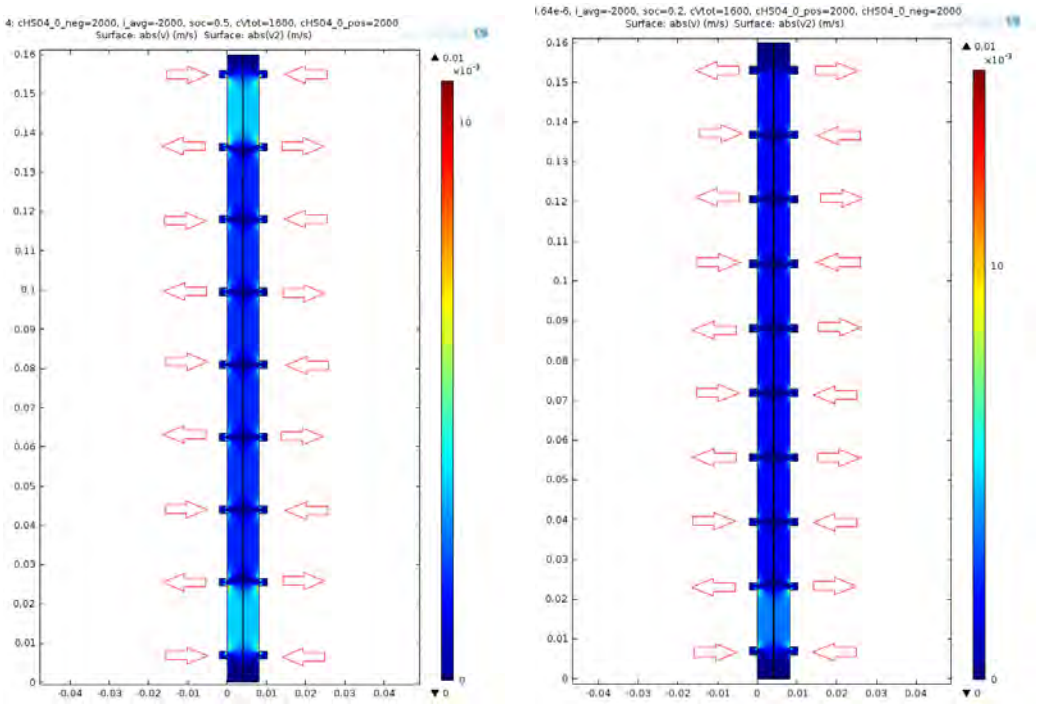

(a) *VRFB cell with an odd number of interdigitated channels.*

(b) *VRFB cell with an even number of interdigitated channels.*

Figure 3.19: Different velocity fields for odd and even number of channels

3.3.3 Analysis of the 2D flow field results

With this model it is also possible to verify how the velocity field is distributed. There is the possibility to optimize the distribution of the interdigitated channels, to have an homogeneous flow field into the cell:

- the zones of the porous electrode where the fresh electrolyte fluid is supplied by the external channels have a lower discharge rate of the vanadium ions due to the higher flow rate.
- the extremities of the porous electrode region receive a minimum amount of new electrolyte, therefore diffusion mechanisms become more important than the flow field itself. This makes necessary to put the external channels as near as possible to the boundary of the cell.
- To have a symmetric behavior of the cell, the number of the inflow channels must differ from the number of the outflow channels by one unit. In this way the number of channel is odd and therefore the external channels are both inflow or outflow channels (Fig 3.19)

3.3.4 Towards a full 3D modeling

You et al. [22] have created a simplified $3D$ model of a VRFB with interdigitated channels. By taking that work as a reference, the following idea is to develop a

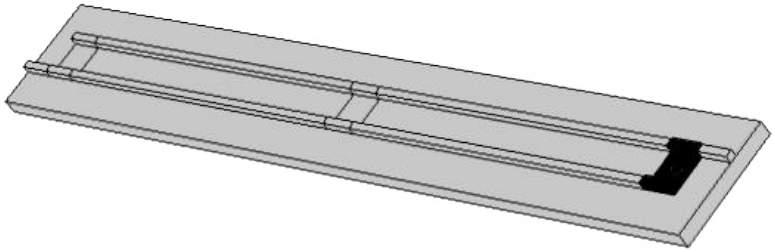

Figure 3.20: $3D$ fluid flow model with the three regions chosen to solve the electrochemical model

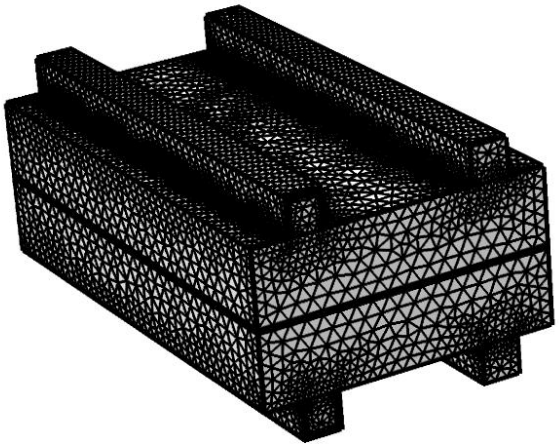

Figure 3.21: $3D$ fluid flow model with the three regions chosen to solve the electrochemical model (see fig 3.20)

$3D$ multiphysics model that consider the flow field of the complete $3D$ fluid flow model.
Since a multiphysics simulation of the whole VRFB cell, with $260 \times 160 mm^2$ area is unfeasible with a standard workstation, while the simulation of the $3D$ fluid flow were already performed.

The idea therefore was to solve the $3D$ electrochemical model only in a small part of the cell, with the solved flow field of the previous simulation as an input value. For this problem three region were chosen (Fig. 3.20):

- one near the inlet
- one in the middle of the height
- one near the outlet

The $3D$ model was set up according to Fig 3.21

3.4 Further developments

The present multiphysics model, that solves both the flow field and the electrochemistry of a VRFB, can be used for observing the cell behavior on different operating conditions.

The simplest evaluation allowed by the model is the value of the average concentration at the outlet of the channel. By knowing the initial concentration, the average outflow concentration and the volume of the tank, it is possible to evaluate the time required to a complete charge or discharge of the VRFB. The variation of the inlet concentration can be approximated from the following mass balance, which assume instantaneous mixing and negligible reaction in the reservoir of volume $V[m^3]$ [14]

$$\frac{dc_i^{in}}{dt} = \frac{\omega}{V}(c_i^{out} - c_i^{in}) \quad [mol/m^3 s], \quad c_i^{in}(0) = c_i^0 \quad [mol/m^3] \tag{3.21}$$

where the volumetric flow at the outlet boundaries, with cross-sectional area A_{out}, is $\omega = \nu_{in}\varepsilon A_{out}$.

Chapter 4

Conclusion

The first part of the work has been focused on the analysis of the VRFB technology. The equations that describe this systems have been explained and organized together with their references. After analyzing the state of the art models it has been possible to say that one of the problems that needed further investigation is the study of the flow field. A simple $2D$ electrochemical model, already developed in COMSOL®, was selected as the basis for the development of a more detailed model.

The second part has been the analysis of this simple model and how it is implemented in COMSOL. Then the parameter of this model were set to be in accord with the system with interdigitated channels being studied in the laboratory of Computational Electrical Engineering. The results given by this model were not adequate to represent the behavior of the VRFB system. The pressure gradient and the flow rate necessary to maintain the imposed current were order of magnitude greater than the required values.

The third part of the work therefore was focused on the research of the equations to describe the fluid flow field, their interface conditions and the implementation of them in the COMSOL model and how to simulate the 3D cell with a 2D model.

After an assumption on the 3D flow field, with the developed model is possible to simulate properly an interdigitated channel VRFB cell. The performed simulations highlight the fact that, differently from the literature, the distribution of the electrolyte into the porous electrode for an optimal range of the flow rate, with this geometry, is uneven. This distribution of the electrolyte may led to "hotspot". But if the temperature of the cell overcome a limit value, the vanadium ions start to precipitate, making the cell useless. For this reason some measures can be taken to guarantee an even and homogeneous distribution of the electrolyte into the cell, such as different spacing of the channels.

Since the interdigitated channels flow field is a key technology, there is the need of further analysis. The only available model with this kind of channels state that the uneven pressure drop between the external channels and the internal is obtained for low flow rates, but this is not in agreement with the optimal flow factor α reported in [27] because a flow factor of 7 has been used for the $2D$ multiphysics simulation and the flow field is still uneven (see fig 3.19) and a higher flow rate

could reduce the overall efficiency of the VRFB system. Therefore a solution to this problem could be find from the solution of the 3D electrochemical model with the solved 3D flow field that remains an open task. A further step in the improvement of the model therefore could be the implementation of the heat transfer physics. In this way it could be possible to evaluate the temperature distribution into the cell and avoid the precipitation of the vanadium ions by increasing the flow rate.

Appendices

Appendix A

Equations of the simple model

A.1 Negative electrode: Tertiary current distribution

1. **Porous electrode, negative**, the equations of the Domain1 (fig A.1) are:

   - Current source:
     $Q_{si} = 0[A/m^3]$,

     SO_4

   - Concentration of SO_4:
     $cSO_4 = \frac{(-cHSO_4 \times z_{cHSO_4} - cH \times z_{cH} - cV_2 \times z_{cV_2} - cV_3 \times z_{cV_3})}{z_{cSO_4} + eps}[mol/m^3]$ where eps is the machine epsilon, an upper bound to the relative error due to rounding in floating point arithmetic. In this case used to avoid division for zero.

   - Diffusion coefficient
     $$\mathbf{D_{c_{SO_4}}} = \begin{bmatrix} D_{xx} & D_{xy} & D_{xz} \\ D_{yx} & D_{yy} & D_{yz} \\ D_{zx} & D_{zy} & D_{zz} \end{bmatrix} = \begin{bmatrix} D_{SO_4}\varepsilon^{1,5} & 0 & 0 \\ 0 & D_{SO_4}\varepsilon^{1,5} & 0 \\ 0 & 0 & D_{SO_4}\varepsilon^{1,5} \end{bmatrix} [m^2/s]$$

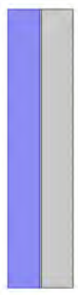

Figure A.1: Domain1

- Average diffusion coefficient
  $D_{av_{SO_4}} = \frac{1}{2}(D_{xx_{SO_4}} + D_{yy_{SO_4}})[m^2/s]$
- Total flux
  $$Tflux_{cSO_4} = \begin{bmatrix} Tflux_x \\ Tflux_y \\ Tflux_y \end{bmatrix} =$$
  $$= \begin{bmatrix} D_{xx_{cSO_4}} \frac{\partial cSO_4}{\partial x} - D_{xy_{cSO_4}} \frac{\partial cSO_4}{\partial y} + Cflux_{x,cSO_4} + Mflux_{x,cSO_4} \\ D_{yx_{cSO_4}} \frac{\partial cSO_4}{\partial x} - D_{yy_{cSO_4}} \frac{\partial cSO_4}{\partial y} + Cflux_{y,cSO_4} + Mflux_{y,cSO_4} \\ D_{zx_{cSO_4}} \frac{\partial cSO_4}{\partial x} - D_{zy_{cSO_4}} \frac{\partial cSO_4}{\partial y} + Cflux_{z,cSO_4} + Mflux_{z,cSO_4} \end{bmatrix} [m^2/s]$$
- Diffusive flux
  $$Dflux_{cSO_4} = \begin{bmatrix} Dflux_x \\ Dflux_y \\ Dflux_y \end{bmatrix} = \begin{bmatrix} D_{xx_{cSO_4}} \frac{\partial cSO_4}{\partial x} - D_{xy_{cSO_4}} \frac{\partial cSO_4}{\partial y} \\ D_{yx_{cSO_4}} \frac{\partial cSO_4}{\partial x} - D_{yy_{cSO_4}} \frac{\partial cSO_4}{\partial y} \\ D_{zx_{cSO_4}} \frac{\partial cSO_4}{\partial x} - D_{zy_{cSO_4}} \frac{\partial cSO_4}{\partial y} \end{bmatrix} [m^2/s]$$
- Concentration gradient
  $$\begin{bmatrix} \nabla_x \\ \nabla_y \\ \nabla_z \end{bmatrix} = \begin{bmatrix} \frac{\partial cSO_4}{\partial x} \\ \frac{\partial cSO_4}{\partial y} \\ 0 \end{bmatrix} [mol/m^4]$$
- Diffusive flux magnitude
  $DfluxMag_{cSO_4} = \sqrt{Dflux^2_{x,cSO_4} + Dflux^2_{y,cSO_4} + Dflux^2_{z,cSO_4}}[mol/m^2s]$
- Total flux magnitude
  $TfluxMag_{cSO_4} = \sqrt{Tflux^2_{x,cSO_4} + Tflux^2_{y,cSO_4} + Tflux^2_{z,cSO_4}}[mol/m^2s]$

$\mathbf{HSO_4}$

- Concentration of HSO_4:
  $cHSO_4 = \frac{(-cHHSO_4 \times z_{cHHSO_4} - cH \times z_{cH} - cV_2 \times z_{cV_2} - cV_3 \times z_{cV_3})}{z_{cHSO_4} + eps}[mol/m^3]$
- Diffusion coefficient
  $$\mathbf{D_{c_{HSO_4}}} = \begin{bmatrix} D_{xx} & D_{xy} & D_{xz} \\ D_{yx} & D_{yy} & D_{yz} \\ D_{zx} & D_{zy} & D_{zz} \end{bmatrix} = \begin{bmatrix} D_{HSO_4}\varepsilon^{1,5} & 0 & 0 \\ 0 & D_{HSO_4}\varepsilon^{1,5} & 0 \\ 0 & 0 & D_{HSO_4}\varepsilon^{1,5} \end{bmatrix} [m^2/s]$$
- Average diffusion coefficient
  $D_{av_{HSO_4}} = \frac{1}{2}(D_{xx_{HSO_4}} + D_{yy_{HSO_4}})[m^2/s]$
- Total flux
  $$Tflux_{cHSO_4} = \begin{bmatrix} Tflux_x \\ Tflux_y \\ Tflux_y \end{bmatrix} =$$
  $$= \begin{bmatrix} D_{xx_{cHSO_4}} \frac{\partial cHSO_4}{\partial x} - D_{xy_{cHSO_4}} \frac{\partial cHSO_4}{\partial y} + Cflux_{x,cHSO_4} + Mflux_{x,cHSO_4} \\ D_{yx_{cHSO_4}} \frac{\partial cHSO_4}{\partial x} - D_{yy_{cHSO_4}} \frac{\partial cHSO_4}{\partial y} + Cflux_{y,cHSO_4} + Mflux_{y,cHSO_4} \\ D_{zx_{cHSO_4}} \frac{\partial cHSO_4}{\partial x} - D_{zy_{cHSO_4}} \frac{\partial cHSO_4}{\partial y} + Cflux_{z,cHSO_4} + Mflux_{z,cHSO_4} \end{bmatrix} [m^2/s]$$
- Diffusive flux
  $$Dflux_{cHSO_4} = \begin{bmatrix} Dflux_x \\ Dflux_y \\ Dflux_y \end{bmatrix} = \begin{bmatrix} D_{xx_{cHSO_4}} \frac{\partial cHSO_4}{\partial x} - D_{xy_{cHSO_4}} \frac{\partial cHSO_4}{\partial y} \\ D_{yx_{cHSO_4}} \frac{\partial cHSO_4}{\partial x} - D_{yy_{cHSO_4}} \frac{\partial cHSO_4}{\partial y} \\ D_{zx_{cHSO_4}} \frac{\partial cHSO_4}{\partial x} - D_{zy_{cHSO_4}} \frac{\partial cHSO_4}{\partial y} \end{bmatrix} [m^2/s]$$

- Concentration gradient
$$\begin{bmatrix} \nabla_x \\ \nabla_y \\ \nabla_z \end{bmatrix} = \begin{bmatrix} \frac{\partial cHSO_4}{\partial x} \\ \frac{\partial cHSO_4}{\partial y} \\ 0 \end{bmatrix} [mol/m^4]$$
- Diffusive flux magnitude
$$DfluxMag_{cHSO_4} = \sqrt{Dflux^2_{x,cHSO_4} + Dflux^2_{y,cHSO_4} + Dflux^2_{z,cHSO_4}}$$
- Total flux magnitude
$$TfluxMag_{cHSO_4} = \sqrt{Tflux^2_{x,cHSO_4} + Tflux^2_{y,cHSO_4} + Tflux^2_{z,cHSO_4}}$$

H

- Concentration of H:
$cH = \frac{(-cHH \times z_{cHH} - cH \times z_{cH} - cV_2 \times z_{cV_2} - cV_3 \times z_{cV_3})}{z_{cH} + eps} [mol/m^3]$
- Diffusion coefficient
$$\mathbf{D_{cH}} = \begin{bmatrix} D_{xx} & D_{xy} & D_{xz} \\ D_{yx} & D_{yy} & D_{yz} \\ D_{zx} & D_{zy} & D_{zz} \end{bmatrix} = \begin{bmatrix} D_H \varepsilon^{1,5} & 0 & 0 \\ 0 & D_H \varepsilon^{1,5} & 0 \\ 0 & 0 & D_H \varepsilon^{1,5} \end{bmatrix} [m^2/s]$$
- Average diffusion coefficient
$D_{av_H} = \frac{1}{2}(D_{xx_H} + D_{yy_H})[m^2/s]$
- Total flux
$$Tflux_{cH} = \begin{bmatrix} Tflux_x \\ Tflux_y \\ Tflux_y \end{bmatrix} = \begin{bmatrix} D_{xx_{cH}} \frac{\partial cH}{\partial x} - D_{xy_{cH}} \frac{\partial cH}{\partial y} + Cflux_{x,cH} + Mflux_{x,cH} \\ D_{yx_{cH}} \frac{\partial cH}{\partial x} - D_{yy_{cH}} \frac{\partial cH}{\partial y} + Cflux_{y,cH} + Mflux_{y,cH} \\ D_{zx_{cH}} \frac{\partial cH}{\partial x} - D_{zy_{cH}} \frac{\partial cH}{\partial y} + Cflux_{z,cH} + Mflux_{z,cH} \end{bmatrix} [m^2/s]$$
- Diffusive flux
$$Dflux_{cH} = \begin{bmatrix} Dflux_x \\ Dflux_y \\ Dflux_y \end{bmatrix} = \begin{bmatrix} D_{xx_{cH}} \frac{\partial cH}{\partial x} - D_{xy_{cH}} \frac{\partial cH}{\partial y} \\ D_{yx_{cH}} \frac{\partial cH}{\partial x} - D_{yy_{cH}} \frac{\partial cH}{\partial y} \\ D_{zx_{cH}} \frac{\partial cH}{\partial x} - D_{zy_{cH}} \frac{\partial cH}{\partial y} \end{bmatrix} [m^2/s]$$
- Concentration gradient
$$\begin{bmatrix} \nabla_x \\ \nabla_y \\ \nabla_z \end{bmatrix} = \begin{bmatrix} \frac{\partial cH}{\partial x} \\ \frac{\partial cH}{\partial y} \\ 0 \end{bmatrix} [mol/m^4]$$
- Diffusive flux magnitude
$$DfluxMag_{cH} = \sqrt{Dflux^2_{x,cH} + Dflux^2_{y,cH} + Dflux^2_{z,cH}}$$
- Total flux magnitude
$$TfluxMag_{cH} = \sqrt{Tflux^2_{x,cH} + Tflux^2_{y,cH} + Tflux^2_{z,cH}}$$

$\mathbf{V_2}$

- Concentration of V_2:
$cV_2 = \frac{(-cHV_2 \times z_{cHV_2} - cH \times z_{cH} - cV_2 \times z_{cV_2} - cV_3 \times z_{cV_3})}{z_{cV_2} + eps} [mol/m^3]$
- Diffusion coefficient
$$\mathbf{D_{cV_2}} = \begin{bmatrix} D_{xx} & D_{xy} & D_{xz} \\ D_{yx} & D_{yy} & D_{yz} \\ D_{zx} & D_{zy} & D_{zz} \end{bmatrix} = \begin{bmatrix} D_{V_2} \varepsilon^{1,5} & 0 & 0 \\ 0 & D_{V_2} \varepsilon^{1,5} & 0 \\ 0 & 0 & D_{V_2} \varepsilon^{1,5} \end{bmatrix} [m^2/s]$$

- Average diffusion coefficient
  $D_{av_{V_2}} = \frac{1}{2}(D_{xx_{V_2}} + D_{yy_{V_2}})[m^2/s]$
- Total flux
  $$Tflux_{cV_2} = \begin{bmatrix} Tflux_x \\ Tflux_y \\ Tflux_y \end{bmatrix} = \begin{bmatrix} D_{xx_{cV_2}} \frac{\partial cV_2}{\partial x} - D_{xy_{cV_2}} \frac{\partial cV_2}{\partial y} + Cflux_{x,cV_2} + Mflux_{x,cV_2} \\ D_{yx_{cV_2}} \frac{\partial cV_2}{\partial x} - D_{yy_{cV_2}} \frac{\partial cV_2}{\partial y} + Cflux_{y,cV_2} + Mflux_{y,cV_2} \\ D_{zx_{cV_2}} \frac{\partial cV_2}{\partial x} - D_{zy_{cV_2}} \frac{\partial cV_2}{\partial y} + Cflux_{z,cV_2} + Mflux_{z,cV_2} \end{bmatrix} [m^2/s$$
- Diffusive flux
  $$Dflux_{cV_2} = \begin{bmatrix} Dflux_x \\ Dflux_y \\ Dflux_y \end{bmatrix} = \begin{bmatrix} D_{xx_{cV_2}} \frac{\partial cV_2}{\partial x} - D_{xy_{cV_2}} \frac{\partial cV_2}{\partial y} \\ D_{yx_{cV_2}} \frac{\partial cV_2}{\partial x} - D_{yy_{cV_2}} \frac{\partial cV_2}{\partial y} \\ D_{zx_{cV_2}} \frac{\partial cV_2}{\partial x} - D_{zy_{cV_2}} \frac{\partial cV_2}{\partial y} \end{bmatrix} [m^2/s]$$
- Concentration gradient
  $$\begin{bmatrix} \nabla_x \\ \nabla_y \\ \nabla_z \end{bmatrix} = \begin{bmatrix} \frac{\partial cV_2}{\partial x} \\ \frac{\partial cV_2}{\partial y} \\ 0 \end{bmatrix} [mol/m^4]$$
- Diffusive flux magnitude
  $DfluxMag_{cV_2} = \sqrt{Dflux^2_{x,cV_2} + Dflux^2_{y,cV_2} + Dflux^2_{z,cV_2}}$
- Total flux magnitude
  $TfluxMag_{cV_2} = \sqrt{Tflux^2_{x,cV_2} + Tflux^2_{y,cV_2} + Tflux^2_{z,cV_2}}$

$\mathbf{V_3}$

- Concentration of V_3:
  $cV_3 = \frac{(-cHV_3 \times z_{cHV_3} - cH \times z_{cH} - cV_3 \times z_{cV_3} - cV_3 \times z_{cV_3})}{z_{cV_3} + eps}[mol/m^3]$
- Diffusion coefficient $\mathbf{D_{c_{V_3}}} = \begin{bmatrix} D_{xx} & D_{xy} & D_{xz} \\ D_{yx} & D_{yy} & D_{yz} \\ D_{zx} & D_{zy} & D_{zz} \end{bmatrix} = \begin{bmatrix} D_{V_3}\varepsilon^{1,5} & 0 & 0 \\ 0 & D_{V_3}\varepsilon^{1,5} & 0 \\ 0 & 0 & D_{V_3}\varepsilon^{1,5} \end{bmatrix} [m^2/s]$
- Average diffusion coefficient
  $D_{av_{V_3}} = \frac{1}{2}(D_{xx_{V_3}} + D_{yy_{V_3}})[m^2/s]$
- Total flux
  $$Tflux_{cV_3} = \begin{bmatrix} Tflux_x \\ Tflux_y \\ Tflux_y \end{bmatrix} =$$
  $$= \begin{bmatrix} D_{xx_{cV_3}} \frac{\partial cV_3}{\partial x} - D_{xy_{cV_3}} \frac{\partial cV_3}{\partial y} + Cflux_{x,cV_3} + Mflux_{x,cV_3} \\ D_{yx_{cV_3}} \frac{\partial cV_3}{\partial x} - D_{yy_{cV_3}} \frac{\partial cV_3}{\partial y} + Cflux_{y,cV_3} + Mflux_{y,cV_3} \\ D_{zx_{cV_3}} \frac{\partial cV_3}{\partial x} - D_{zy_{cV_3}} \frac{\partial cV_3}{\partial y} + Cflux_{z,cV_3} + Mflux_{z,cV_3} \end{bmatrix} [m^2/s]$$
- Diffusive flux
  $$Dflux_{cV_3} = \begin{bmatrix} Dflux_x \\ Dflux_y \\ Dflux_y \end{bmatrix} = \begin{bmatrix} D_{xx_{cV_3}} \frac{\partial cV_3}{\partial x} - D_{xy_{cV_3}} \frac{\partial cV_3}{\partial y} \\ D_{yx_{cV_3}} \frac{\partial cV_3}{\partial x} - D_{yy_{cV_3}} \frac{\partial cV_3}{\partial y} \\ D_{zx_{cV_3}} \frac{\partial cV_3}{\partial x} - D_{zy_{cV_3}} \frac{\partial cV_3}{\partial y} \end{bmatrix} [m^2/s]$$
- Concentration gradient
  $$\begin{bmatrix} \nabla_x \\ \nabla_y \\ \nabla_z \end{bmatrix} = \begin{bmatrix} \frac{\partial cV_3}{\partial x} \\ \frac{\partial cV_3}{\partial y} \\ 0 \end{bmatrix} [mol/m^4]$$

- Diffusive flux magnitude
  $DfluxMag_{cV_3} = \sqrt{Dflux^2_{x,cV_3} + Dflux^2_{y,cV_3} + Dflux^2_{z,cV_3}}$
- Total flux magnitude
  $TfluxMag_{cV_3} = \sqrt{Tflux^2_{x,cV_3} + Tflux^2_{y,cV_3} + Tflux^2_{z,cV_3}}$
- Porosity
  $\varepsilon_p = \varepsilon[1]$
- Velocity field
  $\begin{bmatrix} u \\ v \\ w \end{bmatrix} = \begin{bmatrix} model.input.u1 \\ model.input.u2 \\ model.input.u3 \end{bmatrix} [m/s]$
- Convective flux
  $SO_4\ Cflux = \begin{bmatrix} Cflux_{x,SO_4} \\ Cflux_{y,SO_4} \\ Cflux_{z,SO_4} \end{bmatrix} = \begin{bmatrix} cSO_4model.input.u1 \\ cSO_4model.input.u2 \\ cSO_4model.input.u3 \end{bmatrix}$
- Convective flux magnitude
  $CfluxMag_{cSO_4} = \sqrt{Cflux^2_{x,cSO_4} + Cflux^2_{y,cSO_4} + Cflux^2_{z,cSO_4}}$
- Convective flux
  $HSO_4\ Cflux = \begin{bmatrix} Cflux_{x,HSO_4} \\ Cflux_{y,HSO_4} \\ Cflux_{z,HSO_4} \end{bmatrix} = \begin{bmatrix} cHSO_4model.input.u1 \\ cHSO_4model.input.u2 \\ cHSO_4model.input.u3 \end{bmatrix}$
- Convective flux magnitude
  $CfluxMag_{cHSO_4} = \sqrt{Cflux^2_{x,cHSO_4} + Cflux^2_{y,cHSO_4} + Cflux^2_{z,cHSO_4}}$
- Convective flux
  $H\ Cflux = \begin{bmatrix} Cflux_{x,H} \\ Cflux_{y,H} \\ Cflux_{z,H} \end{bmatrix} = \begin{bmatrix} cHmodel.input.u1 \\ cHmodel.input.u2 \\ cHmodel.input.u3 \end{bmatrix}$
- Convective flux magnitude
  $CfluxMag_{cH} = \sqrt{Cflux^2_{x,cH} + Cflux^2_{y,cH} + Cflux^2_{z,cH}}$
- Convective flux
  $V_2\ Cflux = \begin{bmatrix} Cflux_{x,V_2} \\ Cflux_{y,V_2} \\ Cflux_{z,V_2} \end{bmatrix} = \begin{bmatrix} cV_2model.input.u1 \\ cV_2model.input.u2 \\ cV_2model.input.u3 \end{bmatrix}$
- Convective flux magnitude
  $CfluxMag_{cV_3} = \sqrt{Cflux^2_{x,cV_3} + Cflux^2_{y,cV_3} + Cflux^2_{z,cV_3}}$
- Convective flux
  $V_3\ Cflux = \begin{bmatrix} Cflux_{x,V_3} \\ Cflux_{y,V_3} \\ Cflux_{z,V_3} \end{bmatrix} = \begin{bmatrix} cV_3model.input.u1 \\ cV_3model.input.u2 \\ cV_3model.input.u3 \end{bmatrix}$
- Convective flux magnitude
  $CfluxMag_{cV_3} = \sqrt{Cflux^2_{x,cV_3} + Cflux^2_{y,cV_3} + Cflux^2_{z,cV_3}}$

- electrolyte potential
  $V = \phi_l[V]$
- Charge number
  $z_{cSO_4} = 1[1]$
- Mobility
  $$\mathbf{um_{SO_4}} = \begin{bmatrix} um_{SO_4,xx} & um_{SO_4,xy} & um_{SO_4,xz} \\ um_{SO_4,yx} & um_{SO_4,yy} & um_{SO_4,yz} \\ um_{SO_4,zx} & um_{SO_4,zy} & um_{SO_4,zz} \end{bmatrix} =$$
  $$= \frac{1}{R_{const} Temp} \begin{bmatrix} D_{cSO_4,xx} & D_{cSO_4,xy} & D_{cSO_4,xz} \\ D_{cSO_4,yx} & D_{cSO_4,yy} & D_{cSO_4,yz} \\ D_{cSO_4,zx} & D_{cSO_4,zy} & D_{cSO_4,zz} \end{bmatrix} [s \cdot mol/kg]$$
- Electrophoretic flux
  $$Mflux_{cSO_4} = \begin{bmatrix} Mflux_{x,cSO_4} \\ Mflux_{y,cSO_4} \\ Mflux_{z,cSO_4} \end{bmatrix} = \begin{bmatrix} z_{cHSO_4} F \cdot cSO_4(-um_{SO_4,xx} \frac{\partial V}{\partial x} - um_{SO_4,xy} \frac{\partial V}{\partial y} \\ z_{cHSO_4} F \cdot cSO_4(-um_{SO_4,yx} \frac{\partial V}{\partial x} - um_{SO_4,yy} \frac{\partial V}{\partial y} \\ z_{cHSO_4} F \cdot cSO_4(-um_{SO_4,zx} \frac{\partial V}{\partial x} - um_{SO_4,zy} \frac{\partial V}{\partial y} \end{bmatrix}$$
- Charge number
  $z_{cHSO_4} = -1[1]$
- Mobility
  $$\mathbf{um_{HSO_4}} = \begin{bmatrix} um_{SO_4,xx} & um_{SO_4,xy} & um_{SO_4,xz} \\ um_{SO_4,yx} & um_{SO_4,yy} & um_{SO_4,yz} \\ um_{SO_4,zx} & um_{SO_4,zy} & um_{SO_4,zz} \end{bmatrix} =$$
  $$= \frac{1}{R_{const} Temp} \begin{bmatrix} D_{cSO_4,xx} & D_{cSO_4,xy} & D_{cSO_4,xz} \\ D_{cSO_4,yx} & D_{cSO_4,yy} & D_{cSO_4,yz} \\ D_{cSO_4,zx} & D_{cSO_4,zy} & D_{cSO_4,zz} \end{bmatrix} [s \cdot mol/kg]$$
- Electrophoretic flux
  $$Mflux_{cHSO_4} = \begin{bmatrix} Mflux_{x,cHSO_4} \\ Mflux_{y,cHSO_4} \\ Mflux_{z,cHSO_4} \end{bmatrix} =$$
  $$= \begin{bmatrix} z_{cHHSO_4} F \cdot cHSO_4(-um_{SO_4,xx} \frac{\partial V}{\partial x} - um_{SO_4,xy} \frac{\partial V}{\partial y} \\ z_{cHHSO_4} F \cdot cHSO_4(-um_{SO_4,yx} \frac{\partial V}{\partial x} - um_{SO_4,yy} \frac{\partial V}{\partial y} \\ z_{cHHSO_4} F \cdot cHSO_4(-um_{SO_4,zx} \frac{\partial V}{\partial x} - um_{SO_4,zy} \frac{\partial V}{\partial y} \end{bmatrix}$$
- Charge number
  $z_{cH} = 1[1]$
- Mobility
  $$\mathbf{um_H} = \begin{bmatrix} um_{SO_4,xx} & um_{SO_4,xy} & um_{SO_4,xz} \\ um_{SO_4,yx} & um_{SO_4,yy} & um_{SO_4,yz} \\ um_{SO_4,zx} & um_{SO_4,zy} & um_{SO_4,zz} \end{bmatrix} =$$
  $$= \frac{1}{R_{const} Temp} \begin{bmatrix} D_{cSO_4,xx} & D_{cSO_4,xy} & D_{cSO_4,xz} \\ D_{cSO_4,yx} & D_{cSO_4,yy} & D_{cSO_4,yz} \\ D_{cSO_4,zx} & D_{cSO_4,zy} & D_{cSO_4,zz} \end{bmatrix} [s \cdot mol/kg]$$
- Electrophoretic flux

$$Mflux_{cH} = \begin{bmatrix} Mflux_{x,cH} \\ Mflux_{y,cH} \\ Mflux_{z,cH} \end{bmatrix} = \begin{bmatrix} z_{cH}F \cdot cH(-um_{SO_4,xx}\frac{\partial V}{\partial x} - um_{SO_4,xy}\frac{\partial V}{\partial y} \\ z_{cH}F \cdot cH(-um_{SO_4,yx}\frac{\partial V}{\partial x} - um_{SO_4,yy}\frac{\partial V}{\partial y} \\ z_{cH}F \cdot cH(-um_{SO_4,zx}\frac{\partial V}{\partial x} - um_{SO_4,zy}\frac{\partial V}{\partial y} \end{bmatrix}$$

- Charge number
  $z_{cV_2} = -1[1]$

- Mobility
  $$\mathbf{um_{V_2}} = \begin{bmatrix} um_{SO_4,xx} & um_{SO_4,xy} & um_{SO_4,xz} \\ um_{SO_4,yx} & um_{SO_4,yy} & um_{SO_4,yz} \\ um_{SO_4,zx} & um_{SO_4,zy} & um_{SO_4,zz} \end{bmatrix} =$$
  $$= \frac{1}{R_{const}Temp} \begin{bmatrix} D_{cSO_4,xx} & D_{cSO_4,xy} & D_{cSO_4,xz} \\ D_{cSO_4,yx} & D_{cSO_4,yy} & D_{cSO_4,yz} \\ D_{cSO_4,zx} & D_{cSO_4,zy} & D_{cSO_4,zz} \end{bmatrix} [s \cdot mol/kg]$$

- Electrophoretic flux
  $$Mflux_{cV_2} = \begin{bmatrix} Mflux_{x,cV_2} \\ Mflux_{y,cV_2} \\ Mflux_{z,cV_2} \end{bmatrix} = \begin{bmatrix} z_{cV_2}F \cdot cV_2(-um_{V_2,xx}\frac{\partial V}{\partial x} - um_{V_2,xy}\frac{\partial V}{\partial y} \\ z_{cV_2}F \cdot cV_2(-um_{V_2,yx}\frac{\partial V}{\partial x} - um_{V_2,yy}\frac{\partial V}{\partial y} \\ z_{cV_2}F \cdot cV_2(-um_{V_2,zx}\frac{\partial V}{\partial x} - um_{V_2,zy}\frac{\partial V}{\partial y} \end{bmatrix}$$

- Charge number
  $z_{cV_3} = -1[1]$

- Mobility
  $$\mathbf{um_{V_3}} = \begin{bmatrix} um_{V_3,xx} & um_{V_3,xy} & um_{V_3,xz} \\ um_{V_3,yx} & um_{V_3,yy} & um_{V_3,yz} \\ um_{V_3,zx} & um_{V_3,zy} & um_{V_3,zz} \end{bmatrix} =$$
  $$= \frac{1}{R_{const}Temp} \begin{bmatrix} D_{cV_3,xx} & D_{cV_3,xy} & D_{cV_3,xz} \\ D_{cV_3,yx} & D_{cV_3,yy} & D_{cV_3,yz} \\ D_{cV_3,zx} & D_{cV_3,zy} & D_{cV_3,zz} \end{bmatrix} [s \cdot mol/kg]$$

- Electrophoretic flux
  $$Mflux_{cV_3} = \begin{bmatrix} Mflux_{x,cV_3} \\ Mflux_{y,cV_3} \\ Mflux_{z,cV_3} \end{bmatrix} = \begin{bmatrix} z_{cHV_3}F \cdot cV_3(-um_{SO_4,xx}\frac{\partial V}{\partial x} - um_{SO_4,xy}\frac{\partial V}{\partial y} \\ z_{cHV_3}F \cdot cV_3(-um_{SO_4,yx}\frac{\partial V}{\partial x} - um_{SO_4,yy}\frac{\partial V}{\partial y} \\ z_{cHV_3}F \cdot cV_3(-um_{SO_4,zx}\frac{\partial V}{\partial x} - um_{SO_4,zy}\frac{\partial V}{\partial y}) \end{bmatrix}$$

- Element size
  $helem = h[m]$

- Equation residual

$$
\begin{aligned}
Res_{cHSO_4} = & -D_{cHSO_{4,xx}}\frac{\partial^2 cHSO_4}{\partial x^2} - D_{cHSO_{4,xy}}\frac{\partial^2 cHSO_4}{\partial x \partial y} \\
& - D_{cHSO_{4,yx}}\frac{\partial^2 cHSO_4}{\partial y \partial x} - D_{cHSO_{4,yy}}\frac{\partial^2 cHSO_4}{\partial y^2} + \\
& + \frac{\partial}{\partial x}(cHSO_4 z_{cHSO_4} F(-um_{HSO_{4,xx}}\frac{\partial \phi_l}{\partial x} - um_{HSO_{4,xy}}\frac{\partial \phi_l}{\partial y})) \\
& + \frac{\partial}{\partial y}(cHSO_4 z_{cHSO_4} F(-um_{HSO_{4,yx}}\frac{\partial \phi_l}{\partial x} - um_{HSO_{4,xy}}\frac{\partial \phi_l}{\partial y})) + \\
& + u\frac{\partial cHSO_4}{\partial x} + v\frac{\partial cHSO_4}{\partial y} - R_{cHSO_4}[mol/m^3 s]
\end{aligned}
\tag{A.1}
$$

- Equation residual

$$
\begin{aligned}
Res_{cH} = & -D_{cH_{xx}}\frac{\partial^2 cH}{\partial x^2} - D_{cH_{xy}}\frac{\partial^2 cH}{\partial x \partial y} \\
& - D_{cH_{yx}}\frac{\partial^2 cH}{\partial y \partial x} - D_{cH_{yy}}\frac{\partial^2 cH}{\partial y^2} + \\
& + \frac{\partial}{\partial x}(cH z_{cH} F(-um_{H_{xx}}\frac{\partial \phi_l}{\partial x} - um_{H_{xy}}\frac{\partial \phi_l}{\partial y})) \\
& + \frac{\partial}{\partial y}(cH z_{cH} F(-um_{H_{yx}}\frac{\partial \phi_l}{\partial x} - um_{H_{xy}}\frac{\partial \phi_l}{\partial y})) + \\
& + u\frac{\partial cH}{\partial x} + v\frac{\partial cH}{\partial y} - R_{cH}[mol/m^3 s]
\end{aligned}
\tag{A.2}
$$

- Equation residual

$$
\begin{aligned}
Res_{cV_2} = & -D_{cV_{2,xx}}\frac{\partial^2 cV_2}{\partial x^2} - D_{cV_{2,xy}}\frac{\partial^2 cV_2}{\partial x \partial y} \\
& - D_{cV_{2,yx}}\frac{\partial^2 cV_2}{\partial y \partial x} - D_{cV_{2,yy}}\frac{\partial^2 cV_2}{\partial y^2} + \\
& + \frac{\partial}{\partial x}(cV_2 z_{cV_2} F(-um_{V_{2,xx}}\frac{\partial \phi_l}{\partial x} - um_{V_{2,xy}}\frac{\partial \phi_l}{\partial y})) \\
& + \frac{\partial}{\partial y}(cV_2 z_{cV_2} F(-um_{V_{2,yx}}\frac{\partial \phi_l}{\partial x} - um_{V_{2,xy}}\frac{\partial \phi_l}{\partial y})) + \\
& + u\frac{\partial cV_2}{\partial x} + v\frac{\partial cV_2}{\partial y} - R_{cV_2}[mol/m^3 s]
\end{aligned}
\tag{A.3}
$$

- Equation residual

$$
\begin{aligned}
Res_{cV_3} = & -D_{cV_{3,xx}}\frac{\partial^3 cV_3}{\partial x^3} - D_{cV_{3,xy}}\frac{\partial^3 cV_3}{\partial x \partial y} \\
& - D_{cV_{3,yx}}\frac{\partial^3 cV_3}{\partial y \partial x} - D_{cV_{3,yy}}\frac{\partial^3 cV_3}{\partial y^2} + \\
& + \frac{\partial}{\partial x}(cV_3 z_{cV_3} F(-um_{V_{3,xx}}\frac{\partial \phi_l}{\partial x} - um_{V_{3,xy}}\frac{\partial \phi_l}{\partial y})) \\
& + \frac{\partial}{\partial y}(cV_3 z_{cV_3} F(-um_{V_{3,yx}}\frac{\partial \phi_l}{\partial x} - um_{V_{3,xy}}\frac{\partial \phi_l}{\partial y})) + \\
& + u\frac{\partial cV_3}{\partial x} + v\frac{\partial cV_3}{\partial y} - R_{cV_3}[mol/m^3 s]
\end{aligned}
\tag{A.4}
$$

- Electrolyte current density vector

$$
\mathbf{Il} = \begin{bmatrix} Ilx \\ Ily \\ Ilz \end{bmatrix} =
$$

$$
\begin{aligned}
Il_x = & F(z_{cSO_4}(-D_{cSO_{4,xx}}\frac{\partial cSO_4}{\partial x} - D_{cSO_{4,xy}}\frac{\partial cSO_4}{\partial y}) - z_{cSO_4} um_{cSO_{4,xx}} FcSO_4 \frac{\partial \phi_l}{\partial x} + \\
& - z_{cSO_4} um_{cSO_{4,xy}} FcSO_4 \frac{\partial \phi_l}{\partial y}) + \\
& + z_c HSO_4(-D_{cHSO_{4,xx}}\frac{\partial cHSO_4}{\partial x} - D_{cHSO_{4,xy}}\frac{\partial cHSO_4}{\partial y} \\
& - z_{cHSO_4} um_{cHSO_{4,xx}} FcHSO_4 \frac{\partial \phi_l}{\partial x} + \\
& - z_{cHSO_4} um_{cHSO_{4,xy}} FcHSO_4 \frac{\partial \phi_l}{\partial y}) + \\
& + z_{cH}(-D_{cH_{xx}}\frac{\partial cH}{\partial x} - D_{cH_{xy}}\frac{\partial cH}{\partial y} - z_{cH} um_{cH_{xx}} FcH \frac{\partial \phi_l}{\partial x} + \\
& - z_{cH} um_{cH_{xy}} FcH \frac{\partial \phi_l}{\partial y}) + \\
& + z_{cV2}(-D_{cV_{2,xx}}\frac{\partial cV_2}{\partial x} - D_{cV_{2,xy}}\frac{\partial cV_2}{\partial y} - z_{cV_2} um_{cV_{2,xx}} FcV_2 \frac{\partial \phi_l}{\partial x} + \\
& - z_{cV_2} um_{cV_{2,xy}} FcV_2 \frac{\partial \phi_l}{\partial y}) + \\
& + z_{cV_3}(-D_{cV_{3,xx}}\frac{\partial cV_3}{\partial x} - D_{c_V 3,xy}\frac{\partial cV_3}{\partial y} - z_{cV_3} um_{cV_{3,xx}} FcV_3 \frac{\partial \phi_l}{\partial x} + \\
& - z_{cV_3} um_{cV_{3,xy}} FcV_3 \frac{\partial \phi_l}{\partial y})
\end{aligned}
\tag{A.5}
$$

$$
\begin{aligned}
Il_y = F(&z_{cSO_4}(-D_{cSO_{4,yx}}\frac{\partial cSO_4}{\partial x} - D_{cSO_{4,yy}}\frac{\partial cSO_4}{\partial y})+\\
&- z_{cSO_4}um_{cSO_{4,yx}}FcSO_4\frac{\partial \phi_l}{\partial x} - z_{cSO_4}um_{cSO_{4,yy}}FcSO_4\frac{\partial \phi_l}{\partial y})+\\
&+ z_cHSO_4(-D_{cHSO_{4,yx}}\frac{\partial cHSO_4}{\partial x} - D_{cHSO_{4,yy}}\frac{\partial cHSO_4}{\partial y}+\\
&- z_{cHSO_4}um_{cHSO_{4,yx}}FcHSO_4\frac{\partial \phi_l}{\partial x} - z_{cHSO_4}um_{cHSO_{4,yy}}FcHSO_4\frac{\partial \phi_l}{\partial y})+\\
&+ z_{cH}(-D_{cH_{yx}}\frac{\partial cH}{\partial x} - D_{cH_{yy}}\frac{\partial cH}{\partial y} - z_{cH}um_{cH_{yx}}FcH\frac{\partial \phi_l}{\partial x} - z_{cH}um_{cH_{yy}}FcH\frac{\partial \phi_l}{\partial y})+\\
&+ z_{cV2}(-D_{cV_{2,yx}}\frac{\partial cV_2}{\partial x} - D_{cV_{2,yy}}\frac{\partial cV_2}{\partial y} - z_{cV_2}um_{cV_{2,yx}}FcV_2\frac{\partial \phi_l}{\partial x}+\\
&- z_{cV_2}um_{cV_{2,yy}}FcV_2\frac{\partial \phi_l}{\partial y})+\\
&+ z_{cV_3}(-D_{cV_{3,yx}}\frac{\partial cV_3}{\partial x} - D_{c_V3,yy}\frac{\partial cV_3}{\partial y} - z_{cV_3}um_{cV_{3,yx}}FcV_3\frac{\partial \phi_l}{\partial x}+\\
&- z_{cV_3}um_{cV_{3,yy}}FcV_3\frac{\partial \phi_l}{\partial y})
\end{aligned}
\tag{A.6}
$$

$$
\begin{aligned}
Il_z = F(&z_{cSO_4}(-D_{cSO_{4,zx}}\frac{\partial cSO_4}{\partial x} - D_{cSO_{4,zy}}\frac{\partial cSO_4}{\partial y})+\\
&- z_{cSO_4}um_{cSO_{4,zx}}FcSO_4\frac{\partial \phi_l}{\partial x} - z_{cSO_4}um_{cSO_{4,zy}}FcSO_4\frac{\partial \phi_l}{\partial y})+\\
&+ z_cHSO_4(-D_{cHSO_{4,zx}}\frac{\partial cHSO_4}{\partial x} - D_{cHSO_{4,zy}}\frac{\partial cHSO_4}{\partial y}+\\
&- z_{cHSO_4}um_{cHSO_{4,zx}}FcHSO_4\frac{\partial \phi_l}{\partial x} - z_{cHSO_4}um_{cHSO_{4,zy}}FcHSO_4\frac{\partial \phi_l}{\partial y})+\\
&+ z_{cH}(-D_{cH_{zx}}\frac{\partial cH}{\partial x} - D_{cH_{zy}}\frac{\partial cH}{\partial y} - z_{cH}um_{cH_{zx}}FcH\frac{\partial \phi_l}{\partial x}+\\
&- z_{cH}um_{cH_{zy}}FcH\frac{\partial \phi_l}{\partial y})+\\
&+ z_{cV2}(-D_{cV_{2,zx}}\frac{\partial cV_2}{\partial x} - D_{cV_{2,zy}}\frac{\partial cV_2}{\partial y} - z_{cV_2}um_{cV_{2,zx}}FcV_2\frac{\partial \phi_l}{\partial x}+\\
&- z_{cV_2}um_{cV_{2,zy}}FcV_2\frac{\partial \phi_l}{\partial y})+\\
&+ z_{cV_3}(-D_{cV_{3,zx}}\frac{\partial cV_3}{\partial x} - D_{c_V3,zy}\frac{\partial cV_3}{\partial y} - z_{cV_3}um_{cV_{3,zx}}FcV_3\frac{\partial \phi_l}{\partial x}+\\
&- z_{cV_3}um_{cV_{3,zy}}FcV_3\frac{\partial \phi_l}{\partial y})
\end{aligned}
\tag{A.7}
$$

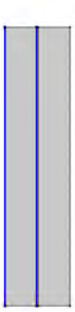

Figure A.2: Boundaries1-4

- Total power dissipation density
  $Qh = -Il_x \frac{\partial \phi_l}{\partial x} - Il_y \frac{\partial \phi_l}{\partial y} - is_x \frac{\partial \phi_s}{\partial x} - is_y \frac{\partial \phi_s}{\partial y} [W/m^3]$
- Current source
  $Q_{li} = 0$
- Electrode current density
  $$\mathbf{I_s} = \begin{bmatrix} Is_x \\ Is_y \\ Is_z \end{bmatrix} = \begin{bmatrix} -\sigma_{xx} \frac{\partial \phi s}{\partial x} - \sigma_{xy} \frac{\partial \phi s}{\partial y} \\ -\sigma_{yx} \frac{\partial \phi s}{\partial x} - \sigma_{yy} \frac{\partial \phi s}{\partial y} \\ -\sigma_{zx} \frac{\partial \phi s}{\partial x} - \sigma_{zy} \frac{\partial \phi s}{\partial y} \end{bmatrix} [A/m^2]$$
- Temperature
  $Temp = mode.input.minput_temperature[K]$
- Electrode reaction source
  $Iv_{tot} = 0[A/m^3]$
- Electrical conductivity
  $$\sigma = \begin{bmatrix} \sigma_{xx} & \sigma_{xy} & \sigma_{xz} \\ \sigma_{yx} & \sigma_{yy} & \sigma_{yz} \\ \sigma_{zx} & \sigma_{zy} & \sigma_{zz} \end{bmatrix} = \begin{bmatrix} \sigma_e & 0 & 0 \\ 0 & \sigma_e & 0 \\ 0 & 0 & \sigma_e \end{bmatrix}$$

2. **Porous electrode, negative** the equations of the boundaries 1 and 4 (fig A.2)

   - Convective boundary flux
     $CBF_{cHSO_4} = 0$
   - Convective boundary flux
     $CBF_{cH} = 0$
   - Convective boundary flux
     $CBF_{cV_2} = 0$
   - Convective boundary flux
     $CBF_{cV_3} = 0$

3. **Reactions** of the domain 1 (fig A.1)

   - Total rate expression
     $R_{cHSO_4} = r_d \varepsilon_p [mol/m^3 s]$

- Total rate expression
  $R_{cH} = -r_d \varepsilon_p [mol/m^3 s]$
- Total rate expression
  $R_{cV_2} = 0 [mol/m^3 s]$
- Total rate expression
  $R_{cV_3} = 0 [mol/m^3 s]$
- Total rate expression
  $R_{cSO_4} = -r_d \varepsilon_p [mol/m^3 s]$

4. **Porous electrode reaction (per),negative** equations of domain 1 (fig A.1)

   - Total rate expression
     $R_{cHSO_4} = R_{cHSO_{4,per}} [mol/(m^3 s)]$
   - Total rate expression
     $R_{cH} = R_{cH_{per}} [mol/(m^3 s)]$
   - Total rate expression
     $R_{cV_2} = R_{cV_{2,per}} [mol/(m^3 s)]$
   - Total rate expression
     $R_{cV_3} = R_{cV_{3,per}} [mol/(m^3 s)]$
   - Total power dissipation density
     $Q_{rev} + Q_{irrev} [W/m^3]$
   - Electrode reaction source
     $iv_{tot} = iv [A/m^3]$
   - Local current source
     $iv = i_{loc} Av [A/m^3]$
   - Local current source
     $pce1.iv = iv [A/m^3]$
   - Cathodic transfer coefficient
     $\alpha_c = \alpha_{neg}$
   - Anodic transfer coefficient
     $\alpha_a = 1 - \alpha_{neg}$
   - Exchange current density
     $i0 = i0_{neg} [A/m^2]$
   - Local current density
     $i_{loc} = i0 \left(e^{\frac{\alpha_a F \eta}{R * Temp}} - e^{\frac{-\alpha_c F \eta}{R * Temp}} \right) [A/m^2]$
   - Total interface current density
     $i_{tot} = i_{loc} [A/m^2]$
   - Active specific surface area
     $Av = a [1/m]$

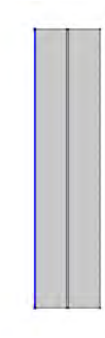

Figure A.3: boundary1

- Irreversible heat source
  $Q_{irrev} = iv\eta[W/m^3]$
- Reversible heat source
  $ivTemp\frac{dE_{eq}}{dt}[W/m^3]$
- Temperature derivative of equilibrium potential
  $\frac{dE_{eq}}{dT} = 0[V/K]$
- Overpotential
  $\phi_s - \phi_l - E_eq[V]$
- Stoichiometric coefficient
  $Vi_{0,cSO_4} = 0[1]$
- Stoichiometric coefficient
  $Vi_{0,cHSO_4} = 0[1]$
- Stoichiometric coefficient
  $Vi_{0,cH} = 0[1]$
- Stoichiometric coefficient
  $Vi_{0,cV_2} = 1[1]$
- Stoichiometric coefficient
  $Vi_{0,cV_3} = -1[1]$
- Total rate expression
  $R_{cHSO_4} = 0$
- Total rate expression
  $R_{cH} = 0$
- Total rate expression
  $R_{cV_2} = -\frac{iv}{F}$
- Total rate expression
  $R_{cV_3} = \frac{iv}{F}$

5. **Electric ground** of boundary1 (fig A.3)

   - Boundary electric potential
     $\phi_{s,BND} = 0[V]$

Figure A.4: boundary2

- Constraint
  $\phi_{s,BND} - \phi_s = 0[V]$

6. **No flux, negative** the equations of the boundaries 1-4 (fig A.2)
   - Convective boundary flux
     $CBF_{HSO_4} = cHSO_4(un_{x,mesh} + vn_{y,mesh} + wn_{z,mesh})$
   - Convective boundary flux
     $CBF_H = cH(un_{x,mesh} + vn_{y,mesh} + wn_{z,mesh})$
   - Convective boundary flux
     $CBF_{V_2} = cV_2(un_{x,mesh} + vn_{y,mesh} + wn_{z,mesh})$
   - Convective boundary flux
     $CBF_{V_3} = cV_3(un_{x,mesh} + vn_{y,mesh} + wn_{z,mesh})$

7. **Concentration,negative** the equation of boundary2 (fig A.4)
   - Concentration
     $c0_{HSO_4} = cHSO_{4,0}[mol/m^3]$
   - Concentration
     $c0_H = cH_0[mol/m^3]$
   - Concentration
     $c0_{V_2} = cV_{2,0}[mol/m^3]$
   - Concentration
     $c0_{V_3} = cV_{3,0}[mol/m^3]$
   - Constraint
     $-cHSO_4 + c0_{HSO_4} = 0[mol/m^3]$
   - Constraint
     $-cH + c0_H = 0[mol/m^3]$
   - Constraint
     $-cV_2 + c0_{V_2} = 0[mol/m^3]$
   - Constraint
     $-cV_3 + c0_{V_3} = 0[mol/m^3]$

Figure A.5: boundary3

8. **Outflow, negative** the equations of boundary 3, weak expressions (fig A.5)

- Integration frame: material

$$
\begin{aligned}
&- z_{cHSO_4} * F * cHSO_4 * (-n_x * (um_{cHSO_{4,xx}} * mean(\frac{\partial \phi_l}{\partial x}) + \\
&+ um_{cHSO_{4,xy}} * mean(\frac{\partial \phi_l}{\partial y}) + um_{cHSO_{4,xz}} * mean(0)) - ny * (um_{cHSO_{4,yx}} * mean(\frac{\partial \phi_l}{\partial x}) + \\
&+ um_{cHSO_{4,yy}} * mean(\frac{\partial \phi_l}{\partial y}) + um_{cHSO_{4,yz}} * mean(0)) - nz * (um_{cHSO_{4,zx}} * mean(\frac{\partial \phi_l}{\partial x}) + \\
&+ um_{cHSO_{4,zy}} * mean(\frac{\partial \phi_l}{\partial y}) + um_{cHSO_{4,zz}} * mean(0))) * test(cHSO_4)
\end{aligned}
\tag{A.8}
$$

- Integration frame: material

$$
\begin{aligned}
&- z_cH * F * cH * (-nx * (um_{cH_{xx}} * mean(\frac{\partial \phi_l}{\partial x}) + \\
&+ um_{cH_{xy}} * mean(\frac{\partial \phi_l}{\partial y}) + um_{cH_{xz}} * mean(0)) - ny * (um_{cH_{yx}} * mean(\frac{\partial \phi_l}{\partial x}) + \\
&+ um_{cH_{yy}} * mean(\frac{\partial \phi_l}{\partial y}) + um_{cH_{yz}} * mean(0)) - nz * (um_{cH_{zx}} * mean(\frac{\partial \phi_l}{\partial x}) + \\
&+ um_{cH_{zy}} * mean(\frac{\partial \phi_l}{\partial y}) + um_{cH_{zz}} * mean(0))) * test(cH)
\end{aligned}
\tag{A.9}
$$

- Integration frame: material

$$
\begin{aligned}
&- z_cV_2 * F * cV_2 * (-nx * (um_{cV_{2,xx}} * mean(\frac{\partial \phi_l}{\partial x}) + \\
&+ um_{cV_{2,xy}} * mean(\frac{\partial \phi_l}{\partial y}) + um_{cV_{2,xz}} * mean(0)) - ny * (um_{cV_{2,yx}} * mean(\frac{\partial \phi_l}{\partial x}) + \\
&+ um_{cV_{2,yy}} * mean(\frac{\partial \phi_l}{\partial y}) + um_{cV_{2,yz}} * mean(0)) - nz * (um_{cV_{2,zx}} * mean(\frac{\partial \phi_l}{\partial x}) + \\
&+ um_{cV_{2,zy}} * mean(\frac{\partial \phi_l}{\partial y}) + um_{cV_{2,zz}} * mean(0))) * test(cV_2)
\end{aligned}
\tag{A.10}
$$

- Integration frame: material

$$
\begin{aligned}
&- z_cV_3 * F * cV_3 * (-nx * (um_{cV_{3,xx}} * mean(\frac{\partial \phi_l}{\partial x}) + \\
&+ um_{cV_{3,xy}} * mean(\frac{\partial \phi_l}{\partial y}) + um_{cV_{3,xz}} * mean(0)) - ny * (um_{cV_{3,yx}} * mean(\frac{\partial \phi_l}{\partial x}) + \\
&+ um_{cV_{3,yy}} * mean(\frac{\partial \phi_l}{\partial y}) + um_{cV_{3,yz}} * mean(0)) - nz * (um_{cV_{3,zx}} * mean(\frac{\partial \phi_l}{\partial x}) + \\
&+ um_{cV_{3,zy}} * mean(\frac{\partial \phi_l}{\partial y}) + um_{cV_{3,zz}} * mean(0))) * test(cV_3)
\end{aligned}
\tag{A.11}
$$

9. **Tertiary current distribution, negative** the equations of domain1, (fig A.1)

- Total rate expression
  $R_{cHSO_4} = 0[mol/(m^3 s)]$
- Total rate expression
  $R_{cH} = 0[mol/(m^3 s)]$
- Total rate expression
  $R_{cV_2} = 0[mol/(m^3 s)]$
- Total rate expression
  $R_{cv_3} = 0[mol/(m^3 s)]$
- Current source
  $Qsi = 0[A/m^3]$
- Domain Flux
  $Domflux(\frac{\partial \phi_l}{\partial x}) = Il_x[A/m^2]$
- Domain Flux
  $Domflux(\frac{\partial \phi_l}{\partial y}) = Il_y[A/m^2]$
- Domain Flux
  $Domflux(\frac{\partial \phi_s}{\partial x}) = Is_x[A/m^2]$
- Domain Flux
  $Domflux(\frac{\partial \phi_s}{\partial x}) = Is_y[A/m^2]$
- Domain Flux
  $Domflux(\frac{\partial cSO_4}{\partial x}) = Dflux_{cSO_{4,x}} + Mflux_{cSO_{4,x}}[mol/(m^2 s)]$
- Domain Flux
  $Domflux(\frac{\partial cSO_4}{\partial y}) = Dflux_{cSO_{4,y}} + Mflux_{cSO_{4,y}}[mol/(m^2 s)]$
- Domain Flux
  $Domflux(\frac{\partial cHSO_4}{\partial x}) = Dflux_{cHSO_{4,x}} + Mflux_{cHSO_{4,x}}[mol/(m^2 s)]$
- Domain Flux
  $Domflux(\frac{\partial cHSO_4}{\partial y}) = Dflux_{cHSO_{4,y}} + Mflux_{cHSO_{4,y}}[mol/(m^2 s)]$
- Domain Flux
  $Domflux(\frac{\partial cH}{\partial x}) = Dflux_{cH_x} + Mflux_{cH_x}[mol/(m^2 s)]$

- Domain Flux
  $Domflux(\frac{\partial cH}{\partial y}) = Dflux_{cH_y} + Mflux_{cH_y}[mol/(m^2 s)]$
- Domain Flux $Domflux(\frac{\partial cV_2}{\partial x}) = Dflux_{cV_{2,x}} + Mflux_{cV_{2,x}}[mol/(m^2 s)]$
- Domain Flux
  $Domflux(\frac{\partial cV_2}{\partial y}) = Dflux_{cV_{2,y}} + Mflux_{cV_{2,y}}[mol/(m^2 s)]$
- Domain Flux
  $Domflux(\frac{\partial cV_3}{\partial x}) = Dflux_{cV_{3,x}} + Mflux_{cV_{3,x}}[mol/(m^2 s)]$
- Domain Flux
  $Domflux(\frac{\partial cV_3}{\partial y}) = Dflux_{cV_{3,y}} + Mflux_{cV_{3,y}}[mol/(m^2 s)]$
- Thickness
  $d = 1[m]$

10. **Tertiary current distribution, negative** the equations of boundaries1-4, (fig A.2)

- Inward electrolyte current density
  $ni_l = 0[A/m^2]$
- Inward electrode current density
  $ni_s = 0[A/m^2]$
- Normal vector
  $\mathbf{N} = \begin{bmatrix} N_x \\ N_y \\ N_z \end{bmatrix} = \begin{bmatrix} dn_x \\ dn_y \\ 0 \end{bmatrix}$
- Normal vector
  $\mathbf{N_{mesh}} = \begin{bmatrix} N_{x,mesh} \\ N_{y,mesh} \\ N_{z,mesh} \end{bmatrix} = \begin{bmatrix} root.dn_{x,mesh} \\ root.dn_{y,mesh} \\ 0 \end{bmatrix}$
- Normal electrolyte current density
  $Ni_l = BNDflux_{\phi_l}[A/m^2]$
- Normal electrolyte current density
  $Ni_s = BNDflux_{\phi_s}[A/m^2]$
- Normal vector
  $\mathbf{N_c} = \begin{bmatrix} N_{x,c} \\ N_{y,c} \\ N_{z,c} \end{bmatrix} = \begin{bmatrix} root.nxc/\sqrt{root.nxc^2 + root.nyc^2} \\ root.nyc/\sqrt{root.nxc^2 + root.nyc^2} \\ 0 \end{bmatrix}$
- Boundary flux
  $BNDflux_{cHSO_4} = -Dflux\_spatial_{cHSO_4}[mol/(m^2 s)]$
- Normal total flux
  $NTflux_{cHSO_4} = BNDflux_{cHSO_4} + Cflux_{cHSO_{4,x}} \cdot n_{x,c} + Cflux_{cHSO_{4,y}} \cdot n_{y,c} + Cflux_{cHSO_{4,z}} \cdot n_{z,c}[mol/(m^2 s)]$
- Normal diffusive flux
  $NDflux_{cHSO_4} = Dflux_{cHSO_{4,x}} \cdot n_{x,c} + Dflux_{cHSO_{4,y}} \cdot n_{y,c} + Dflux_{cHSO_{4,z}} \cdot n_{z,c}[mol/(m^2 s)]$

- Normal convective flux
  $NCflux_{cHSO_4} = Cflux_{cHSO_{4,x}} \cdot n_{x,c} + Cflux_{cHSO_{4,y}} \cdot n_{y,c} + Cflux_{cHSO_{4,z}} \cdot n_{z,c} [mol/(m^2 s)]$
- Normal electrophoretix flux
  $NMflux_{cHSO_4} = Mflux_{cHSO_{4,x}} \cdot n_{x,c} + Mflux_{cHSO_{4,y}} \cdot n_{y,c} + Mflux_{cHSO_{4,z}} \cdot n_{z,c} [mol/(m^2 s)]$
- Boundary flux
  $BNDflux_{cH} = -Dflux\_spatial_{cH} [mol/(m^2 s)]$
- Normal total flux
  $NTflux_{cH} = BNDflux_{cH} + Cflux_{cH_x} \cdot n_{x,c} + Cflux_{cH_y} \cdot n_{y,c} + Cflux_{cH_z} \cdot n_{z,c} [mol/(m^2 s)]$
- Normal diffusive flux
  $NDflux_{cH} = Dflux_{cH_x} \cdot n_{x,c} + Dflux_{cH_y} \cdot n_{y,c} + Dflux_{cH_z} \cdot n_{z,c} [mol/(m^2 s)]$
- Normal convective flux
  $NCflux_{cH} = Cflux_{cH_x} \cdot n_{x,c} + Cflux_{cH_y} \cdot n_{y,c} + Cflux_{cH_z} \cdot n_{z,c} [mol/(m^2 s)]$
- Normal electrophoretix flux
  $NMflux_{cH} = Mflux_{cH_x} \cdot n_{x,c} + Mflux_{cH_y} \cdot n_{y,c} + Mflux_{cH_z} \cdot n_{z,c} [mol/(m^2 s)]$
- Boundary flux
  $BNDflux_{cV_2} = -Dflux\_spatial_{cV_2} [mol/(m^2 s)]$
- Normal total flux
  $NTflux_{cV_2} = BNDflux_{cV_2} + Cflux_{cV_{2,x}} \cdot n_{x,c} + Cflux_{cV_{2,y}} \cdot n_{y,c} + Cflux_{cV_{2,z}} \cdot n_{z,c} [mol/(m^2 s)]$
- Normal diffusive flux
  $NDflux_{cV_2} = Dflux_{cV_{2,x}} \cdot n_{x,c} + Dflux_{cV_{2,y}} \cdot n_{y,c} + Dflux_{cV_{2,z}} \cdot n_{z,c} [mol/(m^2 s)]$
- Normal convective flux
  $NCflux_{cV_2} = Cflux_{cV_{2,x}} \cdot n_{x,c} + Cflux_{cV_{2,y}} \cdot n_{y,c} + Cflux_{cV_{2,z}} \cdot n_{z,c} [mol/(m^2 s)]$
- Normal electrophoretix flux
  $NMflux_{cV_2} = Mflux_{cV_{2,x}} \cdot n_{x,c} + Mflux_{cV_{2,y}} \cdot n_{y,c} + Mflux_{cV_{2,z}} \cdot n_{z,c} [mol/(m^2 s)]$
- Boundary flux
  $BNDflux_{cV_3} = -Dflux\_spatial_{cV_3} [mol/(m^2 s)]$
- Normal total flux
  $NTflux_{cV_3} = BNDflux_{cV_3} + Cflux_{cV_{3,x}} \cdot n_{x,c} + Cflux_{cV_{3,y}} \cdot n_{y,c} + Cflux_{cV_{3,z}} \cdot n_{z,c} [mol/(m^2 s)]$
- Normal diffusive flux
  $NDflux_{cV_3} = Dflux_{cV_{3,x}} \cdot n_{x,c} + Dflux_{cV_{3,y}} \cdot n_{y,c} + Dflux_{cV_{3,z}} \cdot n_{z,c} [mol/(m^2 s)]$
- Normal convective flux
  $NCflux_{cV_3} = Cflux_{cV_{3,x}} \cdot n_{x,c} + Cflux_{cV_{3,y}} \cdot n_{y,c} + Cflux_{cV_{3,z}} \cdot n_{z,c} [mol/(m^2 s)]$
- Normal electrophoretix flux
  $NMflux_{cV_3} = Mflux_{cV_{3,x}} \cdot n_{x,c} + Mflux_{cV_{3,y}} \cdot n_{y,c} + Mflux_{cV_{3,z}} \cdot n_{z,c} [mol/(m^2 s)]$

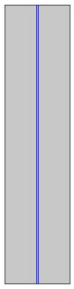

Figure A.6: domain2

- Normal total flux
  $NTflux_{cSO_4} = BNDflux_{cSO_4} + Cflux_{cSO_{4,x}} \cdot n_{x,c} + Cflux_{cSO_{4,y}} \cdot n_{y,c} + Cflux_{cSO_{4,z}} \cdot n_{z,c}[mol/(m^2 s)]$
- Normal diffusive flux
  $NDflux_{cSO_4} = Dflux_{cSO_{4,x}} \cdot n_{x,c} + Dflux_{cSO_{4,y}} \cdot n_{y,c} + Dflux_{cSO_{4,z}} \cdot n_{z,c}[mol/(m^2 s)]$
- Normal convective flux
  $NCflux_{cSO_4} = Cflux_{cSO_{4,x}} \cdot n_{x,c} + Cflux_{cSO_{4,y}} \cdot n_{y,c} + Cflux_{cSO_{4,z}} \cdot n_{z,c}[mol/(m^2 s)]$
- Normal electrophoretix flux
  $NMflux_{cSO_4} = Mflux_{cSO_{4,x}} \cdot n_{x,c} + Mflux_{cSO_{4,y}} \cdot n_{y,c} + Mflux_{cSO_{4,z}} \cdot n_{z,c}[mol/(m^2 s)]$

A.2 Membrane: Secondary current distribution

1. **Electrolyte, membrane** the equations of domain 2, (fig A.6)

   - Electric field
     $$\begin{bmatrix} E_x \\ E_y \\ E_z \end{bmatrix} = \begin{bmatrix} -\frac{\partial \phi_{l_m}}{\partial x} \\ -\frac{\partial \phi_{l_m}}{\partial y} \\ 0 \end{bmatrix} [V/m]$$
   - Current Source $Qli = 0[A/m^3]$
   - Electrode current density
     $$\begin{bmatrix} il_x \\ il_y \\ il_z \end{bmatrix} = \begin{bmatrix} \sigma_{l,xx}\frac{\partial \phi_{l_m}}{\partial x} - \sigma_{l,xy}\frac{\partial \phi_{l_m}}{\partial y} \\ \sigma_{l,yx}\frac{\partial \phi_{l_m}}{\partial x} - \sigma_{l,yy}\frac{\partial \phi_{l_m}}{\partial y} \\ \sigma_{l,zx}\frac{\partial \phi_{l_m}}{\partial x} - \sigma_{l,zy}\frac{\partial \phi_{l_m}}{\partial y} \end{bmatrix} [A/m^2]$$
   - Electrolyte current density vector
     $$\begin{bmatrix} Il_x \\ Il_y \\ Il_z \end{bmatrix} = \begin{bmatrix} il_x \\ il_y \\ il_z \end{bmatrix} [A/m^2]$$

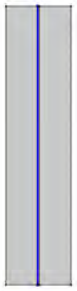

Figure A.7: boundary4

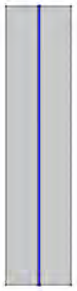

Figure A.8: boundary7

- Electrolyte conductivity
  $\sigma_{\mathbf{m}} = \begin{bmatrix} \sigma_{xx} & \sigma_{xy} & \sigma_{xz} \\ \sigma_{yx} & \sigma_{yy} & \sigma_{yz} \\ \sigma_{zx} & \sigma_{zy} & \sigma_{zz} \end{bmatrix} = \begin{bmatrix} \sigma_m & 0 & 0 \\ 0 & \sigma_m & 0 \\ 0 & 0 & \sigma_m \end{bmatrix} [S/m]$
- Total power dissipation
  $Qh = -Il_x \frac{\partial \phi_{l_m}}{\partial x} - Il_y \frac{\partial \phi_{l_m}}{\partial y} [W/m^3]$

2. **Poinwise constraint 1, membrane** equations of the boundary 4 (fig A.7)
   - Constraint
     $\phi_{l,neg} - Nernst(0, \phi_l, \frac{aH}{AH_m}) - \phi_{l_m} = 0[V]$
   - Constraint force
     $\phi_{l,neg} + \frac{cH}{F} - \phi_{l_m} = 0$

3. **Poinwise constraint 2, membrane** equations of the boundary 7 (fig A.8)
   - Constraint
     $\phi_{l,pos} - Nernst(0, \phi_l, \frac{aH}{AH_m}) - \phi_{l_m} = 0[V]$
   - Constraint force
     $\phi_{l,pos} + \frac{cH}{F} - \phi_{l_m} = 0$

4. **Secondary current distribution, membrane** equation of the domain 2 (fig A.6)

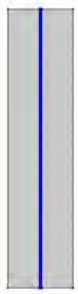

Figure A.9: boundary4-7

- Current source
  $Qsi = 0[A/m^3]$
- Domain Flux
  $Domflux(\frac{\partial \phi_{l_m}}{\partial x}) = Il_x[A/m^2]$
- Domain Flux
  $Domflux(\frac{\partial \phi_{l_m}}{\partial y}) = Il_y[A/m^2]$
- Domain Flux
  $Domflux(\frac{\partial \phi_s}{\partial x}) = root.comp.1.siec.Isx$
- Domain Flux
  $Domflux(\frac{\partial \phi_s}{\partial y}) = root.comp.1.siec.Isy$
- Thickness
  $d = 1[m]$

5. **Secondary current distribution, membrane** equations of the boundaries 4-7 (fig A.9)
   - Inward electrolyte current density
     $nil = 0[A/m^2]$
   - Inward electrode current density $nis = 0[A/m^2]$
   - Normal electrolyte current density $nIl = BNDflux_{\phi_{l_m}}[A/m^2]$
6. **Secondary current distribution, membrane** equations of the boundary 4 (fig A.7)
   - Normal vector $\begin{bmatrix} n_x \\ n_y \\ n_z \end{bmatrix} = \begin{bmatrix} un_x \\ un_y \\ 0 \end{bmatrix}$
   - Normal vector (mesh) $\begin{bmatrix} n_{x,mesh} \\ n_{y,mesh} \\ n_{z,mesh} \end{bmatrix} = \begin{bmatrix} root.unxmesh \\ root.unymesh \\ 0 \end{bmatrix}$
   - Boundary flux $BNDflux_{\phi_{l_m}} = -uflux_spatial(\phi_{l_m})[A/m^2]$

7. **Secondary current distribution, membrane** equations of the boundaries 5-7
   - Normal vector $\begin{bmatrix} n_x \\ n_y \\ n_z \end{bmatrix} = \begin{bmatrix} dnx \\ dny \\ 0 \end{bmatrix}$
   - Normal vector (mesh) $\begin{bmatrix} n_{x,mesh} \\ n_{y,mesh} \\ n_{z,mesh} \end{bmatrix} = \begin{bmatrix} root.dnxmesh \\ root.dnymesh \\ 0 \end{bmatrix}$
   - Boundary flux $BNDflux_{\phi_{l_m}} = -dflux_spatial(\phi_{l_m})[A/m^2]$

A.3 Positive electrode: Tertiary current distribution

For the positive electrode, the equation are the same of the negative electrode, with the substitution of V_2 and V_3 with V_5 and V_4

Appendix B

Matlab Codes

Code to create the curves of the electric potential for different charge and discharge current densities.

```
%script to make the charge/discharge curves
%from the files exported from COMSOL



clear all
clc
%import of the datas
table = sprintf('test2.csv');
delimiterIn = ',';
headerlinesIn = 5;
Data = importdata(table,delimiterIn,headerlinesIn);
Data = Data.data;

col3 = Data(:,3);

tab = [];

%file prepared for 19 soc levels
numsoc=19;
%and 10 current levels
numcurr=10;
for j=1:numsoc

col=[];
for i=1:numcurr
    col = [col;col3(i+(j-1)*numcurr)];
end

tab = [tab col];
end
%for each current, there are both the "-" sign and the
%"+" sign; by doing this, it is possible to consider
```

```
%both the discharge and the charge
curves = [];
for k=1:5
    reg = tab(k,:);
    inv = fliplr(tab(11-k,:));
    row = [reg inv];
    curves = [curves; row];
end
curve = fliplr(curve);

currents = [200,150,100,50,25];
soc=linspace(1,2*numsoc,2*numsoc);
surf(soc,currents,curves);

%calculation of the electric efficiency
eta_v = [];
for j=1:5
totpotc=0;
totpotd=0;
for i=1:numsoc
    totpotc=totpotc+curve(j,i);
    totpotd = totpotd + curve(j,(2*numsoc+1)-i);
end
pot_c_m = totpotc/numsoc;
pot_d_m = totpotd/numsoc;
eta_v(j) = pot_d_m/pot_c_m;
end
```

Bibliography

[1] C. Blanc. *Modeling of a Vanadium Redox Flow Battery Electricity Storage System*. PhD thesis, Ecole Polytechnique Federale de Lausanne, 2009.

[2] Electricity Storage Association. Storage technology comparison, 2014. [Online; accessed 30-September-2014].

[3] P. Alotto, M. Guarnieri, and F. Moro. Redox flow batteries for the storage of renewable energy: A review. *Renewable and Sustainable Energy Reviews*, 29, 2014.

[4] B. Scrosati and J. Garche. Lithium batteries: Status, prospects and future. *Journal of Power Sources*, 195, 2010.

[5] M. Skyllas-Kazacos, M. H. Chakrabarti, S. A. Hajimolana, F. S. Mjalli, and M. Saleem. Progress in flow battery research and development. *Journal of the Electrochemical Society*, 158, 2011.

[6] E. Sum and M. Skyllas-Kazacos. A study of the V(II)/V(III) redox couple for redox flow applications. *Journal of Power Sources*, 15, 1985.

[7] E. Sum, M. Rychick, and M. Skyllas-Kazacos. Investigation of the V(V)/V(IV) system for use in the positive half cell of a redox battery. *Journal of Power Sources*, 16, 1985.

[8] C. Blanc and A. Rufer. Multiphysics and energetic modeling of a vanadium redox flow battery. *Ieee International Conference on Sustainable Energy Technologies*, 2008.

[9] L. Joerissen, J. Garche, Ch. Fabjan, and G. Tomazic. Possible use of vanadium redox-flow batteries for energy storage in small grids and stand-alone photovoltaic systems. *Journal of Power Sources*, 127, 2004.

[10] T Shigematsu. Redox flow battery for energy storage. *SEI Technical Review*, 73, 2011.

[11] M. Skyllas-Kazacos et al. All-vanadium redox battery patent, 1986.

[12] A. Z. Weber, M. M. Mench, J. P. Meyers, P. N. Ross, J. T. Gostick, and Q. Liu. Redox flow batteries: a review. *Journal of Applied Electrochemistry*, 2011.

[13] W. Schmickler and E. Santos. *Interfacial Electrochemistry*. Springer, 2010.

[14] A. A. Shah, M. J. Watt-Smith, and F. C. Walsh. A dynamic performance model for redox-flow batteries involving soluble species. *Electrochimica Acta*, 53, 2008.

[15] D. You, H. Zhang, and J. Chen. A simple model for the vanadium redox battery. *Electrochimica Acta*, 54, 2009.

[16] M. Vynnycky. Analysis of a model for the operation of vanadium redox battery. *Energy*, 36, 2011.

[17] K. W. Knehr and E. C. Kumbur. Open circuit voltage of vanadium redox flow batteries: Discrepancy between models and experiments. *Electrochemistry Communications*, 13, 2011.

[18] K. W. Knehr, E. Agar, C. R. Dennison, and E. C. Kalidindi, A. R.and Kumbur. A transient vanadium flow battery model incorporating vanadium crossover and water transport through the membrane. *Journal of The Electrochemical Society*, 159, 2012.

[19] C. L. Chen, H. K. Yeoh, and M. H. Chakrabarti. An enhancement to vynniky's model for the all-vanadium redox flow battery. *Electrochimica Acta*, 120, 2014.

[20] Q. Xu, T. S. Zhao, and P. K. Leung. Numerical investigations of flow field design for vanadium redox flow batteries. *Applied Energy*, 105, 2013.

[21] Y. Wang and S. C. Cho. Analysis and three-dimensional modeling of vanadium flow batteries. *Journal of the Electrochemical Society*, 161, 2014.

[22] C. Yin, Y. Gao, S. Guo, and H. Tang. A coupled three dimensional model of vanadium redox flow battery for flow field designs. *Energy*, 74, 2014.

[23] A. Tang, S. Ting, J. Bao, and M. Skyllas-Kazacos. Thermal modelling and simulation of the all-vanadium redox flow battery. *Journal of Power Sources*, 203, 2012.

[24] A. Tang, J. Bao, and M. Skyllas-Kazacos. Thermal modelling of a battery configuration and self-discharge reactions in vanadium redox flow battery. *Journal of Power Sources*, 216, 2012.

[25] B. Turker, S. Arroyo Klein, E. M. Hammer, B. Lenz, and L. Komsiyska. Modeling a vanadium redox flow battery system for large scale applications. *Energy Conversion and Management*, 66, 2013.

[26] K. Bromberger, J. Kaunert, and T. Smolinka. A model for all- vanadium redox flow batteries: Introducing electrode-Compression effects on voltage losses and hydraulics. *Energy Technology*, 2, 2014.

[27] A. Tang, J. Bao, and M. Skyllas-Kazacos. Studies on pressure losses and flow rate optimization in vanadium redox flow battery. *Journal of Power Sources*, 248, 2014.

[28] COMSOL Multiphysics®. Vanadium redox flow battery model, 2013. `http://www.comsol.com/model/download/184561/models.bfc.v_flow_battery.pdf` [Online; accessed 15-March-2014].

[29] Wikipedia. Mathematical model — wikipedia, the free encyclopedia, 2014. `http://en.wikipedia.org/w/index.php?title=Mathematical_model&oldid=627316508` [Online; accessed 1-October-2014].

[30] Wikipedia. Simulation — wikipedia, the free encyclopedia, 2014. `http://en.wikipedia.org/w/index.php?title=Simulation&oldid=627147166` [Online; accessed 1-October-2014].

[31] Wikipedia. Finite element method — wikipedia, the free encyclopedia, 2014. `http://en.wikipedia.org/w/index.php?title=Finite_element_method&oldid=627076387` [Online; accessed 1-October-2014].

[32] Dietrich Braess. *Finite Elements*. Cambridge University Press, third edition, 2007. Cambridge Books Online.

[33] COMSOL Multiphysics®. Comsol multiphysics 4.4 users guide, 2013.

[34] T. Yamamura, N. Watanabe, T. Yano, and Y. Shiokawa. Electron-Transfer kinetics of Np^{3+}/Np^{4+}, NpO_2^+/NpO_2^{2+}, V^{2+}/V^{3+}, and VO^{2+}/VO_2^+. *Journal of the Electrochemical Society*, 152, 2005.

[35] J. Newman and K. E. Thomas-Alyea. *Electrochemical Systems*. Wiley, 2012.

[36] H. Zhou, H. Zhang, P. Zhao, and B. Yi. A comparative study of carbon felt and activated carbon based electrodes for for sodium polysulfide/bromine redox flow battery. *Electrochimica Acta*, 51, 2006.

[37] M. Pourbaix. *Atlas of electrochemical equilibria in aqueous solutions*. National Association of Corrosion Engineers, 1974.

[38] M. Le Bars and M. Grae Worster. Interfacial conditions between a pure fluid and a porous medium: implication for a binary alloy solidification. *Journal of Fluid Mechanics*, 550, 2006.

[39] P. Xu and B. Yu. Developing a new form of permeability and Kozeny-Carman constant for homogeneous porous media by means of fractal geometry. *Advances in Water Resources*, 31, 2008.